Spring 2013

Structure Determination by X-Ray Diffraction Methods and Physicochemical Characterization of Quaternary Diamond-Like Semiconductors

Carl David Brunetta

STRUCTURE DETERMINATION BY X-RAY DIFFRACTION METHODS AND PHYSICOCHEMICAL CHARACTERIZATION OF QUATERNARY DIAMOND-LIKE SEMICONDUCTORS

A Dissertation

Submitted to the Bayer School of Natural and Environmental Sciences

Duquesne University

In partial fulfillment of the requirements for

the degree of Doctor of Philosophy

By

Carl D. Brunetta

May 2013

STRUCTURE DETERMINATION BY X-RAY DIFFRACTION METHODS AND PHYSICOCHEMICAL CHARACTERIZATION OF QUATERNARY DIAMOND-LIKE SEMICONDUCTORS

By

Carl D. Brunetta

Approved December 12, 2012

Jennifer A. Aitken Associate Professor of Chemistry (Committee Chair)	Ellen Gawalt Associate Professor of Chemistry (Committee Member)
Jeffry D. Madura Professor of Chemistry (Committee Member)	Ralph Wheeler Professor of Chemistry (Committee Member)
Peter Wildfong Associate Professor of Pharmacy (Outside Reader)	
David W. Seybert Dean, Bayer School of Natural and Environmental Sciences Professor of Chemistry	Ralph Wheeler Chair, Department of Chemistry Professor of Chemistry

ABSTRACT

STRUCTURE DETERMINATION BY X-RAY DIFFRACTION METHODS AND PHYSICOCHEMICAL CHARACTERIZATION OF QUATERNARY DIAMOND-LIKE SEMICONDUCTORS

By

Carl D. Brunetta

May 2013

Dissertation supervised by Professor Jennifer A. Aitken

Diamond-like semiconductors (DLSs) are a class of semiconductor materials having structures similar to that of either cubic or hexagonal diamond. These normal valence compounds are of interest for their wide variety of technologically useful properties that can be tuned for specific applications. Until recently, DLS research has been focused on binary and ternary compositions due to their relative ease of synthesis. However, quaternary DLSs have gained considerable popularity due to their increased compositional flexibility and their potential as multifunctional materials. Despite their growing reputation, the vast number of possible combinations and conceivable solid solutions, DLSs remain fairly unexplored.

This work focuses on quaternary DLSs of the formula Ag_2-II-IV-S_4 in order to advance the knowledge of structure-property relationships for this entire class of

materials. Toward this goal, a more complete understanding of the crystal structures of these materials is necessary. This task is often problematic due to the presence of isoelectronic, or nearly isoelectonic elements, that can complicate X-ray structure refinements. In this work, Ag_2CdGeS_4 is used as a case study to demonstrate that this problem can be resolved with careful consideration of bonding environments as well as the use of high-resolution X-ray sources. For the novel DLS Ag_2ZnSiS_4, the relationship between the structure and optical properties is probed with the combination of single crystal X-ray diffraction, optical diffuse reflectance spectroscopy and electronic structure calculations using the software package Wien2k. Finally, the current set of predictive tools employed to forcast diamond-like structures are reviewed, including the adherence of these guidelines to the novel compound Ag_2FeSiS_4 as well all over 60 ternary and quaternary diamond-like materials currently reported in the literature. Furthermore, the most common radii sets used for the prediction of bond distance and cell parameters in these materials are compared to the observed bond distances in quaternary diamond-like nonoxide materials.

ACKNOWLEDGEMENT

I would first like to thank my family, without their love and support I would not have been able to accomplish so much. I would especially like to thank my father David Brunetta and my grandfather Daniel Komarinski for not only encouraging me to do my best, but also for teaching me what it means to be a good man. I would also like to thank a mentor, Major General Thomas S. Jones U.S.M.C. (ret) who inspired me to pursue my academic goals to their full potential and for teaching me, among many things, that dreams + actions really do equal reality. I would also like to thank my advisor, Dr. Jennifer Aitken who has helped me to become a better chemist and person by not giving up on me and encouraging me to always do better. Thank you also to my committee for your patience and support.

I would like to thank my labmates and friends Dr. Nathan Takas and Dr. Jonathan Lekse for welcoming me into the lab and helping me start my research. Thanks to Dr. Jin Lei Yao, Dr. Balamurugan Karuppannan, Johanna Burnett and Matt Srnec for all of your help and support. I would also specifically like to thank Jacilynn Brant for her work on Li_2FeSnS_4 and Li_2FeGeS_4 which is prominently featured in this work, as well as Kim Rosmus for all of her help on my projects and her consistent reminders to "Keep Calm." I would also not have been able to accomplish this work without our very talented undergraduate students; Stephen Wisneski, Kimberly Daley, Kylie Henline, Danielle Massi, and Bill Minsterman who have all helped me at various points of my research.

Very special thanks to all my friends for helping me and encouraging me to complete this work especially Jason Campbell, Mike Wozniak, Justin Taddeo, Dr. Chris

Kabana, and Joe Rosmus. Also a very special thanks to our instrument shop; Daniel Bodnar, Lance Crosby, Ben Lauterbach, and Dave Hardesty who not only kept our instruments running but allowed me to help and learn all that I could about them.

Thanks to Dr. Charles Lake (Indiana University of Pennsylvania) for his help with X-ray refinements, synchrotron collection and many fruitful crystallography discussions. I would also like to thank Dr. Brian Toby (Argonne National Laboratory) for his help with Rietveld refinements.

Thank you to the Bayer School of Natural and Environmental Sciences and the National Science Foundation (DMR-0645304 and DMR-1201729) for funding. Instrumentation was purchased through National Science Foundation grants; DUE-0511444 for the Panalytical X'Pert Pro diffractometer, CRIF-0234872 for the Bruker Apex 2 diffractometer, and MRI-CHE-0923183 for the Hitachi S3400n scanning electron microscope. I would also like to thanks the U.S. Department of Energy, Office of Science, Office of Basic Energy Science, under contract DE-AC02-06CH11357 for the use of the Advanced Photon Source at Argonne National Laboratory.

TABLE OF CONTENTS

Page

LIST OF TABLES

Page

LIST OF FIGURES

Page

1 An Introduction to Quaternary Diamond-like Semiconductors

1.1 Introduction

Over the past 50 years, materials science and the study of semiconductors have become a very active area of research. From the development of new materials with designed properties, to new synthesis techniques for existing essential components, this field generates materials that have become an essential part of our everyday lives. Semiconductor materials can be found almost everywhere including in the personal computer, cell phones, solar cells, fiber optics, and even lasers. As technology advances a need arises for smaller, faster, and more efficient components, further propelling this exciting field of research. While the study of new DLSs does not always produce improved materials, these compounds have a redeeming quality; the information gained from the study of these semiconductors provides a deeper understanding of the structure-property and composition-property relationships. This knowledge in turn contributes to the development of predictive tools for the next generation of useful semiconductor materials.

1.2 Diamond-Like Semiconductors (DLSs)

The term diamond-like semiconductors (DLSs) refers to the class of normal valence materials with structures that resemble that of either cubic or hexagonal diamond and posses a band gap generally less than 4 eV.[1,2] The normal valence nature of these materials refers to the component elements' eagerness to achieve an octet by either

sharing, donating, or accepting electrons. The result of this phenomenon is that the bonding within these compounds can range from mostly ionic to mostly covalent and any level of iono-covalent bonding in-between.[3]

These materials also generally abide by four guidelines.[1,6] The first is that the average number of valence electrons per atom is four. This guideline ensures that the overall packing is similar to diamond, where each carbon atom possesses four valence electrons. For example, the well know DLS stannite, Cu_2FeSnS_4, is comprised of eight atoms; two copper atoms, one iron atom, one tin atom, and four sulfur atoms.[4] Each copper atom has one valence electron, the iron atom has two valence electrons, the tin atom has four valence electrons, and each sulfur atom has six valence electrons, for a total of thirty two valence electrons. Therefore, the average number of valence electrons is four, which can be generalized for quaternary compounds as:

$$\overline{\mathrm{X}}\mathrm{ve} = \frac{\left((\mathrm{n}_{\mathrm{cation1}} * \mathrm{ve}_{\mathrm{cation1}}) + (\mathrm{n}_{\mathrm{cation2}} * \mathrm{ve}_{\mathrm{cation2}}) + (\mathrm{n}_{\mathrm{cation3}} * \mathrm{ve}_{\mathrm{cation3}}) + (\mathrm{n}_{\mathrm{anion}} * \mathrm{ve}_{\mathrm{anion}})\right)}{(\mathrm{n}_{\mathrm{cation1}} + \mathrm{n}_{\mathrm{cation2}} + \mathrm{n}_{\mathrm{cation3}} + \mathrm{n}_{\mathrm{anion}})}$$

Where $\overline{\mathrm{X}}\mathrm{ve}$ is the average number of valence electrons; $\mathrm{n}_{\mathrm{cation1}}$, $\mathrm{n}_{\mathrm{cation2}}$, $\mathrm{n}_{\mathrm{cation3}}$, and $\mathrm{n}_{\mathrm{anion}}$ are the number of respective atoms in the formula unit and $\mathrm{ve}_{\mathrm{cation1}}$, $\mathrm{ve}_{\mathrm{cation2}}$, $\mathrm{ve}_{\mathrm{cation3}}$, and $\mathrm{ve}_{\mathrm{anion}}$ are the number of valence electrons per cation or anion.

The second guideline is that the average number of valence electrons per anion is eight. In other words, the octet of each anion must be satisfied and, therefore, the overall material must charge balance to contain an equal number of cations and anions. Using Cu_2CdGeS_4 as an example, the total number of valence electrons is thirty two, with each of the two copper atoms contributing two valence electrons, the cadmium atom

contributing two valence electrons, the germanium atom with four valence electrons, and each of the four sulfur atoms contributing six valence electrons.[5] The division of the total number of valence electrons (thirty two) by the number of anions (four) results in an average of valence electrons per anion ($\overline{X}_{ve}/_{anion}$) of eight, represented by the following general equation for quaternary compounds:

$$\overline{X}_{ve}/_{anion} = \frac{\left((n_{cation1} * ve_{cation1}) + (n_{cation2} * ve_{cation2}) + (n_{cation3} * ve_{cation3}) + (n_{anion} * ve_{anion})\right)}{(n_{anion})}$$

The third guideline states that the octet of each anion must be satisfied by the cations in its immediate coordination sphere. This guideline is also commonly known as Pauling's electrostatic valency principle, as it was first established in Pauling's 1929 publication on the structures of complex crystals.[6] Adherence to this guideline can be determined through the examination of valence bond sums or the amount of electrostatic charge that each cation contributes to each bound anion. The charge of the valence bond (*s*) can be described as:

$$s = \frac{z}{v}$$

Where *z* is the charge of the cation and *v* is the coordination number or the number of bound anions on the cation. For this guideline to be satisfied, the sum of the valence bonds to each anion must be equal to the negative charge on the anion in order for the

structure in question to be electrostatically stable. Therefore, if the charge of the anion is -ζ the relation can be described as:

$$\zeta = \sum_i s_i = \sum_i \frac{z_i}{v_i}$$

However, complete adherence to this particular guideline is not necessary for a material to exist, or to be close to diamond-like. As noted by Pauling, the charge of the anion can deviate from the charge of the valence bonds as long as the difference is compensated for within the structure through structural distortions. For instance, if ζ is greater than sum of the valance bonds, the cations will be more strongly attracted to the anion and the bonds will contract to compensate. In contrast, if ζ is less than the sum of the valence bonds, the cations will less strongly attracted and an elongation of the bonds occurs.6 These situations can still result in a stable structure; however, it will be significantly distorted relative to the usual diamond-like structure, although the diamond-like motif may still be structurally noticeable.

The final guideline for diamond-like materials is that all atoms must be tetrahedrally coordinated. This guideline ensures that these materials will have similar packing arrangements to that of cubic diamond or hexagonal diamond (lonsdaleite4) which are based on cubic and hexagonal closest packing of anions, respectively. The adherence to this rule can easily be determined post synthesis via X-ray structure studies; however, the application of this guideline as a predictive tool is somewhat problematic. Traditionally, Pauling's radius ratio rule is used to predict the coordination of ions in potential compounds. This rule states that the ratio between the cation radius and the

anion radius can be used to predict the coordination environment of the cation. If the radius ratio falls between 0.22 and 0.41, a coordination number of four (tetrahedral geometry) is predicted.6 However, every quaternary diamond-like sulfide and selenide reported to date, as further explained in Chapter 4, exhibits the prerequisite tetrahedral coordination, despite radius ratios above Pauling's limit for CN=4. This result is not completely unexpected; Pauling himself notes that this rule is not likely to hold true for softer anions such as sulfur and selenium.[3,6] Furthermore, this rule assumes a hard sphere model of bonding where no covalent overlap of the orbitals are considered. Since the iono-covalent character of the bonding within these materials is well known, the purely ionic model is not expected to be a an adequate representation.

The application of these guidelines to predict new materials is fairly straightforward. The possible oxidation states and configurations of valence electrons across the periodic table are well known, as well as the formulae of diamond-like materials that satisfy the first three guidelines. Table 1.1 shows the known formulae for binary, ternary, and quaternary DLS materials with the number of valence electrons represented by roman numerals and the number of atoms per formula unit represented by subscripts. Compounds of the I_2-II-IV-VI_4 formula are the primary focus of this work. However, the prediction of tetrahedral geometry remains elusive, not only for the reasons listed above, but also due to the lack of complete or "accurate" radii sets that can describe the bonding of these materials. Currently the best predictor for tetrahedral geometry is to search the literature for example compounds where the elements in question reside in a tetrahedral bonding environment. Although this method in no way guarantees that the desired diamond-like compound will form, this method of prediction has been used

effectively in this work to predict and ultimately synthesize the two new DLSs Ag_2ZnSiS_4, and Ag_2FeSiS_4.[7]

Table 1.1 Known formulae for DLS materials with the focus of this work indicated in red.[2]

Binary	Ternary	Ternary	Quaternary	Quaternary
I-VII	III_3-IV_2-VII	I-IV_2-V_3	I-IV-V-VI	I-III-IV_2-V_4
II-VI	III_2-IV-VI	II-IV-V_2	II-III-V-VI	II-III_2-IV-V_4
III-V	II_2-V-VII	I-III-VI_2	II-III-IV-VII	I-II_2-III-VI_4
IV-IV	II_3-IV-VII_2	I_2-IV-VI_3	I-III-V-VII	**I_2-II-IV-VI_4**
	II_4-III-VII_3	I_3-V-VI_4	I-II-VI-VII	

1.3 Structure

The structure of diamond-like materials resembles that of either the cubic-closest packed (ccp) diamond or the hexagonal-closest packed (hcp) lonsdaleite (hexagonal diamond).[8,9] The progression to binary compounds, as shown in Figure 1.1, can be imagined through the replacement of half the carbon sites with cations and the other half with anions. One of the most well studied binary compounds is ZnS. This II-VI semiconductor can adapt either a ccp or a hcp structure forming the minerals sphalerite and wurtzite, respectively.[10,11] If further ordered substitution is envisioned on the cation sites, ternary and quaternary compounds can be derived from each of the closest packing models. The ternary DLS $AgInS_2$ is another example of a compound that can adopt either packing arrangement dependant on synthetic conditions, growing in either a ccp chalcopyrite or hcp wurtz-chalcopyrite structure.[12,13]

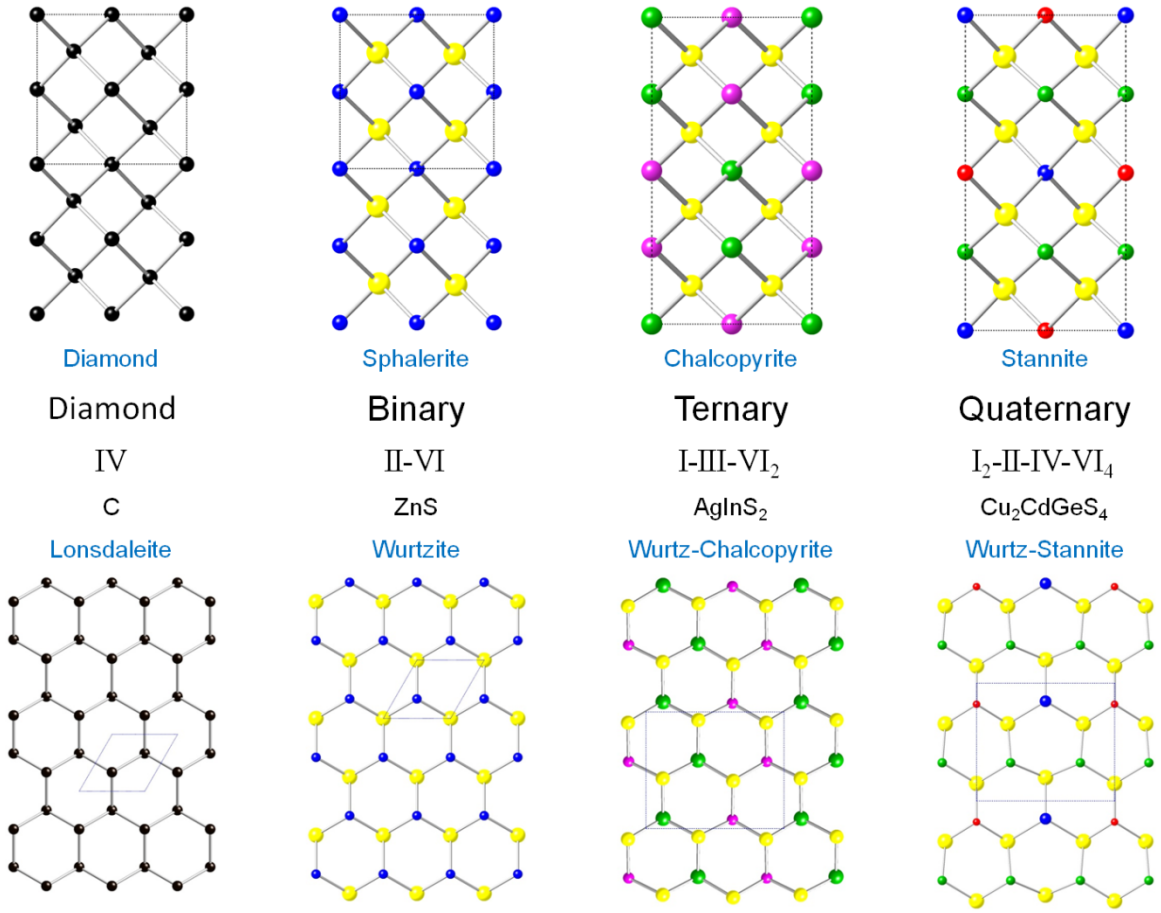

Figure 1.1 Progression of DLS from diamond to quaternary materials for both cubic-closest packing (top) and hexagonal-closest packing (bottom) with example compounds and common structure types.

Although the structure types listed in Figure 1.1 for ternary and quaternary DLS materials are those most commonly found in the literature, other structure types are possible when considering the ordering of the cations. Quaternary DLSs in hcp arrangements are known to possess structures in the space groups *Pn* (no. 7), $Pmn2_1$ (no. 31), *and* $Pna2_1$ (no. 33). Each of these structures is comprised of the same arrangement of anions and only differs in cation ordering. This can lead to challenges in structure refinements, especially in situations where cations are similar in size or

isoelectronic, as well as difficulties in differentiating between them using standard laboratory X-ray diffraction techniques.[14]

1.4 Synthesis

DLS materials can be synthesized in a variety of ways including high-temperature solid-state (HTSS) synthesis, chemical vapor transport (CVT), flux synthesis, and solvothermal methods, to name just a few. This work primarily focuses on the HTSS synthetic approach with some samples prepared using CVT. Both of these approaches are considered solid-state syntheses owing to the solid phase of both the starting and ending materials at room temperature and they are by far the most reported techniques used to prepare diamond-like materials.

1.4.1 High-Temperature Solid-State (HTSS) Synthesis

The HTSS approach is a low-waste, high-yield technique, which ideally results in complete conversion of starting materials to product. However, the phase purity of the products of this technique is very sensitive to temperature, because the most thermodynamically stable compound usually forms. This process consists of combining the elements or binary starting materials in stoichiometric amounts under an inert atmosphere, vacuum sealing the reagents in a fused-silica reaction tube, and heating the samples in a programmable furnace. The heating profiles of these reactions are usually composed of five steps; initial heating or ramp up, dwell, slow cooling or ramp down, annealing, and final cooling. A diagram of a typical heating profile is shown in Figure 1.2.

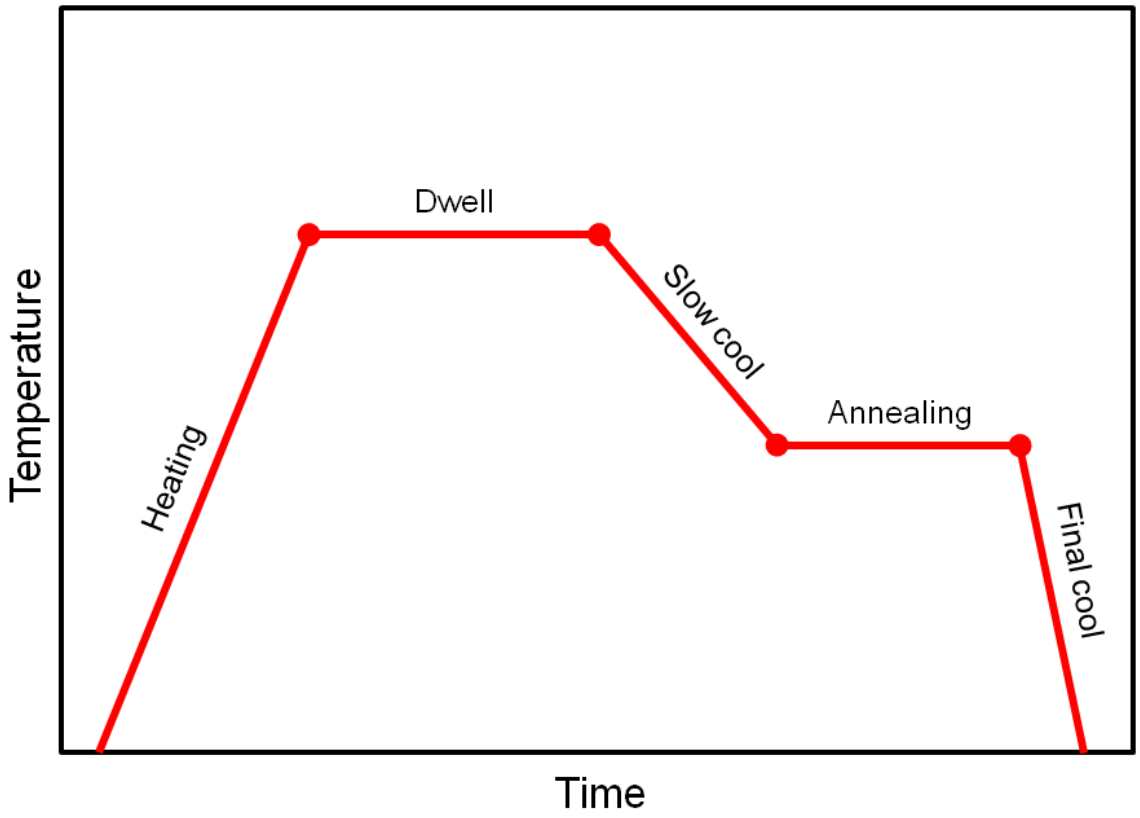

Figure 1.2 A diagramed standard heating profile used for high-temperature solid-state synthesis.

The initial heating step generally reaches a temperature higher than the melting point of the desired material. For quaternary DLSs this step is typically between 500°C and 1200°C. The purpose of this step is to render the starting materials molten so that the atoms can more easily diffuse and arrange into the ordering necessary for the desired product. This diffusion and arrangement is further facilitated by the dwell step or a hold at high temperature. The timescale of this step can range from hours to weeks, but typically lasts a few days. The crystal growth of the product is then facilitated by a cooling step, typically slow (~5°C/hour) enough to reduce the thermal motion of the atoms until a supersaturated solution and nucleation/growth can occur. The speed at

which this cooling takes place can determine which product is formed. Faster cooling rates and even quenches can be utilized to access less stable products and are sometimes preferable for quaternary systems where binary byproducts are often more thermodynamically stable than the desired product.

The annealing step is optional step and holds the product, after crystallization, at a temperature approximately 2/3 of the melting temperature of the material. This supplies thermal energy to the system without melting the material, to allow solid-state diffusion to take place, thus permitting the atoms to slowly rearrange and effectively "repair" defects, minimize grain boundaries, and remove minor impurities. This step normally last days to weeks and is sometimes employed after the product has been allowed to completely cool and has been processed in some way, such as grinding. The last step of the process is the final cooling. Generally this final cooling step is rapid and normally carried out radiatively. Since the material is already solid when this step takes place, little to no change occurs in the sample.

1.4.2 Chemical Vapor Transport (CVT)

Chemical vapor transport (CVT) is a synthetic approach used when relatively large, high-quality crystals are desired. This approach requires more time than the more common HTSS process, often on the order of weeks to months. CTV also requires more material, produces waste products, and requires a multi-zone, high-temperature furnace. For this process starting materials are combined according to the desired stoichiometry and placed in a fused-silica tube. A volatile transport agent such as iodine is added to the tube in a ratio of 5 mg/cm^3 according to the total volume of the reaction vessel.[15] The

reaction tube is then vacuum sealed at a diameter to length ratio of 1 to 10 for optimal crystal growth. Crystal growth in this process is facilitated by a temperature gradient created by the two-zone furnace. The end of the reaction tube containing the starting materials is held at a temperature approximately 200°C higher than the cool end of the tube, as depicted in Figure 1.3.[15] During the long dwell at these temperatures, a convection current is created within the reaction tube caused by the volatile transport agent. As the iodine heats, it weakly bonds to the starting materials and it migrates to the cooler end of the tube where it deposits the materials and returns to the warmer end.

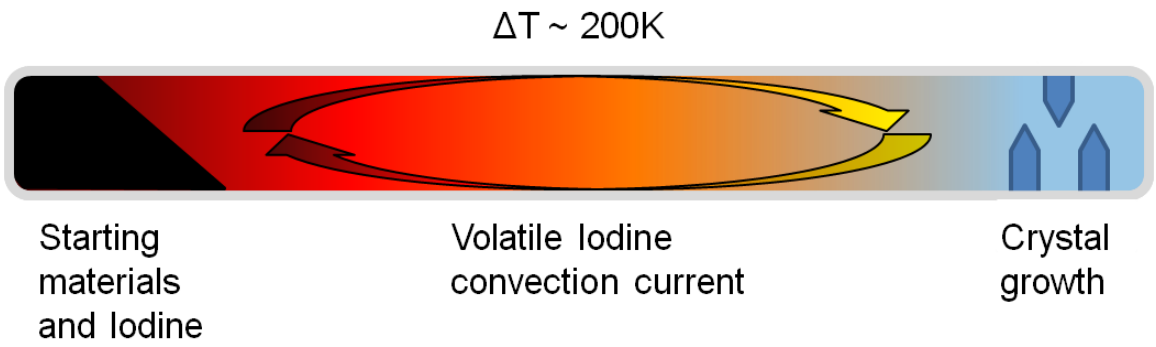

Figure 1.3 Diagram of chemical vapor transport synthesis.

1.5 Previous Work

Quaternary DLSs first appeared in the literature in the late 1950's and for decades appeared to be novel compounds with few apparent uses. Although many quaternary DLSs were already known as naturally occurring minerals, such as stannite (Cu_2FeSnS_4)4 and cernyite (Cu_2CdSnS_4)[16], DLS synthesis proved difficult and the naturally doped character of these minerals led to large amounts of impurities, making property characterization difficult. Early research on these compounds primarily focused on structure and composition studies, relying mainly on "shotgun" synthesis studies in which

numerous compositions, according to the stoichiometry of predicted quaternary systems, were targeted.[5,17] The materials produced in these studies were structurally characterized using X-ray powder diffraction refinements or simple lattice parameter calculations, without the measurement of further properties. However, these studies helped to establish the range of compositions that can form diamond-like structures, as well as the materials' ability to be doped and to form solid-solutions.

Quaternary materials did not receive notable recognition until the mid 1990s with the discovery of Cu_2ZnSnS_4 (CZTS) and its nearly ideal band gap for solar energy conversion.[18] This shifted some of the focus from the relatively established ternary photovoltaic materials $CuInS_2$ and $CuInSe_2$ to the new, more cost effective quaternary material comprised of earth abundant elements.[12] Over the next two decades research into these materials boomed, focusing on new preparations, compositions, nanoscale syntheses, thin films, and more complete property characterizations. This eventually led to further characterization of these materials and the discovery of numerous potential properties and applications such as photovoltaics,[19-21] non-linear optics,[22,23] magnetism,[24,25] and thermoelectrics.[26,27,28]

1.6 Properties

1.6.1 Photovoltaics

In the search for more earth-abundant and sustainable energy sources, solar energy conversion has become a leading technology. Although solar cells are already in use for space vehicles and satellites; low efficiency and high cost of production prevents photovoltaic (PV) energy from becoming the dominant power source.[29,30] Even though

the majority of commercially available solar cells are based on silicon, multi-cation DLS materials are gaining interest due to their inherent compositional flexibility. This leads to tunable band gaps in the range of 1.1 eV to 1.7 eV, which is predicted to be the optimal range for PV applications.[21] Furthermore, DLS such as (CZTS) and $Cu_2ZnSnSe_4$ (CZTSe) have band gaps of 1.45 eV and 1.41 eV, respectively, and are composed of non-toxic, earth abundant elements, which are drastically increasing the interest in diamond-like materials.[18,26]

Research on quaternary DLS materials for PV applications has boomed even in the past decade with projects focusing mainly on application specific syntheses,[19,31-43] the tunability of the band gaps through changes in composition,[44-47] and structure-property relationships formulated with the aid of electronic structures.[36,48] The synthetic work on these materials for solar cell applications has been centered on the materials' ability to be made into thin films and nanoparticulate inks for use as the essential solar radiation absorption layer.[49] However, studies on composition and electronic structures have been focused on increasing the efficiency of the resulting solar cells through the adjustment of the band gap. Even though the efficiency of the quaternary DLS solar cells are not yet as high as their silicon-based counterparts,[50] the tunable nature and the vast number of possible compositions of these materials make them viable candidates for the future of solar cells.

1.6.2 Non-Linear Optics

The field of non-linear optics (NLO) refers to a material's ability to alter incident light as it passes through it. Although this field can refer to many physical phenomena,

DLSs are of interest specifically for the occurrence of second harmonic generation (SHG). This property, also known as frequency doubling, refers to the phenomenon when two incident phonons combine within a material to produce one phonon with double the frequency and half the wavelength.[51] SHG materials have been found to be useful as tunable light sources for spectroscopy and laser applications.[52]

Quaternary DLS materials are of particular interest for NLO phenomena because of their noncentrosymmetric structures (a prerequisite for SHG materials) and generally wide band gaps which leads to higher laser-damage thresholds. Typically ternary DLS materials are used commercially such as $AgGaS_2$,[53-55] $AgGaSe_2$,[56] and $CuGaS_2$[57] for their SHG response in the IR region. However, quaternary Li-containing DLSs have recently been reported with SHG responses 100 times that of standard α-quartz.[58] These studies on Li_2CdGeS_4 and Li_2CdSnS_4 have demonstrated the viability of quaternary DLS materials for SHG applications and are helping to fuel a growing interest for new NLO materials.[23,58]

1.6.3 Thermoelectrics

Thermoelectric (TE) devices are semiconductor systems that can employ either the Seebeck effect or the Peltier effect. The Seebeck effect refers to a system's ability to generate electricity from an applied temperature gradient.[59] This process has potential applications as waste heat collectors for low efficiency procedures such as combustion engines[59] and as power sources for human-implantable devices such as pacemakers.[60] Inversely, the Peltier effect is a system's ability to create a temperature gradient when supplied with a potential difference. This process is of particular interest for applications

including solid-state refrigeration, laser diode coolers, car seat heater/coolers and electronic heat sinks.[59]

Thermoelectric materials are classified by a dimensionless figure-of-merit, ZT, which can be described as:

$$ZT = \left(\frac{\sigma S^2}{(\kappa_{latt} + \kappa_E)}\right) T$$

The value of ZT is determined by the electrical conductivity (σ), Seebeck coefficient (S), lattice thermal conductivity (κ_{latt}), electrical thermal conductivity (κ_E), and the absolute temperature (T) of the material. In order to gain perspective, for a TE system to be as efficient as a commercially available refrigerant system the material would have to possess a ZT of approximately 9.[61] As is apparent in the above formula, this can potentially be achieved by maximizing the electrical conductivity and the Seebeck coefficient while minimizing the thermal conductivity.

The interest in DLSs for thermoelectric applications arise from the structure of these materials and the presence of high atomic mass elements leading to inherently low thermal conductivities. Although the presence of heavy elements normally results in low electrical conductivities, these effects can be mediated through doping procedures as is the case for $Cu_{2+x}Zn_{1-x}SnSe_4$ and $Cu_2ZnSn_{1-x}In_xSe_4$.[26,27] Table 1.2 summarizes the current quaternary DLSs that are being targeted for these applications and lists their ZT values and band gaps. Even though the best TE quaternary DLS materials have ZT values around 1 and research on these materials for this application have been limited to only a handful of studies,[28,63] the ability to increase ZT through doping combined with the

structural flexibility and unexplored compositions of these materials makes TE the fastest growing area of interest for DLSs.

Table 1.2 Thermoelectric figures of merit (ZT) for quaternary diamond-like materials.

Compound	E_g (eV)	T (K)	ZT	Reference
Cu_2ZnSnS_4	1.49	700	0.039	26
$Cu_{2.1}Zn_{0.9}SnS_4$	1.48	700	0.36	26
$Cu_2ZnSnSe_4$	1.41	700	0.18	26
$Cu_{2.1}Zn_{0.9}SnSe_4$	1.39	700	0.45	26
$Cu_{2.1}Zn_{0.9}SnSe_4$	1.39	860	0.91	26
$Cu_2ZnSnSe_4$	1.44	700	0.28	27
$Cu_2ZnSn_{1-x}In_xSe_4$	-	700	0.37	27
$Cu_2ZnSn_{1-x}In_xSe_4$	-	850	0.95	27
$Cu_2CdSnSe_4$	0.98	700	0.19	26
$Cu_{2.1}Cd_{0.9}SnSe_4$	0.95	700	0.65	26

1.6.4 Magnetism

Another potential property of interest for DLSs is ferromagnetism. This phenomenon occurs when the material possesses a magnetic moment arising from the presence of magnetic elements such as Fe or Mn and, consequently, their unpaired electrons. These materials are of interest for potential applications in electronic devices, specifically circuit boards and spintronic devices for the transfer, storage, and processing of electronic information.[64,65] One method to find these potential materials is to synthetically target quaternary DLSs of the formula I_2-II-IV-VI_4 where II is either Fe or Mn.[66-75] This was the approach used by Woolley *et al.* in their study of the diamond-like

material Ag_2FeGeS_4, which was found to be antiferromagnetic with a Néel temperature (T_N), or a temperature that above which the material is paramagnetic, of 240K.[71] Another avenue of research has been to dope Fe or Mn onto the II site in diamagnetic materials.[76,77] This approach produces materials known as dilute magnetic semiconductors where the specific ferromagnetic characteristics may be tailored by site occupation and doping levels. An example of this approach is the work of Quintero *et al.*, where they created a solid-solution of $Cu_2Cd_{0.25}Fe_{0.75}GeSe_4$ that was found to be antiferromagnetic with a T_N of 12K.

1.7 Conclusion

This work focuses on the synthesis and physicochemical characterization of quaternary DLSs with the general formula I_2-II-IV-VI_4 for the elucidation of structure-property relationships, as well as a critical review of the predictive tools used for these materials. In other words the purpose of this work is to further the knowledge of what compositions and structures cause the physicochemical properties in these materials in order to determine how to predict them. This allows for materials to be targeted for specific applications rather than the more common approach of synthesizing a new material and then determining its useful properties. Due to the vast number of conceivable compositions for quaternary diamond-like materials, predictive tools including property targeting techniques are a necessity for the advancement of DLS research and a key component for the development of new materials for real-world applications. Therefore, careful structural studies, including crystal and electronic

structures, are of paramount importance in these materials for the establishment of structure-property relationships.

1.8 Reference

1 Goryunova, N.A. *The Chemistry of Diamond-Like Semiconductors*; Anderson, J.C. Ed.; The MIT Press: Cambridge, U.K. **1965**.

2 E. Parthé, E. *Crystal Chemistry of Tetrahedral Structures*; Gordon and Breach Science Publishers: New York, NY, **1964**.

3 Pauling L. *The Nature of the Chemical Bond, 3rd ed.*; Cornell University Press: Ithaca, NY, **1960**.

4 Brockway L. O. "The crystal structure of stannite, Cu_2FeSnS_4" *Z. Kristallogr. Krist.* **1934**, *89*, 434-441.

5 Parthé, E.; Yvon, K.; Dietech, R. H. "Crystal structure of Cu_2CdGeS_4 and other quaternary normal tetrahedral structure compounds" *Acta Crystallogr., Sect. B* **1969**, *25(6)*, 1164-1174.

6 Pauling, L. "The principles determining the structure of complex ionic crystals" *J. Am. Chem. Soc.* **1929**, *51*, 1010-1026.

7 Brunetta, C. D.; Balamurugan, K.; Rosmus, K. A.; Aitken, J. A. "The crystal and electronic band structure of the diamond-like semiconductor Ag_2ZnSiS_4" *J. Alloy. Compd.* **2012**, *516*, 65-72.

8 Frondel, C.; Marvin, U. B. "Lonsdaleite, a hexagonal polymorph of diamond" *Nature* **1967**, *214*, 587-589.

9 Straumanis, M. E.; Aka, E. Z. "Precision determination of lattice parameter, coefficient of thermal expansion, and atomic weight of carbon in diamond" *J. Am. Chem. Soc.* **1951**, *73*, 5643-5646.

10 Jamieson, J.C.; Demarest, H. H. "A note on the compression of cubic zinc sulfide" *J. Phys. Chem. Solid* **1980**, *41(9)*, 963-964.

11 Chao, G. Y.; Gault, R. A. "The occurrence of two rare polytypes of wurtzite, 4H and 8H, at Mont Saint-Hilaire, Quebec" *Can. Mineral.* **1998**, *36(3)*, 775-778.

12 Hahn, H.; Frank, G.; Klingler, W.; Meyer, A. D.; Stoerger, G. "Investigations of ternary chalcogenides, ternary chalcogenides with chalcopyrite structures" *Z. Anorg. Allg. Chem.* **1953**, *271*, 153-170.

13 Vaipolin, A. A.; Rud, Yu. V.; Rozhdestvenskaya, I. V. "Interatomic interaction aspect of phase transition in silver indium sulfide ($AgInS_2$) crystals" *Cryst. Res. Technol.* **1988**, *23(3)*, 337-341.

14 Brunetta, C. D.; Minsterman, W. C.; Lake, C. H.; Aitken, J. A. "Cation ordering and physicochemical characterization of the quaternary diamond-like semiconductor Ag_2CdGeS_4" *J. Solid State Chem.* **2012**, *187*, 177-185.

15 Zuo, R.; Wang, W. "Theoretical study on chemical vapor transport of ZnS-I_2 system" *J. Cryst. Growth* **2002**, *236(4)*, 687-710.

16 Szymański, J. T. "The crystal structure of cernyite, Cu_2CdSnS_4, a cadmium analog of stannite" *Can. Mineral.* **1978**, *16(2)*, 147-151.

17 Schäfer, W.; Nitsche, R. "Tetrahedral quaternary chalcogenides of the type Cu_2-II-IV-$S_4(Se_4)$" *Mater. Res. Bull.* **1974**, *9(5)*, 645-654.

18 Nakayama, N.; Ito, K. "Sprayed films of stannite Cu_2ZnSnS_4" *Appl. Surf. Sci.* **1996**, *92*, 171-175.

19 Guo, Q.; Hillhouse, H. W.; Agrawal, R. "Synthesis of Cu_2ZnSnS_4 nanocrystal ink and its use for solar cells" *J. Am. Chem. Soc.* **2009**, *131(33)*, 11672-11673.

20 Ford, G. M.; Guo, Q.; Agrawal, R.; Hillhouse, H. W.; Hugh, W. "Earth abundant element $Cu_2Zn(Sn_{1-x}Ge_x)S_4$ nanocrystals for tunable band gap solar cells: 6.8% efficient device fabrication" *Chem. Mater.* **2011**, *23(10)*, 2626-2629.

21 Goetzberger, A.; Hebling, C.; Schock, H. W. "Photovoltaic materials, history, status and outlook" *Mater. Sci. Eng. R.* **2003**, *40(1)*, 1-46.

22 Levcenco, S.; Dumcenco, D.; Huang, Y. S.; Arushanov, E.; Tezlevan, V. "Polarization-dependent electrolyte electroreflectance study of Cu_2ZnSiS_4 and $Cu_2ZnSiSe_4$ single crystals" *J. Alloys Compd.* **2011**, *509(25)*, 7105-7108.

23 Li, Y.; Fan, W.; Sun, H.; Cheng, X.; Li, P.; Zhao X. "Electronic, optical and lattice dynamic properties of the novel diamond-like semiconductors Li_2CdGeS_4 and Li_2CdSnS_4" *J. Phys. Condens, Matter* **2011**, *23(22)*, 225401.

24 McCabe, G. H.; Fries, T.; Liu, M. T.; Shapira, Y.; Ram-Mohan, L. R.; Kershaw, R.; Wold, A.; Fau, C.; Averous, M.; McNiff, E. J. "Bound magnetic polarons in p-type $Cu_2Mn_{0.9}Zn_{0.1}SnS_4$" *Phys. Rev. B.* **1997**, *56(11)*, 6673-6680.

25 Pearton, S. J.; Abernathy, C. R.; Norton, D. P.; Hebard, A. F.; Park, Y. D.; Boatner, L. A.; Budai, J. D. "Advances in wide bandgap materials for semiconductor spintronics" *Mater. Sci Eng. R.* **2003**, *40(4)*, 137-168.

26 Liu, M. L.; Chen, I. W.; Huang, F. Q.; Chen, L. D. "Improved thermoelectric properties of Cu-doped quaternary chalcogenides of $Cu_2CdSnSe_4$" *Adv. Mater.* **2009**, *21(37)*, 3808-3812.

27 Shi, X. Y.; Huang, F. Q.; Liu, M. L.; Chen, L. D. "Thermoelectric properties of tetrahedrally bonded wide-gap stannite compounds $Cu_2ZnSn_{1-x}In_xSe_4$" *Appl. Phys. Lett.* **2009**, *94(12)*, 122103.

28 Sevik, C.; Ćağin, T. "Ab initio study of thermoelectric transport properties of pure and doped quaternary compounds" *Phys. Rev. B* **2010**, *82(4)*, 045202.

29 Miles, R. W.; Zoppi, G.; Forbes, I. "Inorganic photovoltaic cells" *Mater. Today* **2007**, *10(11)*, 20-27.

30 Stanbery, B. J. "Copper indium selenides and related materials for photovoltaic devices" *Rev. Solid State Mater. Sci.* **2002**, *27(2)*, 73-117.

31 Zhao, H.; Persson, C. "Optical properties of $Cu(In,Ga)Se_2$ and $Cu_2ZnSn(S,Se)_4$" *Thin Solid Films* **2011**, *519(21)*, 7508-7512.

32 Shavel, A.; Arbiol, J.; Cabot, A. "Synthesis of quaternary chalcogenide nanocrystals: stannite $Cu_2Zn_xSn_ySe_{1+x+2y}$" *J. Am. Chem. Soc.* **2010**, *132(13)*, 4514-4515.

33 Steinhagen, C.; Panthani, M. G.; Akhavan, V.; Goodfellow, B.; Koo, B.; Korgel, B. A. "Synthesis of Cu_2ZnSnS_4 nanocrystals for use in low-cost photovoltaics" *J. Am. Chem. Soc.* **2009**, *131(35)*, 12554-12555.

34 Weber, A.; Krauth, H.; Perlt, S.; Schubert, B.; Kötschau, I.; Schorr, S.; Schock, H. W. "Multi-stage evaporation of Cu_2ZnSnS_4 thin films" *Thin Solid Films* **2009**, *517(7)*, 2524-2526.

35 Mellikov, E.; Meissner, D.; Varema, T.; Altosaar, M.; Kauk, M.; Volobujeva, O.; Raudoja, J.; Timmo, K.; Danilson, M. "Monograin materials for solar cells" *Sol. Energy Mater. Sol. Cells* **2009**, *93(1)*, 65-68.

36 Maeda, T.; Nakamura, S.; Wada, T. "First principles calculations of defect formation in in-free photovoltaic semiconductors Cu_2ZnSnS_4 and $Cu_2ZnSnSe_4$" *Jpn. J. Appl. Phys.* **2011**, *50(4)*, 04DP07.

37 Katagiri, H.; Jimbo, K.; Maw, W. S.; Oishi, K.; Yanazaki, M.; Araki, H.; Takeuchi, A. "Development of CZTS-based thin film solar cells" *Thin Solid Films* **2009**, *517(7)*, 2455-2460.

38 Scragg, J. J.; Dale, P. J.; Peter, L. M.; Zoppi, G.; Forbes, I. "New routes to sustainable photovoltaics: evaluation of Cu_2ZnSnS_4 as an alternative absorber material" *Phys. Stat. Sol. B* **2008**, *245(9)*, 1772-1778.

39 Babu, G. S.; Kumar, Y. B.; Bhaskar, P. U.; Raja, V. S. "Effect of post-deposition annealing on the growth of $Cu_2ZnSnSe_4$ thin films for a solar cell absorber layer" *Semicond. Sci. Technol.* **2008**, *23(8)*, 085023.

40 Tanaka, K.; Moritake, N.; Uchiki, H. "Preparation of Cu_2ZnSnS_4 thin films by sulfurizing sol-gel deposited precursors" *Sol. Energy Mater. Sol. Cells* **2007**, *91(13)*, 1199-1201.

41 Kamoun, N.; Bouzouita, H.; Rezig, B. "Fabrication and characterization of Cu_2ZnSnS_4 thin films deposited by spray pyrolysis technique" *Thin Solid Films* **2007**, *515(15)*, 5949-5952.

42 Matsushita, H.; Ochiai, T.; Katsui, A. "Preparation and characterization of $Cu_2ZnGeSe_4$ thin filmsby selenization method using the Cu-Zn-Ge evaporated layer precursors" *J. Cryst. Growth* **2005**, *275*, 995-999.

43 Katagiri, H.; Saitoh, K.; Washio, T.; Shinohara, H.; Kurumadani, T.; Miyajima, S. "Development of thin film solar cell based on Cu_2ZnSnS_4 thin films" *Sol. Energy Mater. Sol. Cells* **2001**, *65*, 141-148.

44 Nakamura, S.; Maeda, T.; Wada, T. "Phase stability and electronic structure of in-free photovoltaic materials $Cu_2IISnSe_4$ (II: Zn, Cd, Hg)" *Jpn. J. Appl. Phys.* **2011**, *50(5)*, 05FF01.

45 Zoppi, G.; Forbes, I.; Miles, R. W.; Dale, P. J.; Scragg, J. J.; Peter, L. M. "$Cu_2ZnSnSe_4$ thin film solar cells produced by selenisation of magnetron sputtered precursors" *Prog. Photovolt: Res. Appl.* **2009**, *17(5)*, 315-319.

46 Altosaar, M.; Raudoja, J.; Timmo, K.; Danilson, M.; Grossberg, M.; Krustok, J.; Mellikov, E. "$Cu_2Zn_{1-x}Cd_xSn(Se_{1-y}S_y)_4$ solid solutions as absorber materials for solar cells" *Phys. Stat. Sol. A* **2008**, *205(1)*, 167-170.

47 Raulot, J. M.; Domain, C.; Guillemoles, J. F. "Ab initio investigation of potential indium and gallium free chalcopyrite compounds for photovoltaic application" *J. Phys. Chem. Solids* **2005**, *66(11)*, 2019-2023.

48 Persson, C. "Electronic and optical properties of Cu_2ZnSnS_4 and $Cu_2ZnSnSe_4$" *J. Appl. Phys.* **2010**, *107(5)*, 053710.

49 Beach, J. D.; McCandless, B. E. "Materials challenges for CdTe and $CuInSe_2$ photovoltaics" *MRS Bull.* **2007**, *32(3)*, 225-229.

50 Green, M. A.; Emery, K.; Hisikawa, Y.; Warta, W. “Solar cell efficiency tables” *Prog. Photovolt: Res. Appl.* **2007**, *15(5)*, 425-430.

51 Franken, P. A.; Hill, A. E.; Peters, C. W.; Weinrich, G. “Generation of optical harmonics” *Phys. Rev. Lett.* **1961**, *7(4)*, 118-119.

52 Kim, Y.; Martin, S. W.; Ok, K. M.; Halasyamani, P. S. "Synthesis of the thioborate crystal $Zn_xBa_2B_2S_{5+x}$ (x~0.2) for second order nonlinear optical applications" *Chem. Mater.* **2005**, *17(8)*, 2046-2051.

53 Ruderman, W.; Maffetone, J.; Zelman, D.; D. Poirier, D. "Laser damage studies of silver gallium sulfide single crystals" *Mater. Res. Soc. Symp. Proc.* **1998**, *484*, 519-524.

54 Bhar, G. C.; Smith, R. C. "Optical properties of II-IV-V_2 and I-III-VI_2 crystals with particular reference to transmission limits" *Phys. Status Solidi* **1972**, *13(1)*, 157-168.

55 Chemla, D. S.; Kupecek, P. J.; Robertson, D. S.; Smith, R. C. "Silver thiogallate, a new material with potential for infrared devices" *Opt. Commun.* **1971**, *3(1)*, 29-31.

56 Catella, G. C.; Burlage, D. "Crystal growth and optical properties of $AgGaS_2$ and $AgGaSe_2$" *MRS Bull.* **1998**, *23(7)*, 28-36.

57 Jackson, A. G.; Ohmer, M. C.; LeClair, S. R. "Relationship of the second order nonlinear optical coefficient to energy gap in inorganic non-centrosymmetric crystals" *Infrared Phys. Technol.* **1997**, *38(4)*, 233-244.

58 Lekse, J. W.; Moreau, M. A.; McNerny, K. L.; Yeon, J.; Halasyamani, P. S.; Aitken, J. A. "Second-harmonic generation and crystal structure of the diamond-

like semiconductors Li_2CdGeS_4 and Li_2CdSnS_4" *Inorg. Chem.* **2009**, *48(16)*, 7516-7518.

59 Bell, L. E. "Cooling, heating, generating power, and recovering waste heat with thermoelectric systems" *Science* **2008**, *321*, 1457-1461.

60 Yang, Y.; Wei, X. J.; Liu, J. "Suitability of a thermoelectric power generator for implantable medical electronic devices" *J. Phys. D: Appl. Phys.* **2007**, *40(18)*, 5790-5800.

61 DiSalvo, F. J. "Thermoelectric cooling and power generation" *Science* **1999**, *285*, 703-706.

62 Shi, X.; Xi, L.; Fan, J.; Zhang, W.; Chen, L. "Cu-Se bond network and thermoelectric compounds with complex diamondlike structure" *Chem. Mater.* **2010**, *22(22)*, 6029-6031.

63 Sevik, C.; Çağin, T. "Assessment of thermoelectric performance of Cu_2ZnSnX_4, X = S, Se, and Te" *Appl. Phys. Lett.* **2009**, *95(11)*, 112105.

64 Žutić, I.; Fabian, J.; Das Sarma, S. "Spintronics: fundamentals and applications" *Rev. Mod. Phys.* **2004**, *76(2)*, 323-410.

65 Schmidt, G.; Molenkamp, L. W. "Spin injection into semiconductors, physics and experiments" *Semicond. Sci. Technol.* **2002**, *17(4)*, 310-321.

66 Rincón, C.; Quintero, M.; Moreno, E.; Power, C.; Quintero, E.; Henao, J. A.; Macías, M. A.; Delgado, G. E.; Tovar, R.; Morocoima, M. "X-ray diffraction, Raman spectrum and magnetic susceptibility of the magnetic semiconductor Cu_2FeSnS_4" *Solid State Comm.* **2011**, *151(13)*, 947-951.

67 Quintero, E.; Quintero, M.; Moreno, E.; Lara, L.; Morocoima, M.; Pineda, F.; Grima, P.; Tovar, R.; Bocaranda, P.; Henao, J. A.; Macías, M. A. "Magnetic properties for the $Cu_2MnSnSe_4$ and $Cu_2FeSnSe_4$ compounds" *J. Phys. Chem. Solids* **2010**, *71(7)*, 993-998.

68 Fukushima, T.; Yamauchi, K.; Picozzi, S. "Magnetically induced ferroelectricity in Cu_2MnSnS_4 and $Cu_2MnSnSe_4$" *Phys. Rev. B* **2010**, *82(1)*, 014102.

69 Nénert, G.; Palstra, T. T. M. "Magnetoelectric and multiferroic properties of ternary copper chalcogenides $Cu_2MIIMIVS_4$" *J. Phys. Condens. Matter* **2009**, *21(17)*, 176002.

70 Fries, T.; Shapira, Y.; Palacio, F.; Morón, M. C.; McIntyre, G. J.; Kershaw, R.; Wold, A.; McNiff, E. J. "Magnetic ordering of the antiferromagnet Cu_2MnSnS_4 from magnetization and neutron-scattering" *Phys. Rev. B* **1997**, *56(9)*, 5425-5431.

71 Woolley, J. C.; Lamarche, G.; Lamarche, A. M.; Rakoto, H.; Broto, J. M.; Quintero, M.; Morocoima, M.; Quintero, E.; Gonzalez, J.; Tovar, R.; Cadenas, R.; Bocoranda, P.; Ruiz, J. "High field magnetic properties of $Ag_2FeGeSe_4$ in the temperature range 2-300 K" *J. Magn. Magn. Mater.* **2003**, *257(1)*, 87-94.

72 Quintero, M.; Cadenas, R.; Tovar, R.; Quintero, E.; Gonzalez, J.; Ruiz, J.; Woolley, J. C.; Lamarche, G.; Lamarche, A. M.; Broto, J. M.; Rakoto, H.; Barbaste, R. "Magnetic spin-flop and magnetic saturation in $Ag_2FeGeSe_4$, $Ag_2FeSiSe_4$ and $Cu_2MnGeSe_4$ semiconductor compounds" *Physica B* **2001**, *294*, 471-474.

73 Quintero, E.; Tovar, R.; Quintero, M.; Sánchez-Porras, G.; Bocaranda, P.; Broto, J. M.; Rakoto, H.; Barbaste, R.; Woolley, J. C.; Lamarche, G.; Lamarche, A. M.

"Crystallographic, electrical and magnetic properties of the $Cu_2FeGeSe_4$ compound" *Phys. Stat. Sol. B* **2000**, *220(1)*, 417-423.

74 Quintero, E.; Tovar, R.; Quintero, M.; Gonzalez, J.; Broto, J. M.; Rakoto, H.; Barbaste, R.; Woolley, J. C.; Lamarche, G.; Lamarche, A. M. "Magnetic behaviour of $Cu_2FeGeSe_4$" *J. Magn. Magn. Mater.* **2000**, *210*, 208-214.

75 Bernardini, G. P.; Borrini, D.; Caneschi, A.; Di Benedetto, F.; Gatteschi, D.; Ristori, S.; Romanelli, M. "EPR and SQUID magnetometry study of Cu_2FeSnS_4 (stannite) and Cu_2ZnSnS_4 (kesterite)" *Phys. Chem. Minerals* **2000**, *27(7)*, 453-461.

76 Quintero, E.; Quintero, M.; Moreno, E.; Morocoima, M.; Grima, P.; Bocaranda, P.; Henao, J. A.; Pinilla, J. "Magnetic properties of $Cu_2Cd_{1-z}Mn_zGeSe_4$ and $Cu_2Cd_{1-z}Fe_zGeSe_4$ alloys" *J. Alloys Compd.* **2009**, *471*, 16-20.

77 Quintero, E.; Quintero, M.; Morocoima, M.; Bocaranda, P. "Bound magnetic polarons in p-type $Cu_2Cd_{0.25}Fe_{0.75}GeSe_4$ and $Cu_2FeGeTe_4$" *J. Appl. Phys.* **2007**, *102(8)*, 083905.

2 Cation Ordering and Physicochemical Characterization of the Quaternary Diamond-Like Semiconductor Ag_2CdGeS_4

2.1 Introduction

Although quaternary diamond-like semiconductors (DLSs) were first discovered in the 1960s[78,79] these compounds have recently seen increased attention.[80-90] This is due to their promising, tunable properties stemming from their flexible compositions and stable structures. These normal valence compounds have structures that resemble that of either cubic or hexagonal diamond, as seen in Figure 2.1.[78,79,91] Diamond-like semiconductor compounds adhere to a series of simple guidelines, which helps to predict new compounds that will possess these structures. The first guideline is that the average number of valence electrons per ion must be 4. Next, the average valence electron concentration per anion must be 8.[78,79] Additionally, all ions are required to be in tetrahedral environments; Pauling's rule of radius ratios (1^{st} rule) has been recommended as a good predictor.[78,79,92] Lastly, the octet of each anion must be fulfilled by the cations in its immediate coordination sphere, as dictated by Pauling's electrostatic valence sum rule (2^{nd} rule).[78,79,92]

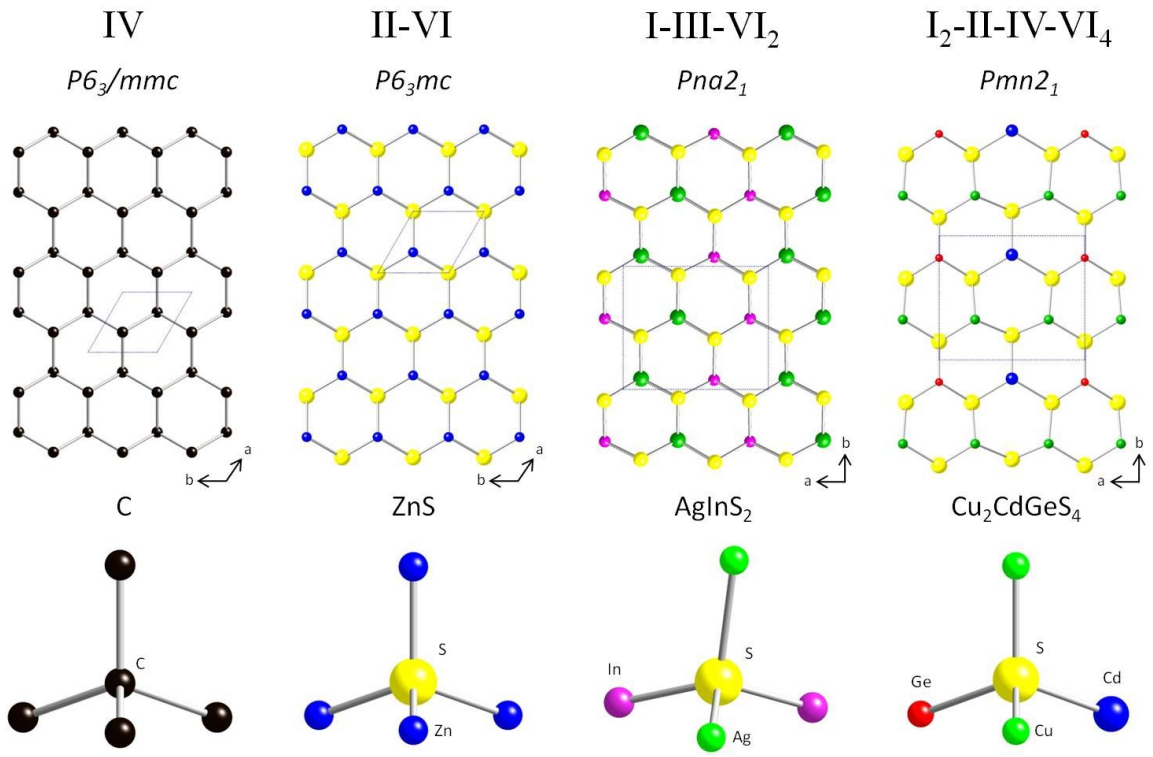

Figure 2.1 Structural progression of the common space groups of hexagonal DLSs.

Over the years a large number of binary and ternary DLSs have been synthesized and characterized owing to their relative ease of synthesis.[78,79,93,94] Although quaternary systems often present synthetic challenges, a search of recent literature shows an amplified interest in quaternary DLSs, due to their increased compositional flexibility and technologically useful properties.[83-90,94] Provided that the guidelines of DLSs are not violated, a large number of ions can be used to construct these materials, making them ideal as tunable semiconductors.[84,90,95,96] Physical properties of DLSs such as band gap,[83,84,97,98] magnetism,[95,99] second harmonic generation (SHG),[81,98,100] and electrical properties[93] can be tailored to a specific application by altering the composition of the material. This makes quaternary DLSs attractive materials in the areas of photovoltaics,[83,84,101] spintronics,[99,102] non-linear optics,[81,88] and thermoelectrics.[89,90,103]

However, the resulting physicochemical properties of these quaternary DLSs are not only a result of their composition, but also the structural arrangement of the ions. A universal understanding of how structure (i.e. cation ordering) is related to each of these properties is not yet known. This knowledge is necessary for materials scientists to predict applications for new DLSs. For this purpose, a complete understanding of each compound's structure as well as its physicochemical characteristics is required.

Earlier work on Ag_2CdGeS_4 by Parthè et al.[104] and Parasyuk et al.[105-107] focused only on the structure of this compound from laboratory X-ray powder diffraction data; no other properties were explored. Both of these prior studies concluded that this compound crystallizes in the orthorhombic, noncentrosymmetric space group $Pmn2_1$, a well known space group for DLSs, often called the wurtz-stannite structure.[78,79,108] A detailed comparison of the structure in $Pna2_1$ presented here, $Pmn2_1$ proposed previously[104,107], and the computationally predicted *Pn* space group[109] is described. Additionally this work reports diffuse reflectance UV/Vis/NIR spectroscopy, optical microscopy, scanning electron microscopy, energy dispersive spectroscopy, and inductively coupled plasma optical emission spectroscopy for Ag_2CdGeS_4.

2.2 Experimental

2.2.1 Reagents

Chemicals used in this work were utilized as obtained unless otherwise noted : (1) silver powder, ~325 mesh, 99.99%, Cerac Milwaukee, WI; (2) cadmium powder, 99.999%, Strem Newburyport, MA; (3) germanium pieces were first ground using an impact mortar and pestle until the large pieces were broken up into a coarse powder and

then ground for 5 min in a ceramic mortar and pestle before use, 99.999%, Strem Newburyport, MA; (4) sulfur powder, sublimed, 99.5%, Fisher Scientific Pittsburgh, PA.

2.2.2 Synthesis

Single crystals of Ag_2CdGeS_4 were produced by weighing 2 mmols of Ag, 1 mmol of Cd, 1 mmol of Ge, and 4.1 mmol of S in an argon-filled glove box. These reagents were combined and ground for 20 mins using an agate mortar and pestle and transferred to 9 mm o.d. fused-silica tube. The tube was then flame-sealed under a vacuum of approximately 10^{-3} mbar and placed in a programmable furnace. The sample was heated to 800°C over 12 hrs and held at that temperature for 96 hrs. After a slow cooling step of 5°C/hr (60 hrs) to 500°C, the sample was allowed to cool to ambient temperature. Next, the tube was opened and the contents were examined with a light microscope. The product was comprised of mostly orange crystals and a small amount of dark green and red crystals. X-ray powder diffraction and energy dispersive spectroscopy indicated that the orange crystals were Ag_2CdGeS_4. Using the same techniques, the red crystals were identified as Ag_8GeS_6[110] and the dark green crystals were determined to be an unidentified cadmium-germanium-sulfide phase. Both ternaries were manually separated from the orange crystals under a light microscope. Analysis of the ground, hand-selected orange crystals by synchrotron X-ray powder diffraction showed that the large majority of the sample consisted of Ag_2CdGeS_4, with only trace amounts (less than 1%) of germanium sulfide and germanium.

2.2.3 Physical Property Measurements

2.2.3.1 Optical Microscopy

Optical images were collected using a Keyence Digital Microscope System, VHX-600. Images with increased depth of field were obtained by using the Keyence Profile Measurement Unit VHX-S15 with an antivibration system. The Keyence VH-Z100R Real Zoom Lens with magnification range of x100 – x1000 was used.

2.2.3.2 Scanning Electron Microscopy and Energy Dispersive Spectroscopy

Scanning electron microscopy and energy dispersive spectroscopy (SEM/EDS) was performed on a Hitachi S-3400N scanning electron microscope equipped with a Bruker Quantax model 400 energy dispersive spectrometer using an XFlash® 5010 EDS detector with a 129 eV resolution. Samples were mounted on double-sided carbon tape affixed to an aluminum specimen holder. Images were taken at a working distance of 10 mm with an accelerating voltage ranging from 2.5 to 15 kV. EDS spectra were also collected at a working distance of 10 mm and an accelerating voltage of 15 kV for 3 min live time.

2.2.3.3 Inductive Coupled Plasma Optical Emission Spectroscopy

Quantitative analysis of Ag, Cd, Ge and S was performed by RJ Lee Group Inc. (Monroeville, PA) using inductivity coupled plasma optical emission spectrometry (ICP-OES). Samples were prepared for analysis via a microwave-assisted acid digestion. High-pressure XP1500 vessels in a MarsExpress CEM Microwave system were used. The

digested samples were analyzed in a Varian 730ES ICP-OES for Ag, Cd, Ge and S. The recovery was quantitative.

2.2.3.4 Single-Crystal X-ray Diffraction: Data Collection and Reduction

A Bruker SMART Apex 2 CCD single crystal X-ray diffractometer using graphite monochromatized molybdenum K_α radiation was used to collect data at ambient temperature. Data were collected with a tube power of 50 kV and 30 mA for 35 sec per frame. SAINT was used to integrate the data and SADABS was employed to perform the absorption correction.[111,112] XPREP was used for space group determination and to create files for SHELXTL.[113] Based on systematic absences, two space groups were initially considered, $Pna2_1$ and *Pnma*. The space group $Pna2_1$ (No. 33) was selected because all DLSs are noncentrosymmetric. The additional systematic absences, $h0l$ for $h = 2n + 1$ clearly supported $Pna2_1$ over the previously reported $Pmn2_1$.

2.2.3.5 Single-Crystal X-ray Diffraction: Solution and Refinement

The SHELXTL-PC[113] software package was used to solve and refine the crystal structure, Figure. 2.2. All atoms were located at general positions. The sites occupied by the Ag^{1+} and Cd^{2+} ions were nearly indistinguishable as these ions are isoelectronic, having nearly identical X-ray scattering factors and similar coordination geometries.

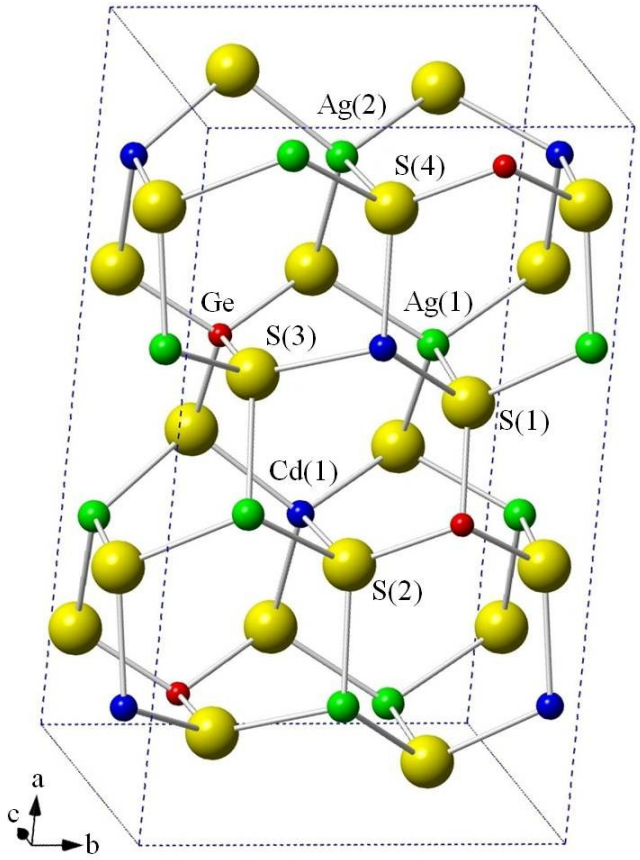

Figure 2.2 The *Pna2₁* structure of Ag_2CdGeS_4 (Model S) viewed slightly tilted from the crystallographic c-axis.

Various arrangements of Ag^{1+} and Cd^{2+} ions were refined at the three nearly identical 46 electron peaks in the electron density maps, maintaining a 2:1 ratio of ions (both disordered and ordered models were investigated). These sites will hereafter be referred to as M(1), M(2) and M(3). The best model determined from refinement of the single crystal X-ray diffraction data is denoted as model S. Crystallographic details are reported in Table 2.1. Table 2.2 lists the refined atomic coordinates and isotropic

displacement parameters for model S as well as alternative assignments of the cations that were considered.

Table 2.1 Crystallographic data and experimental details for Ag_2CdGeS_4 (Model S).

Empirical Formula	Ag_2CdGeS_4
Size	0.21 x 0.11 x 0.05 mm
Color	Orange
Habit	Rod
Formula weight	528.97 g mol^{-1}
Temperature	296(2)K
Wavelength	0.71073 Å
Space group	*Pna2₁*
Unit cell dimensions	a = 13.7415(8) Å
	b = 8.0367(5) Å
	c = 6.5907(4) Å
	α = β = γ = 90°
Volume	727.85(8) $Å^3$
Z	4
Calculated density	4.827 Mg m^{-3}
Flack parameter	0.03(1)
F(000)	952
Reflections collected/independent	9573 / 1600
Data/restraints/parameters	1600 / 1 / 75
Completeness to theta=27.07	100.0%
Goodness of Fit	1.112
Final R indices [I>2sigma(I)]	$R1$ = 0.0235, wR^2 = 0.0583
R indices (all data)	$R1$ = 0.0267, wR^2 = 0.0620
Largest peak/hole	1.43/-0.56 e$Å^{-3}$

Refinement of F^2 was made against all reflections. $R_1 = \frac{\Sigma||F_o|-|F_c||}{\Sigma|F_o|}$, $wR_2 = \sqrt{\frac{\Sigma\left[w(F_o^2-F_c^2)^2\right]}{\Sigma\left[w(F_o^2)^2\right]}}$,

$w = \frac{1}{(\sigma^2(F_o^2)+(aF_o)^2+bP)}$, $P = [2F_c^2 + Max(F_o^2, 0)]/3$

Table 2.2 M(1), M(2) and M(3) assignments for several structural models and fractional atomic coordinates and equivalent isotropic displacement parameters ($Å^2x10^3$) for Ag_2CdGeS_4, (Model S).

Site	Model S	Model S'	Model S''	SOF	Model SD*	SOF
M(1)	Ag(1)	Cd(1)	Ag(1)	1	Ag(1)	1
M(2)	Ag(2)	Ag(2)	Cd(1)	1	Ag(2)	0.83
					Cd(2)	0.17
M(3)	Cd(1)	Ag(1)	Ag(2)	1	Ag(3)	0.17
					Cd(3)	0.83

Site	x	y	z	$U_{(eq)}$**
M(1)	0.42446(4)	0.23807(5)	0.2165(1)	40(1)
M(2)	0.15876(3)	0.49941(5)	0.1976(1)	38(1)
M(3)	0.34215(2)	0.48665(4)	0.70491(8)	22(1)
Ge(1)	0.09086(3)	0.24090(5)	0.7118(1)	13(1)
S(1)	0.4403(1)	0.2426(1)	0.8286(3)	19(1)
S(2)	0.16390(9)	0.0134(1)	0.8216(3)	19(1)
S(3)	0.0931(1)	0.2432(1)	0.3753(3)	20(1)
S(4)	0.16580(8)	0.4696(1)	0.8176(3)	18(1)

* Model SD is a disordered version of Model S

** $U_{(eq)}$ is defined as 1/3 the trace of the orthogonal tensor U_{ij}.

In model S, the structure was refined with Ag on the M(1) and M(2) sites and Cd on the M(3) site with an R1(I>2σ(I)) of 0.0235. Other refinements with this model were carried out using different cation assignments adhering to an ordered structure, Table 2. In model S', Cd was refined on the M(1) site with Ag on sites M(2) and M(3). After refinement of this model, the R1(I>2σ(I)) increased to 0.0310. In model S'', Cd was refined on the M(2) site with Ag on the M(1) and M(3) sites. The R1(I>2σ(I)) of 0.0296 resulting from the refinement of this model increased in comparison to model S.

In model SD, Ag/Cd disorder was considered for the M(1), M(2), and M(3) sites. It was not possible to create a model where the M(1) site contained both Ag and Cd. Attempts to introduce disorder on the M(1) site were made during several stages of the refinement, but were always unsuccessful because the refinement became unstable. However, Ag/Cd disorder could be successfully refined on the M(2) and M(3) sites. When the amount of Ag/Cd was allowed to refine freely on these two sites, the resulting chemical formula was $Ag_{1.94}Cd_{1.06}GeS_4$. Next, a constraint was added to obtain a charge-balanced formula of Ag_2CdGeS_4 with an R1($I>2\sigma(I)$) of 0.0236. Although this model is disordered, it should be noted that the M(2) site in this model is still comprised of mostly Ag (83%), and the M(3) site mostly Cd, (83%).

An alternative structure model was obtained from the structure solution (expo2009)[114] and Rietveld refinement (GSAS/EXPGUI)[115,116] of synchrotron X-ray powder diffraction data and will be referred to as model P. This model, also in *Pna2₁*, possesses an alternate set of cation sites distributed amongst a hexagonally closest-packed network of sulfide ions, Figure. 2.3. Model P, which will be further discussed in the results and discussion section, converged with Rp = 7.46% in GSAS/EXPGUI. Refinement of model P using the single crystal X-ray diffraction data refined with R1($I>2\sigma(I)$) = 6.10%.

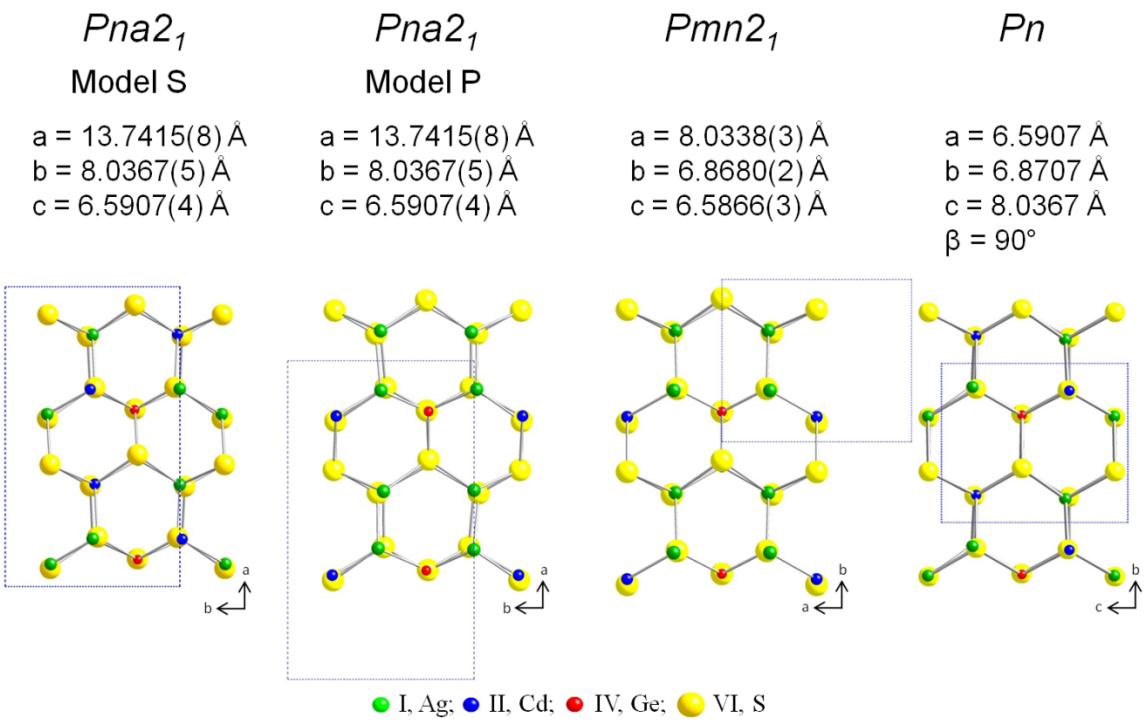

Figure 2.3 The structural comparison of Ag_2CdGeS_4 in space groups *Pna2₁*, *Pmn2₁* and *Pn*.

An additional refinement model was considered using the previously proposed *Pmn2₁* space group[104-107]. The unit cell was obtained by a cell transformation resulting in the halving of the *a*-axis as well as switching the *a* and *b* axes. The *Pmn2₁* space group did not fit the observed systematic absences, but was manually entered. The "forcing" of this space group resulted in the use of only 854 reflections out of the collected 1600. Six crystallographically unique atoms were located: 1 Ag, 1 Cd, 1 Sn and 3 S. This refinement resulted in an R1(I>2σ(I)) of 0.0254. Despite the "good" refinement, this model is not favored because it does not fit approximately half of the observed data.

After the use of chemical reasoning and the Hamilton R test,[117,118] model S was determined to be most probable structure. The ratio of wR2(S)/wR2(P) was determined to be 2.166, greater than the Hamilton confidence level for 99.5% certainty of 1.034.

This test was employed for all models considered, Table 2.3. Only the disordered model, SD, failed the Hamilton test indicating that it could not be rejected at 99.5% certainty.

Table 2.3 The results of the Hamilton R test comparing the weighted R factors determined from the refinement of several structural models using single crystal X-ray diffraction data to that of Model S.

Model	Cd	Ag	R1 (I>2σ(I))	wR2 (all data)	wR2 ratio	R'
S	M(3)	M(1), M(2)	0.0235	0.0620	N/A	N/A
S'	M(1)	M(2), M(3)	0.0280	0.1240	1.997	1.034
S"	M(2)	M(1), M(3)	0.0266	0.1256	2.023	1.034
SD	M(2),M(3)	M(1), M(2), M(3)	0.0236	0.0622	1.002	1.004
P*	N/A	N/A	0.0610	0.1343	2.166	1.034

*The cations reside in different crystallographic sites in Model P and cannot be directly compared to sites M(1), M(2) and M(3).

2.2.3.6 Laboratory X-ray Powder Diffraction

X-ray powder diffraction studies were performed on a Panalytical X'Pert Pro MPD powder X-ray diffractometer. Data were collected from 5° to 145° 2θ with a step size of 0.0083556° and scan rate of 0.010644°/sec. The incident beam optics were comprised of a 0.02 rad soller slit, a divergent slit of 1/4° and an anti-scatter slit of 1/2°; whereas, the diffracted beam optics were comprised of a 0.02 rad soller slit and an anti-scatter slit of 1/4°. The samples were prepared for analysis by fixing the material on glass slides using double-sided tape and were held still, not rotated, during the scan. The incident radiation was generated from a copper source using a voltage of 45 kV and current of 40 mA, which produced X-rays with a wavelength of 1.541871 Å. Phase identification of crystalline components was carried out using the X'Pert HighScore Plus software package[119] and the International Center for Diffracted Data (ICDD) database.

Rietveld refinements of laboratory X-ray powder diffraction data were carried out using the GSAS software package with the EXPGUI interface.[115,116] Peak profiles were fitted using a pseudo-Voigt function with asymmetric terms and low angle support.[120,121] The background was modeled using a shifted Chebyschev polynomial with 6 to 12 terms.[122] Phase parameter refinements were carried out for the unit cell, atomic coordinates, and isotropic displacement parameters of the cations. Peak shapes were expressed through the refinement of the Cagliotti Gaussian terms and a scaling factor.[123] Site occupation factors were assumed to be 1 and no other physical or chemical constraints were used in the refinement.

2.2.3.7 Synchrotron X-ray Powder Diffraction

High resolution synchrotron X-ray powder diffraction data were collected using beamline 11-BM at the Advanced Photon Source (APS), Argonne National Laboratory using an average wavelength of 0.413838 Å. Discrete detectors covering an angular range from -6 to 16º 2θ were scanned over a 34º 2θ range, with data points collected every 0.001º 2θ and a scan speed of 0.01º/s.

The 11-BM instrument uses X-ray optics with two platinum-striped mirrors and a double-crystal Si(111) monochromator, where the second crystal has an adjustable sagittal bend.[124] Ion chambers monitor incident flux. A vertical Huber 480 goniometer, equipped with a eidenhain encoder, positions an analyzer system comprised of twelve perfect Si(111) analyzers and twelve Oxford-Danfysik $LaCl_3$ scintillators, with a spacing of 2º 2θ.[125] The sample was spun during data collection. A Mitsubishi robotic arm was used to mount and dismount the sample on the diffractometer.[124] An Oxford

Cryosystems, Cryostream Plus device was used to maintain the sample temperature at 100 K.

The diffractometer was controlled via EPICS.[126] Data were collected while continually scanning the diffractometer 2θ arm. A mixture of NIST standard reference materials, Si (SRM 640c) and Al_2O_3 (SRM 676) was used to calibrate the instrument, where the Si lattice constant determines the wavelength for each detector. Corrections were applied for detector sensitivity, 2θ offset, small differences in wavelength between detectors, and the source intensity, as noted by the ion chamber before merging the data into a single set of intensities evenly spaced in 2θ.

The data were indexed with N-TREOR in expo2009[114] and the lattice parameters were refined with GSAS/EXPGUI[115,116] to a = 13.7407(1) Å, b = 8.0164(1) Å, c = 6.5927(1) Å, $\alpha = \beta = \gamma = 90°$. The structure was solved with expo2009 and Rietveld refinement was accomplished with GSAS/EXPGUI. The space group was determined as $Pna2_1$ based on systematic absences. Eight atoms were located in general positions resulting in model P. Additionally, Rietveld refinements in GSAS/EXPGUI were carried out using model S which was determined from single crystal X-ray diffraction data.

The background was fitted with a shifted Chebyschev polynomial with ten terms.[122] For both models, Ag^{1+} and Cd^{2+} ions were refined anisiotropically; but, all other atoms were refined isotropically and independently. With this high-quality data, the profiles (i.e. peak shape) are determined more by the sample than the instrument profile and therefore better described by the Lorentzian terms. The reflection profiles contained a significant amount of anisotropic strain broadening which was refined. All data were corrected for absorption with the absorption coefficient being refined to 10.29. All

structure factors were corrected for $\Delta F'$ and $i\Delta F''$ (anomalous dispersion coefficients). Models S and P were used as starting models for Rietveld analysis. Both models converged with similar statistics. For model S the least squares refinement converged with $\chi^2 = 1.423$, Rp = 7.45% (all data) and wRp = 9.65% (all data), while that of model P converged with $\chi^2 = 1.426$, Rp = 7.46% (all data) and wRp = 9.66% (all data). These two models in *Pna2₁* are virtually indistinguishable with powder diffraction data.

2.2.3.8 Diffuse Reflectance UV/Vis/NIR Spectroscopy

Diffuse reflectance UV/Vis/NIR spectra were collected using a Varian Cary 5000 spectrometer equipped with a Harrick Praying Mantis diffuse reflectance accessory. The sample was ground, placed in the sample cup and compared to a similarly prepared 100% reflectance standard, $BaSO_4$. Data were collected from 2500 to 200 nm at a scan rate of 600 nm/min. The collected percent reflectance was converted to absorbance using the Kubelka-Munk equation[127] and wavelength was converted to energy in eV.

2.2.3.9 Differential Thermal Analysis

Thermal studies were carried out on a Shimadzu DTA-50 thermal analyzer using an Al_2O_3 reference that has no thermal events over the studied range of 25°C to 1000°C. The instrument was calibrated using a three-point method utilizing the melting points of indium, zinc, and gold standards. Both the reference and the sample of comparable mass were vacuum-sealed in fused-silica ampoules and placed in the instrument. The ampoules were then heated at a rate of 10°C/min to 1000°C, held at that temperature for 1 min, and cooled at a rate of 10°C/min to 100°C. This cycle was repeated to distinguish between

reversible and irreversible events. DTA residues were further characterized using X-ray powder diffraction.

2.3 Results and Discussion

2.3.1 Synthesis Optimization

A series of samples were prepared with nominal compositions ranging from $Ag_2CdGeS_{3.9}$ to $Ag_2CdGeS_{4.5}$ and heated under various profiles in order to ascertain the ideal conditions for both crystal growth and the production of a phase-pure Ag_2CdGeS_4. The first samples that were made using 4 mmol equivalents of sulfur, were heated to 700°C over 24 hrs and held there for 72 hrs. These samples were then slow-cooled at 4°C/hr to 500°C and then cooled to room temperature over 24 hrs. In all cases, this produced mostly dark red crystals of Ag_8GeS_6 [110] and an unidentified dark green Cd-Ge-S phase with small amounts of orange Ag_2CdGeS_4 powder. Subsequent heating profiles varied holding temperature, holding time, and cooling rates. It was found that when the holding temperature was increased to 800°C, the product changes to mainly orange powder, some orange crystals and a small amount of the darker ternary phases. In the series that produced the largest quantity of Ag_2CdGeS_4 crystals, the samples were heated to 800°C over 12 hrs, held for 96 hrs, and cooled at a rate of 5°C/hr to 500°C. However, these samples did not produce X-ray quality single crystals. The experimental parameters were then expanded further by varying the amount of sulfur added in the starting materials. Each of these samples produced an orange material and some of the ternary phases. The sample that produced the highest quality Ag_2CdGeS_4 crystals was made using the starting stoichiometry of $Ag_2CdGeS_{4.1}$. In this sample crystals of both the

orange Ag_2CdGeS_4 and the darker ternary phases were large enough to be manually separated so that characterization of Ag_2CdGeS_4 could be performed. Phase identification of the orange powder by synchrotron powder X-ray diffraction showed that the large majority of the sample consisted of the Ag_2CdGeS_4 and only trace amounts (less than 1%) of germanium sulfide and germanium.

2.3.2 Morphology and Composition

Optical microscopy was used to image the orange Ag_2CdGeS_4 crystals and the differently colored crystals of the unwanted phases. The colors of these materials are prominently different; examples can be found in Figure 2.4a and 2.4b. These crystals were also imaged with SEM to more carefully study size and morphology. In addition to the noticeable difference in color, the ternary and quaternary phases also have dissimilar habits. The orange crystals are found as single flat needles or in large bundles of planks, while the darker colored crystals form as polyhedra with rounded corners, Figure 2.4c and 2.4d. Sizable crystals of the orange phase were shown to be as long as 1 mm in length while the average size was approximately 600 x 150 μm. Crystals of the darker colored ternary phases were found to have an average size of 450 x 450 μm. These sizes proved to be large enough that the samples could be physically separated under a light microscope using a needle. EDS spectra showed the presence of all four elements in the orange crystals and only three of the intended elements on clean regions of the darker material, Figure 2.4e. Since EDS is only semi-quantitative, the composition of the hand-selected orange crystals was confirmed using ICP-OES. The ICP-OES results yielded a stoichiometry of $Ag_{1.96}Cd_{1.04}Ge_{0.84}S_4$, in relatively close agreement with our predicted formula of Ag_2CdGeS_4.

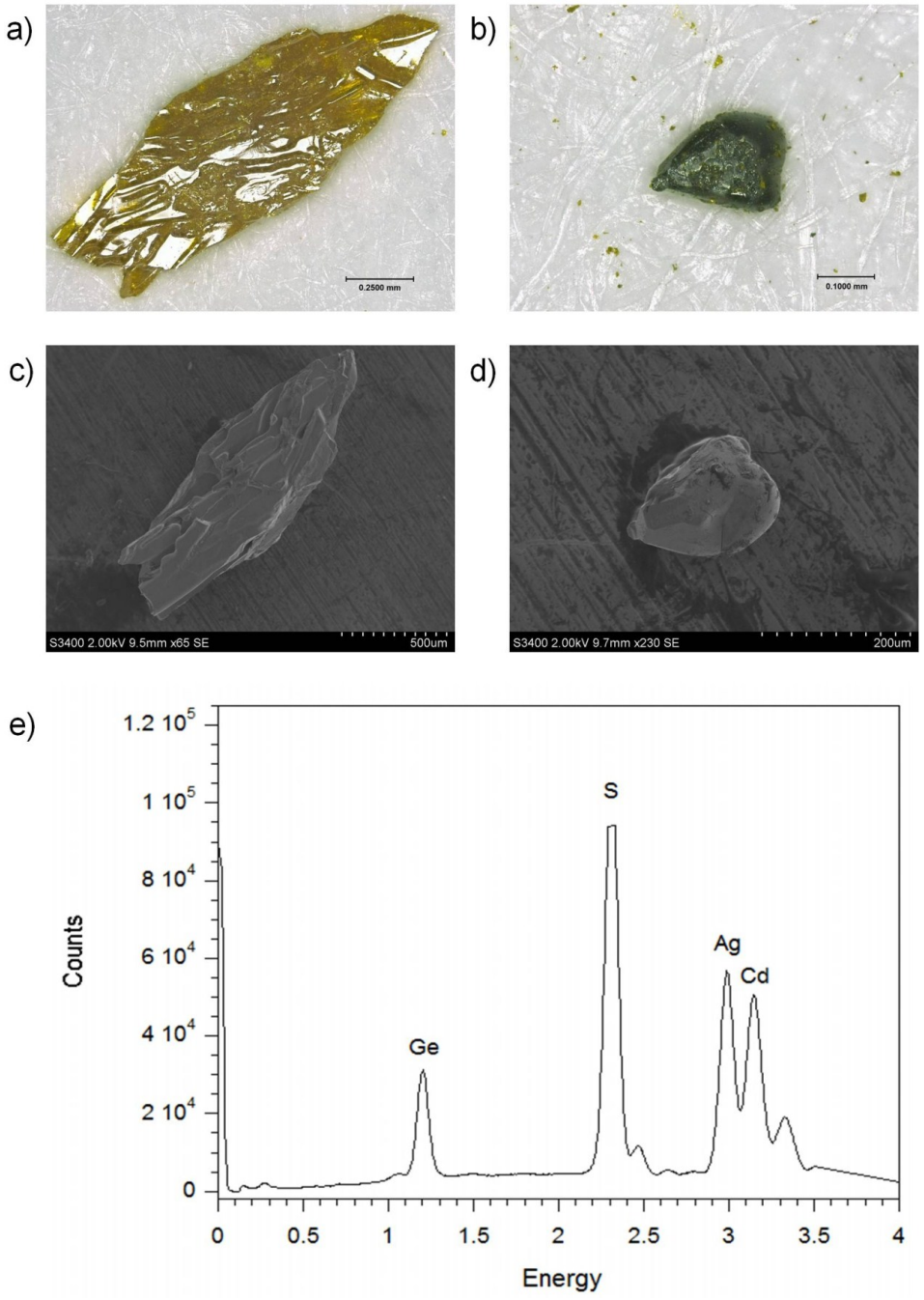

Figure 2.4 (a) Digital image of an orange Ag_2CdGeS_4 crystal, (b) Digital image of the darker Cd-Ge-S phase, (c) SEM micrograph of an orange crystal taken with a magnification of 65x, (d) SEM micrograph of a dark crystal taken with a magnification of 230x, (e) EDS spectra of the orange crystal with the major peak of each element labeled.

2.3.3 Structure

2.3.3.1 Structure Determination Challenges

The structure determination of Ag_2CdGeS_4 is difficult due to Ag^{1+} and Cd^{2+} being isoelectronic. As a result, the calculated X-ray powder diffraction patterns for the compound in the three space groups that were considered, *Pna2₁*, *Pmn2₁*[107] and *Pc*[109], are extremely similar, with additional low intensity peaks and slight intensity changes among common peaks being the only differences present in the calculated patterns. These subtle variations result from differences in the environments around the anion sites as a consequence of the different cation ordering and are manifest in the structure factors. When Ag^{1+} and Cd^{2+} are compared, their atomic X-ray scattering factors are nearly identical, having less than a 5% difference.[109,128] However, the environments surrounding each of the cations in the proposed structures in question are different, which leads to subtle differences in the X-ray structure factors, the resulting symmetry and X-ray powder diffraction patterns. These subtle differences were closely examined in an effort to determine the most likely structure.

Unfortunately, these types of indicators are extremely challenging to observe. Small diffraction peaks of ~1% or less in relative intensity are usually lost in the background of laboratory-collected powder X-ray diffraction data. Additionally, subtle differences in peak intensities can often be attributed to powder sample preparation, which can frequently result in preferred orientation. If these differences are to be used to distinguish between the different structure models, it would be with the use of high-quality powder (i.e. synchrotron) or single crystal X-ray diffraction data. This is because the difference in Ag^{1+} and Cd^{2+} atomic scattering factors for a given reflection increases

with decreasing wavelength.[128] Additionally the use of lower wavelengths gives rise to higher resolution data.

2.3.3.2 Structure Discription

As determined from single crystal X-ray diffraction data, Ag_2CdGeS_4 crystallizes in the orthorhombic noncentrosymetric space group *Pna2₁*. In this structure, all ions are tetrahedrally coordinated and reside in general positions. Due to the difficulty of discerning Ag^{1+} and Cd^{2+} using X-ray data, three ordered structure models that place Cd on the M(1) site (model S'), on the M(2) site (model S'') and on the M(3) site (model S) were considered, Table 2.2. Models S' and S'' refined with higher weighted R factors and were deemed inferior to model S by use of the Hamilton R factor significance test, Table 2.3.[117] In model S, each sulfur anion is surrounded by two silver cations, one cadmium cation, and one germanium cation in accordance to Pauling's 2nd rule of local electroneutrality.[92] Bond distances in Table 4 show an average Ag-S bond length of 2.576(2) Å for Ag(1) and 2.539(3) Å for Ag(2). These distances compare well to those found for the quaternary DLS compounds $AgCd_2GaS_4$ with an average Ag-S bond length of 2.550(2) Å[129], Ag_2HgSnS_4 with an average Ag-S bond length of 2.43(2) Å[130] and Ag_2ZnGeS_4 with an average Ag-S bond length of 2.578(5) Å.[131] The Cd-S bond has an average length of 2.526(2) Å, while the Ge-S bond lengths average 2.214(3) Å. These results are in agreement with bond lengths measured in the chemically related DLS Cu_2CdGeS_4, 2.528(6) Å and 2.28(1) Å, respectively.[132]

The structure of Ag_2CdGeS_4 can be described as a hexagonal, closest-packed array of sulfur anions with Ag^{1+}, Cd^{2+} and Ge^{4+} occupying tetrahedral holes. The model S

structure of Ag_2CdGeS_4 is isostructural to the DLS Li_2CoSiO_4.[133] The structure can be viewed as a corner-sharing, three-dimensional network of MS_4 tetrahedra. The CdS_4 tetrahedra are isolated from one another, as are the GeS_4. The $Ag(1,2)S_4$ alone form a 3-dimensional network, where each AgS_4 connects to four others by sharing corners. When viewed down the *a*-axis (Figure 4) the alternating nature of the cations can be seen. Rows along the *c*-axis of alternating $Ag(1)$-S_4 and $Ge(1)$-S_4 tetrahedra (ABAB) are separated by rows of $Ag(2)$-S_4 and $Cd(1)$-S_4 tetrahedra (CDCD). The pattern is then alternated (BABA) and (DCDC) after which it repeats.

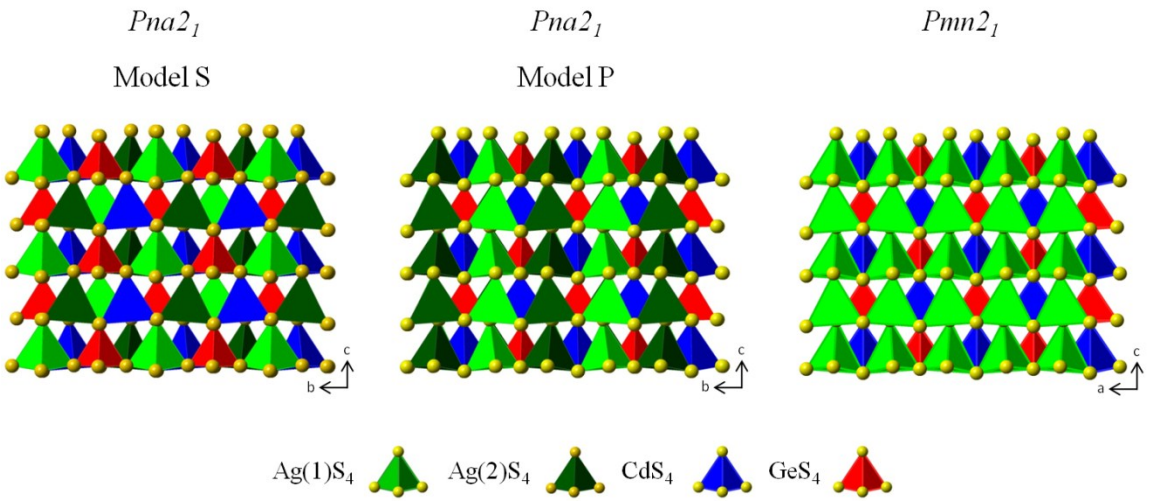

Figure 2.5 Polyhedral representation of Ag_2CdGeS_4 in *Pna2₁* (Models S and P) and *Pmn2₁* viewed down an equivalent axis.

2.3.3.3 Cation Assignments

Due to the difficulty of discerning Ag^{1+} and Cd^{2+} using X-ray data, other ordered structure models that place Cd on the M(1) site (model S') and Cd on the M(2) site (model S'') were considered. These refinements produced weighted R factors of 0.1240 and 0.1256, respectively, for all data in comparison to *w*R2 = 0.0620 for model A. In this

case, the Hamilton R factor significance test[117] was carried out to compare these ordered models, Table 2.3. The tests were performed by comparing the ratios of the weighted R factors for model S to model S' and S". In the case of model S', the ratio of weighted R factors is 1.997. This result is compared to the interpolated significance value of the Hamilton-R-factor ratio, (R'), for 75 parameters, 1525 degrees of freedom and a 0.005 level of significance, $R'_{75,1525,0.005}$=1.0338. Since the ratio of weighted R factors is greater than the significance value, model S′ can be deemed invalid in comparison to model S with 99.5% certainty. The calculation was again employed to compare model S" to model S. Here the ratio of weighted R factors was 2.023. This value was compared to the interpolated significance value for $R'_{75,1525,0.005}$. In this case the ratio of weighted R factors is still greater than the significance value, so the assignment of Cd on the M(2) site is invalid with 99.5% certainty.

The disordered model, model SD, was constructed so that both Ag and Cd were refined on the M(2) and M(3) sites. This model yielded an equivalent R factor in comparison to ordered model S. Since the number of parameters used in each refinement is not equal, the difference in the number of parameters is used to interpolate the R' value. The weighted R factor ratio of ordered to disordered models, wR2(A)/wR2(B), was preformed to prove or disprove the acceptance of model SD in spite of model S. While the weighted R factor ratio of disordered to ordered models, wR2(B)/wR2(A), was employed to determined whether or not the ordered model is significantly better than the disordered model, these ratios of 1.002 and 0.998, respectively, are less than $R'_{2,\ 1525,\ 0.005}$ = 1.003. Therefore, neither model can be rejected using this test at the 99.5% certainty.

The reason for favoring the ordered model S over the disordered model SD is due to the electrostatic valency principle, also known as Pauling's 2nd rule.[92] Here it is predicted that if an anion does not have its octet satisfied by the cations in its immediate coordination sphere there will be structural distortions to relieve the over or under-compensation of electrons.[78,92] For example, in a disordered model, like model SD, it would be possible for a sulfur anion to have three silver cations and one germanium cation around it. In this case the sum of the electrostatic bond strengths (ζ) would be 1.75 instead of the preferred 2. Therefore the M-S bonds around the sulfur anion should get shorter to satisfy the under-compensation of charge. Alternatively, it is also possible in model SD that a sulfur anion could be surrounded by one silver, two cadmium and one germanium cation. In this situation the ζ would be 2.25. Here the anion's charge would be overcompensated, resulting in a lengthening of the M-S bonds. Since the bond distances for this structure are normal it does not seem that Pauling's second rule should be violated. Furthermore, Pauling's 5th rule, the rule of parsimony, states that "the number of essentially different kinds of constituents in a crystal tends to be small."[92] Therefore, the simplest model, in this case the ordered model S, is favored because there are only 4 different types of sulfur tetrahedra that make up this model in comparison to 16 in the disordered model SD.

2.3.3.4 Comparison of *Pmn2₁*, *Pna2₁*, and *Pc* (*Pn*) Structures for Ag_2CdGeS_4

The space group *Pna2₁* has been observed for quaternary oxides, for example Li_2CoSiO_4.[133] Although relatively rare among quaternary DLSs, *Pna2₁* is a common space group for ternary DLSs, such as $AgInS_2$[134] and $LiGaS_2$.[135] However this is not the only space group proposed for Ag_2CdGeS_4, Figure 2.3.

In 1969, Parthé *et al.* reported a wurtz-stannite structure, in space group $Pmn2_1$, and lattice parameters for Ag_2CdGeS_4 from laboratory X-ray powder diffraction data.[104] Later in 2005, Parasyuk *et al.* supported the same space group with a refined structure from laboratory X-ray powder diffraction data.[107] The space group $Pmn2_1$ is a well-known space group for DLSs, such as Cu_2CdGeS_4[136] and Cu_2ZnSiS_4 [82] Additionally, a computational study in 2010 by Chen *et al.* predicted the *Pc* space group for Ag_2CdGeS_4 from Madelung energy calculations.[109] This structure has been observed for other DLSs, first reported in 1969 for Na_2ZnSiO_4[137] and more recently for the compound Li_2ZnSnS_4.[80] The prediction was made by comparing Madelung energies for possible structures abiding by the diamond-like rules and a 2 x 2 x 1 supercell of wurtzite.[109] Although $Pna2_1$ satisfies the rules of diamond-like materials, it has a larger supercell of 4 x 2 x 1 and was not considered in this study. The main difference between the structures reported in $Pna2_1$, $Pmn2_1$ and *Pc* (*Pn*) is the arrangement of the cations.

The difference in the cation arrangement of the $Pmn2_1$ and $Pna2_1$ models is best illustrated by the polyhedral view of the two structures shown in Figure 2.5. In this view both structures are oriented with the tetrahedra pointing in the same direction demonstrating the lack of an inversion center in both structures. It is also easy to notice the higher symmetry of the $Pna2_1$ structure from this view. When comparing the crystallographic sites of the $Pna2_1$ structure to those found in $Pmn2_1$, it can be seen that both structures possess one crystallographically unique Ge. Closer examination of the GeS_4 tetrahedra viewed down each corresponding axis shows that the arrangements of the isolated GeS_4 tetrahedra are identical. Further comparisons were made with the one crystallographically unique Cd in each structure. However, the positions of the Cd atoms

relative to the GeS_4 tetrahedra are different, demonstrating that the Cd sites in the two models are not equivalent, Figure 2.3.

Another model for consideration in the space group *Pna2₁*, model P, was obtained from the solution of the synchrotron powder diffraction data. In this structure, by looking down the *a*-axis, rows of alternating Cd(1)-S_4 and Ge(1)-S_4 tetrahedra (ABAB) separated by rows of Ag(1)-S_4 and Ag(2)-S_4 tetrahedra (CDCD) can be seen. The pattern is then alternated (BABA) and (DCDC) after which it repeats. While this structure has the same general pattern as model S, with the exception that the ions that make up the pattern are different, Figures 2.3 & 2.5. No compound was found in the literature possessing this structure type. The major difference between model P and model S is that in model S each crystallographically unique sulfur anion is surrounded by one of each of the crystallographically unique cations, Ag(1), Ag(2), Cd(1) and Ge(1). However, in model P, one unique sulfur anion is surrounded by Ag(1), Ag(1), Cd(1) and Ge(1), while another one is surrounded by Ag(2), Ag(2), Cd(1) and Ge(1). The other two sulfur anions are connected to one of each of the unique cations. Therefore, although both models contain a hexagonally closest packed array of sulfur anions, the pattern of the crystallographically unique sulfur anions is not the same in the two structure models. At first glance, model P looks very similar to the model in *Pmn2₁*. If only the cation sites are considered, it becomes obvious that the one crystallographically unique Ag in the *Pmn2₁* structure splits into two crystallographically unique Ag cations in model P. However, that is not the only difference. If the sulfur ions are examined more closely, it can be found that the number of crystallographically unique sulfur sites is different (3 for

Pmn2₁ and 4 for *Pna2₁*) and the sulfur anions are arranged in a different pattern in order to generate the hexagonally closest packed array.

A model of Ag_2CdGeS_4 was constructed in the *Pn* space group, an equivalent space group (different setting) to the predicted *Pc*.[109,138] Comparison of this model to the *Pna2₁* structure shows that the locations of the Cd cations in relation to the GeS_4 tetrahedra are not equivalent, which is also found in the comparison to the *Pmn2₁* model. The AgS_4 tetrahedra in the *Pn* model are aligned in diagonal columns in the *ac* plane in contrast to the herringbone configuration in the *Pna2₁* model found in the equivalent *bc* plane.

Another major difference between the models of *Pna2₁*, *Pmn2₁* and *Pn* is the larger unit cell found for the *Pna2₁* model. This may introduce the concern that the measured doubled axis from the single crystal X-ray diffraction data may be not be "real." To check this, careful analysis of the reflections from the single crystal X-ray diffraction data and their *hkl* indexes was performed. Since the *h* parameter corresponds to the doubled axis, the data were separated into odd and even *h* values. Then the measured intensity was compared to the background to determine how many reflections were greater than 4σ. If the data collected only showed measurable intensity from the even sets of *h* values, it could be evidence that the doubled axis is not real. However, this analysis showed the presence of reflections greater than 4σ for both groups, even and odd. Out of 6954 reflections with intensities greater than 4σ, 51.6% had odd *h* values.

2.3.4 X-ray Powder Diffraction

Parasyuk *et al.* determined the structure of Ag_2CdGeS_4 in *Pmn2₁* using laboratory X-ray powder diffraction data with subsequent Rietveld analysis giving an Rp of

0.0983.[107] As previously stated, the powder diffraction patterns for the compound in *Pmn2₁* and *Pna2₁* are very similar, for this reason Rietveld analysis was carried out on laboratory collected samples of Ag_2CdGeS_4 in this work, using models in both space groups. Refinement of the *Pna2₁* model S converged with an Rp value of 0.0720 and a χ^2 of 2.650. However, refinement of the same data using a model constructed with space group *Pmn2₁* did not fit the data as well and yielded an Rp of 0.1209 and a χ^2 of 6.878.

Another refinement was carried out using a *Pn* model.[109] Since Chen *et al.* did not provide lattice parameters or atomic coordinates for their model, a starting model for Rietveld analysis was constructed using the fractional atomic coordinates of the related DLS Li_2ZnSnS_4[80] and the lattice parameters obtained from the single crystal data. The starting lattice parameters were obtained by halving the 13.7415(8) Å parameter of the *Pna2₁* model and arranging the lattice parameters from smallest to largest which is the standard form for the *Pn* space group. This refinement converged with an Rp value of 0.0954 and a χ^2 of 5.620.

A comparison of the calculated powder diffraction patterns for *Pmn2₁*, *Pna2₁*, and *Pn* shows that all of the main peaks of the three patterns appear at the same or very similar positions. However, the doubling of the unit cell volume in *Pna2₁* results in an increase in the number of resolvable planes in the crystals and therefore a more complicated diffractogram. This difference as well as intensity differences between peaks calculated for the three models can account for the difference in Rietveld results. Of the small additional diffraction peaks expected for the *Pna2₁* model, the most notable and largest of these peaks is the (121) located at 26.7582° 2θ (for Cu K_α) with a predicted relative intensity of 1.1%. Other peaks that can be found in the pattern for the *Pna2₁* model, and

not those of the others, are even lower in predicted relative intensity. Unfortunately, these peaks are not observed in laboratory collected X-ray powder diffraction data.

The synchrotron X-ray powder diffraction data set clearly showed the low intensity peaks not present in the collected laboratory X-ray powder diffraction data. Additionally, the systematic absences for the *n*-glide perpendicular to the *a*-axis (0*kl* for $k+l = 2n+1$), the *a*-glide perpendicular to the *b*-axis (*h*0*l* for $h = 2n+1$) and the 2_1 screw axis along the *c*-axis (00*k* for k=2n+1) are clearly apparent in this data set. Interestingly, the structure that was initially solved from the synchrotron X-ray powder diffraction data, model P, is not the same as the preferred model as determined from single crystal X-ray diffraction, model S. When refined against the synchrotron X-ray powder diffraction data, model S and model P are indistinguishable and gave virtually identical statistics and features on the difference Fourier map. This may be indicative of both phases being present in the powder. On the other hand, when model P was refined against the single crystal X-ray data, the statistics are reasonable and the model makes chemical sense; however, the statistics for model S are clearly favored as discussed previously. The Rietveld plot of the synchrotron X-ray powder diffraction data using model S as a starting model is shown in Figure 2.6. While the proposition of yet another structural model adds additional ambiguity to the structure determination of Ag_2CdGeS_4, two things are clearly evident from this data: (1) the larger unit cell is confirmed and (2) the presence of the higher symmetry is apparent.

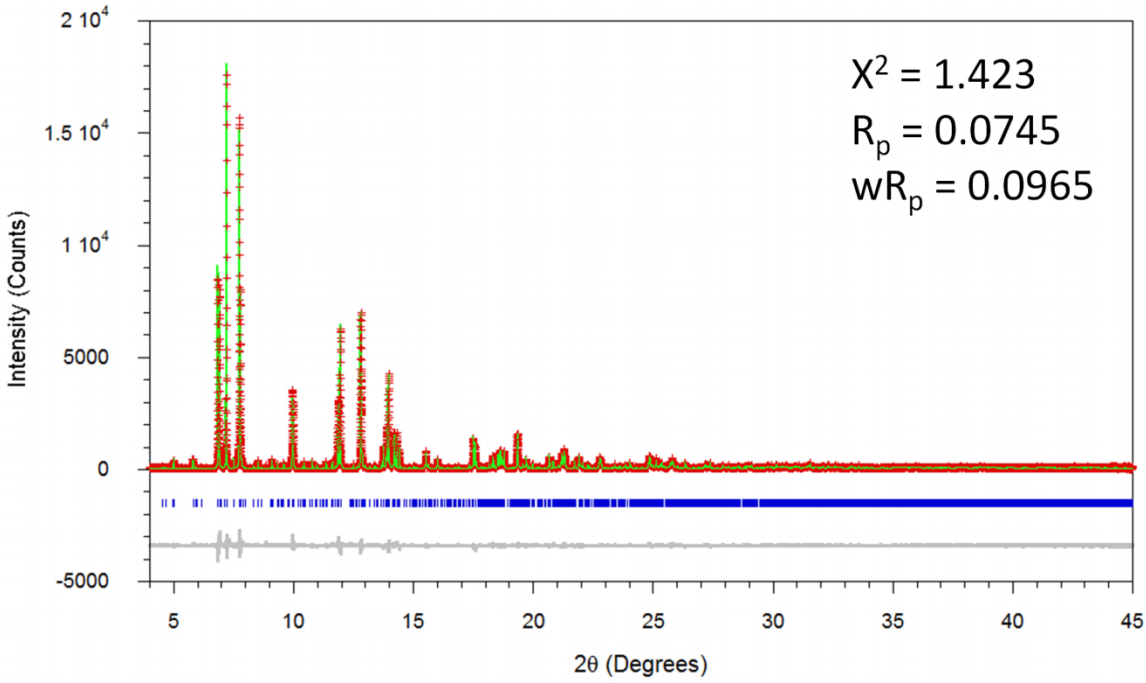

Figure 2.6 Rietveld refinement of Ag_2CdGeS_4 refined in *Pna2₁* (Model S) using synchrotron X-ray powder diffraction data. The observed data (+++) and calculated data (solid line) are overlaid at the top. While tick marks (III) indicating calculated peak locations and a difference plot (solid line) are shown below.

2.3.5 Differential Thermal Analysis

DTA of a ground sample of Ag_2CdGeS_4, Figure 2.7, shows a broad endothermic event that is believed to be the result of a polymorph with a similar melting point. Upon cooling, recrystallization of the phases is clearly evident. In the second cycle of the DTA, the melting points are more clearly defined. However, X-ray powder diffraction of the DTA residue, Figure 2.7, shows that the same diffraction pattern for the Ag_2CdGeS_4 sample is obtained after the experiment, supporting the hypothesis that the observed impurity phase is a polymorph of Ag_2CdGeS_4. This is very interesting because this opens the possibility that Ag_2CdGeS_4 might exist in another structure. In both the publications by Parthé *et al.*[104] and Parasyuk *et al.*[107] the authors were not specific about the synthetic

conditions used to prepare Ag_2CdGeS_4, so it is not possible to directly compare our synthetic procedures. In this study a second phase of Ag_2CdGeS_4 was never observed. Reactions carried out at higher temperatures always produced additional quantities of the unwanted Ag_8GeS_6 phase. Reactions quenched from high temperature yielded almost no Ag_2CdGeS_4, but rather a mixture of Ag_8GeS_6, Ag_2S, GeS_2, Ag_5Cd_8 and a few unidentified diffraction peaks. Interestingly, high-temperature polymorphs are usually of higher symmetry than lower temperature phases. In this work crystals have been isolated with the highest symmetry structure that has been reported for Ag_2CdGeS_4.

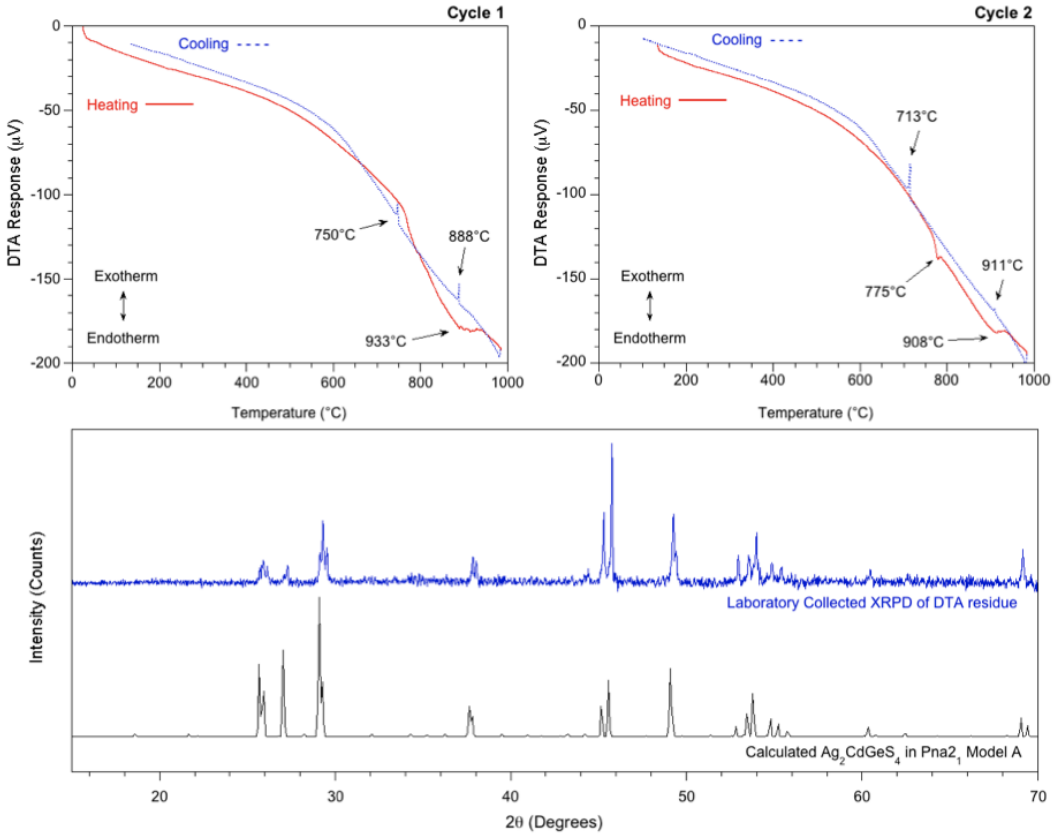

Figure 2.7 Differential thermal analysis of Ag_2CdGeS_4 with heating cycles displayed with a solid line and cooling cycles with a dashed line (top). The observed X-ray powder diffraction pattern of the residue is compared to the calculated pattern for Ag_2CdGeS_4 in *Pna2₁* (Model S) (bottom).

2.3.6 Optical Diffuse Reflectance Spectroscopy

Optical diffuse reflectance UV/Vis/NIR spectroscopy was performed for Ag_2CdGeS_4 in order to estimate the band gap. The resulting spectrum shows an estimated band gap of 2.32 eV, in agreement with the orange color observed for these crystals, Figure 2.8. The presence of only one clean absorption edge supports the X-ray powder diffraction analysis indicating that the sample is visually, nearly phase pure.

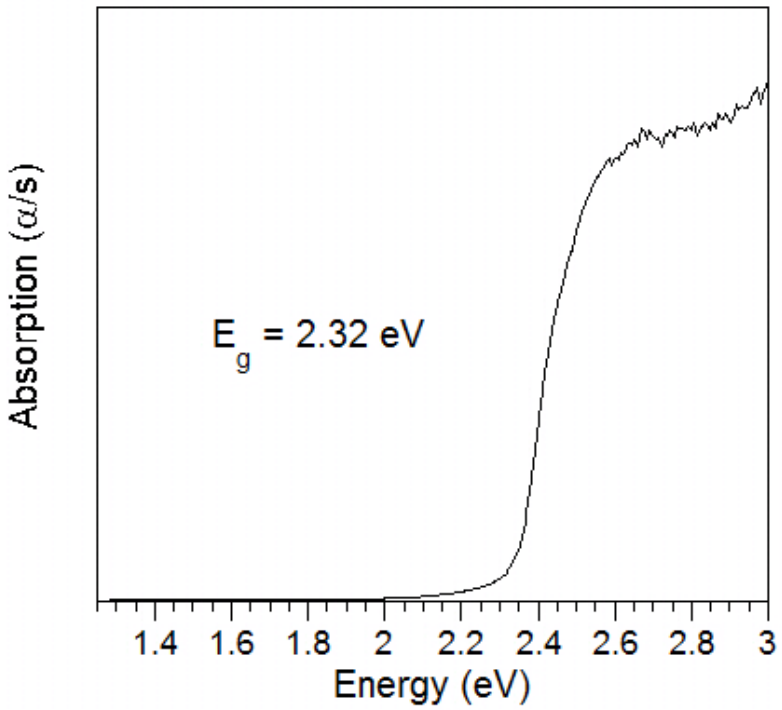

Figure 2.8 Optical diffuse reflectance UV/Vis/NIR spectrum converted to absorption for Ag_2CdGeS_4.

2.4 Conclusion

Single crystals of the diamond-like compound Ag_2CdGeS_4 have been prepared and the structure solved and refined in the space group *Pna2₁*, although two other space groups have been previously proposed for this material. The structure determination of Ag_2CdGeS_4 was challenging due to Ag^{1+} and Cd^{2+} being isoelectronic; however careful analysis of high-quality single crystal and high-resolution synchrotron X-ray powder diffraction data provided significant clues leading to the elucidation of the most probable structure. Model S is clearly favored by the single crystal X-ray diffraction data; however model P makes chemical sense and cannot be distinguished by X-ray powder diffraction data. In fact the structure solution from synchrotron X-ray powder diffraction is a valid structure and would have been acceptable if a single crystal model hadn't been determined. Additionally, the possible presence of multiple polymorphs is suggested by thermal analysis. A partially disordered model was discarded due to the violation of Pauling's second and fifth rules, and the observation of normal bonding distances in this material. While this compound could be a candidate for neutron diffraction studies, the synthesis is challenging, neither a single crystal of appropriate dimensions or a large enough quantity of powder has been successfully prepared, and cadmium is not a neutron-friendly element due to neutron absorption. Future studies will be aimed at preparing the material in pure form, so that it may be further studied (e.g. anomalous dispersion) without the pain-staking, added step of hand-picking the crystals.

2.5 References

Reprinted from the Journal of Solid State Chemistry, 187, Carl D. Brunetta, William C. Minsterman III, Charles H. Lake, and Jennifer A. Aitken, *Cation ordering and physicochemical characterization of the quaternary diamond-like semiconductor* Ag_2CdGeS_4, 177-185, Copyright 2012, with permission from Elsevier.

78 E. Parthé, E. *Crystal Chemistry of Tetrahedral Structures*; Gordon and Breach Science Publishers: New York, NY, **1964**.

79 Goryunova, N.A. *The Chemistry of Diamond-Like Semiconductors*; Anderson, J.C. Ed.; The MIT Press: Cambridge, U.K. **1965**.

80 Lekse, J. W.; Leverett, B. M.; Lake, C. H.; Aitken, J. A. "Synthesis, physicochemical characterization and crystallographic twinning of Li_2ZnSnS_4" *J. Solid State Chem.* **2008**, *181(12),* 3217-3222.

81 Levcenco, S.; Dumcenco, D.; Huang, Y. S.; Arushanov, E.; Tezlevan, V. "Polarization-dependent electrolyte electroreflectance study of Cu_2ZnSiS_4 and $Cu_2ZnSiSe_4$ single crystals" *J. Alloys Compd.* **2011**, *509(25)*, 7105-7108.

82 Rosmus, K. A.; Aitken, J. A. "Cu_2ZnSiS_4" *Acta Cryst.* **2011**, *E67(4)*, i28.

83 Guo, Q.; Ford, G. M.; Yang, W. C.; Walker, B. C.; Stach, E. A.; Hillhouse, H. W.; Agrawal, R. "Fabrication of 7.2% efficient CZTSSe solar cells using CZTS nanocrystals" *J. Am. Chem. Soc.* **2010**, *132(49)*, 17384-17386.

84 Ford, G. M.; Guo, Q.; Agrawal, R.; Hillhouse, H. W.; Hugh, W. "Earth abundant element $Cu_2Zn(Sn_{1-x}Ge_x)S_4$ nanocrystals for tunable band gap solar cells: 6.8% efficient device fabrication" *Chem. Mater.* **2011**, *23(10)*, 2626-2629.

85 Nakamura, S.; Maeda, T.; Wada, T. "Phase stability and electronic structure of in-free photovoltaic materials $Cu_2IISnSe_4$ (II: Zn, Cd, Hg)" *Jpn. J. Appl. Phys.* **2011**, *50(5)*, 05FF01.

86 Rincón, C.; Quintero, M.; Moreno, E.; Power, C.; Quintero, E.; Henao, J. A.; Macías, M. A.; Delgado, G. E.; Tovar, R.; Morocoima, M. "X-ray diffraction, Raman spectrum and magnetic susceptibility of the magnetic semiconductor Cu_2FeSnS_4" *Solid State Comm.* **2011**, *151(13)*, 947-951.

87 Lekse, J. W.; Moreau, M. A.; McNerny, K. L.; Yeon, J.; Halasyamani, P. S.; Aitken, J. A. "Second-harmonic generation and crystal structure of the diamond-like semiconductors Li_2CdGeS_4 and Li_2CdSnS_4" *Inorg. Chem.* **2009**, *48(16)*, 7516-7518.

88 Li, Y.; Fan, W.; Sun, H.; Cheng, X.; Li, P.; Zhao X. "Electronic, optical and lattice dynamic properties of the novel diamond-like semiconductors Li_2CdGeS_4 and Li_2CdSnS_4" *J. Phys. Condens, Matter* **2011**, *23(22)*, 225401.

89 Liu, M. L.; Chen, I. W.; Huang, F. Q.; Chen, L. D. "Improved thermoelectric properties of Cu-doped quaternary chalcogenides of $Cu_2CdSnSe_4$" *Adv. Mater.* **2009**, *21(37)*, 3808-3812.

90 Shi, X. Y.; Huang, F. Q.; Liu, M. L.; Chen, L. D. "Thermoelectric properties of tetrahedrally bonded wide-gap stannite compounds $Cu_2ZnSn_{1-x}In_xSe_4$" *Appl. Phys. Lett.* **2009**, *94(12)*, 122103.

91 Bundy, F. P.; Kasper, J. S. "Hexagonal diamond – a new form of carbon" *J. Chem. Phys.* **1967**, *46(9)*, 3437-3446.

92 Pauling, L. "The principles determining the structure of complex ionic crystals" *J. Am. Chem. Soc.* **1929**, *51*, 1010-1026.

93 Shay, J. L.; Wernick, J. H. *Ternary Chalcopyrite Semiconductors: Growth, Electronic Properties, and Applications*, Pergamon Press, Elmsford, NY, **1975**.

94 Parthé, E. *Intermetallic Compounds: Vol 1, Principles.*, John Wiley and Sons, New York, NY, **1994**.

95 McCabe, G. H.; Fries, T.; Liu, M. T.; Shapira, Y.; Ram-Mohan, L. R.; Kershaw, R.; Wold, A.; Fau, C.; Averous, M.; McNiff, E. J. "Bound magnetic polarons in p-type $Cu_2Mn_{0.9}Zn_{0.1}SnS_4$" *Phys. Rev. B.* **1997**, *56(11)*, 6673-6680.

96 Honig, H.; Shen, H.; Yao, G.; Doverspike, K.; Kershaw, R.; Dwight, K.; Wold, A. "Preparation and characterization of copper zinc manganese germanium sulfide ($Cu_2Zn_{1-x}Mn_xGeS_4$)" *Mater. Res. Bull.* **1998**, *23(3)*, 307-312.

97 Ellis, A. B.; Geselbracht, M. J.; Johnson, B. L.; Lisensky, G. C.; Robinson, W. R. *Teaching General Chemistry: A Materials Science Companion*, American Chemical Society, Washington, DC, **1993**.

98 Catella, G. C.; Burlage, D. "Crystal growth and optical properties of $AgGaS_2$ and $AgGaSe_2$" *MRS Bull.* **1998**, *23(7)*, 28-36.

99 Pearton, S. J.; Abernathy, C. R.; Norton, D. P.; Hebard, A. F.; Park, Y. D.; Boatner, L. A.; Budai, J. D. "Advances in wide bandgap materials for semiconductor spintronics" *Mater. Sci Eng. R.* **2003**, *40(4)*, 137-168.

100 Ohmer, M. C.; Pandey, R. "Emergence of chalcopyrites as nonlinear optical materials" *MRS Bull.* **1998**, *23(7)*, 16-20.

101 Goetzberger, A.; Hebling, C.; Schock, H. W. "Photovoltaic materials, history, status and outlook" *Mater. Sci. Eng. R.* **2003**, *40(1)*, 1-46.

102 Chambers, S. A.; Yoo, Y. K. "New materials for spintronics" *MRS Bull.* **2003**, *28(10)*, 706-710.

103 Sevik, C.; Ćağin, T. "Ab initio study of thermoelectric transport properties of pure and doped quaternary compounds" *Phys. Rev. B* **2010**, *82(4)*, 045202.

104 Parthé, E.; Yvon, K.; Dietech, R. H. "Crystal structure of Cu_2CdGeS_4 and other quaternary normal tetrahedral structure compounds" *Acta Crystallogr., Sect. B* **1969**, *25(6)*, 1164-1174.

105 Parasyuk, O. V.; Piskach, L. V. "The Ag_2SnS_3-CdS system" *Polish J. Chem.* **1998**, *72(5)*, 966-968.

106 Parasyuk, O. V.; Olekseyuk, I. D.; Piskach, L. V.; Volkov, S. V.; Pekhnyo, V. I. "Phase relations in the Ag_2S-CdS-SnS_2 system and the crystal structure of the compounds" *J. Alloys Compd.* **2005**, *399*, 173-177.

107 Parasyuk, O. V.; Piskach, L. V.; Olekseyuk, I. D.; Pekhnyo, V. I. "The quasi-ternary system Ag_2S-CdS-GeS_2 and the crystal structure of Ag_2CdGeS_4" *J. Alloys Compd.* **2005**, *397*, 95-98.

108 Schäfer, W.; Nitsche, R. "Tetrahedral quaternary chalcogenides of the type Cu_2-II-IV-$S_4(Se_4)$" *Mater. Res. Bull.* **1974**, *9(5)*, 645-654.

109 Chen, S.; Walsh, A.; Luo, Y.; Yang, J. H.; Gong, X. G.; Wei, S. H. "Wurtzite-derived polytypes of kesterite and stannite quaternary chalcogenide semiconductors" *Phys. Rev. B* **2010**, *82(19)*, 195203.

110 Eulenberger, G. "The crystal structure of the low temperature form of synthetic argyrodite Ag_8GeS_6" *Monatsh. Chem.* **1977**, *108(4)*, 901-913.

111 Bruker **1998**. *SMART and SAINT*, Bruker AXS Inc., Madison, Wisconsin, USA.

112 Sheldrick, G. M. **2002**. *SADABS*. University of Göttingen, Germany.

113 Bruker **2007**. *SHELXTL-PC, release 6.14*, Bruker AXS Inc., Madison, Wisconsin, USA.

114 Altomare, A.; Camalli, M.; Cuocci, C.; Giacovazzo, C.; Moliterni, A.; Rizzi, R. "EXPO2009: structure solution by powder data in direct and reciprocal space" *J. Appl. Cryst.* **2009**, *42(6)*, 1197-1202.

115 Larson, A. C.; Von Dreele, R. B. *General Structure Analysis System* Los Alamos National Laboratory Report LAUR 86-748, **2004**.

116 Toby, B. H. "EXPGUI, a graphical user interface for GSAS" *J. Appl. Crystallogr.* **2001**, *34(2)*, 210-213.

117 Hamilton, W. C. "Significance tests on the crystallographic R factor" *Acta Cryst.* **1965**, *18(3)*, 502-510.

118 Ladd, M. F. C.; Palmer, R. A. *Structure Determination by X-ray Crystallography*, 3rd ed., Plenum Press, New York, NY, **1994**.

119 X'Pert Highscore Plus, PANalytical B.V., Almelo, the Netherlands.

120 Finger, L. W.; Cox, D. E.; Jephcoat, A. P. "A correction for powder diffraction peak asymmetry due to axial divergence" *J. Appl. Cryst.* **1994**, *27(6)*, 892-900.

121 Van Laar, B.; Yelon, W. B. "The peak in neutron powder diffraction" *J. Appl. Cryst.* **1984**, *17(2)*, 47-54.

122 Abramowitz, M.; Stegun, I.A. eds. *Handbook of Mathematical Functions*, Dover Publications, Dover, NY, **1965**, Ch 22.

123 Caglioti, G.; Paoletti, A.; Ricci, F. P. "Choice of collimators for a crystal spectrometer for neutron diffraction" *Nucl. Instrum. Methods* **1958**, *3*, 223.

124 Wang, J.; Toby, B. H.; Lee, P. L.; Ribaud, L.; Antao, S.; Kurtz, C.; Ramanathan, M.; Von Dreele, R. B.; Beno, M. A. "A dedicated powder diffraction beam-line at the Advanced Photon Source: commissioning and early operational results" *Rev. Sci. Instrum.* **2008**, *79(8)*, 085105.

125 Lee, P. L.; Shu, D.; Ramanathan, M.; Preissner, C.; Wang, J.; Beno, M. A.; Von Dreele, R. B.; Ribaud, L.; Kurtz, C.; Antao, S. M.; Jiao, X.; Toby, B. H. "A twelve-analyzer detector system for high-resolution power diffraction" *J. Synchrotron Radiat.* **2008**, *15*, 427-432.

126 Dalesio, L. R.; Hill, J. O.; Kraimer, M.; Lewis, S.; Murray, D.; Hunt, S.; Watson, W.; Clausen, M.; Dalesio, J. "The experimental physics and industrial control system architecture: past, present, and future" *Nucl. Instrum. Methods Phys. Res., Sect. A.* **1994**, *352*, 197-184.

127 Kubelka, P.; Munk, F. "An article on optics of paint layers" *Zeit. Für Tekn. Physik* **1931**, *12*, 593-601.

128 Wilson, A. J. C.; Prince, E. (Eds.), *International Tables of Crystallography: Volume C Mathematical, Physical, and Chemical Tables*, second ed., Kluwer Academic Publishers, Boston, MA, **1999**.

129 Pervukhina, N. V.; Atuchin, V. V.; Parasyuk, O. V. "Redetermination of the quaternary phase silver dicadmium gallium tetrasulfide, $AgCd_2GaS_4$" *Acta Cryst.* **2005**, *E61(5)*, i91-i93.

130 Parasyuk, O. V.; Chykhrij, S. I.; Bozhko, V. V.; Piskach, L. V.; Bogdanyuk, M. S.; Olekseyuk, I. D.; Bulatetska, L. V.; Pekhnyo, V. I. "Phase diagram of the Ag_2S-HgS-SnS_2 system and single crystal preparation, crystal structure and properties of Ag_2HgSnS_4" *J. Alloys Compd.* **2005**, *399*, 32-37.

131 Parasyuk, O. V.; Fedorchuk, A. O.; Kogut, Yu. M.; Piskach, L. V.; Olekseyuk, I. D. "The Ag_2S-ZnS-GeS_2 system: phase diagram, glass-formation region and crystal structure of Ag_2ZnGeS_4" *J. Alloys Compd.* **2010**, *500*, 26-29.

132 Parasyuk, O. V.; Romanyuk, Y. E.; Olekseyuk, I. D. "Single-crystal growth of Cu_2CdGeS_4" *J. Cryst. Growth* **2005**, *275*, 159-162.

133 Yamaguchi, H.; Akatsuka, K.; Setoguchi, M.; Takaki, Y. "Structure of cobalt dilithium silicate βII-Li_2CoSiO_4" *Acta Cryst. B.* **1979**, *35(11)*, 2680-2682.

134 Delgado, G.; Mora, A. J.; Pineda, C.; Tinoco, T. "Simultaneous Rietveld refinement of three phases in the Ag-In-S semiconducting system from X-ray powder diffraction" *Mater. Res. Bull.* **2001**, *36*, 2507-2517.

135 Leal-Gonzalez, J.; Melibary, S. S.; Smith, A. J. "Structure of lithium gallium sulfide $LiGaS_2$" *Acta Cryst.* **1990**, *46(11)*, 2017-2019.

136 Davidyuk, G. E.; Parasyuk, O. V.; Semenyuk, S. A.; Romanyuk, Y. E. "Electrical and optical properties of Cu_2CdGeS_4 single crystals" *Inorg. Mater.* **2003**, *39(9)*, 919-923.

137 Joubert-Bettan, C. A.; Lachenal, R.; Bertaut, E. F.; Parthé, E. "Crystal structures of Na_2ZnSiO_4, Na_2ZnGeO_4, and Na_2MgGeO_4" *J. Solid State Chem.* **1969**, *1(1)*, 1-5.

138 Hahn, T. (Ed.), *International Tables for Crystallography: Volume A Space-group symmetry*, fifth ed., Kluwer Academic Publishers, Boston, MA, **2002**.

3 The Crystal and Electronic Band Structure of the Diamond-Like Semiconductor Ag_2ZnSiS_4

3.1 Introduction

Over the past few years, multi-cation diamond-like semiconductors (DLSs) have received increased attention for their promising physical properties. A work by Shi *et. al.* showed that $Cu_2Sn_{1-x}In_xSe_3$ possess an impressive thermoelectric figure of merit, ZT, of 1.14 at 850 K indicating its potential use in thermo-electric applications.[139] Newer work on compound $Cu_2ZnSnSe_4$ (CZTSe) has shown that the substitution of In in place of Sn increases ZT from 0.28 in the native compound to 0.95 in the 10% In substituted phase.[140] Other work by Steinhagen *et. al.* has demonstrated that Cu_2ZnSnS_4 (CZTS) can be synthesized as nanocrystals in the kesterite structure which can be used as a cheaper route for the production of photovoltaic devices.[141] Furthermore in 2009, Lekse *et. al.* reported that Li_2CdSnS_4 exhibits a second harmonic generation (SHG) response 100x that of α-quartz and is phase matchable.[142] They suggest that quaternary DLS with larger band gaps should possess increased laser damage thresholds as compared to the commercially available ternary DLSs that are currently used in nonlinear optical applications.[143,144] While these recent studies focus on the technologically useful properties of multi-cation DLSs, one of the key elements in understanding these materials as a class is the correlation between these desirable attributes and structure, both the crystal and electronic structures.

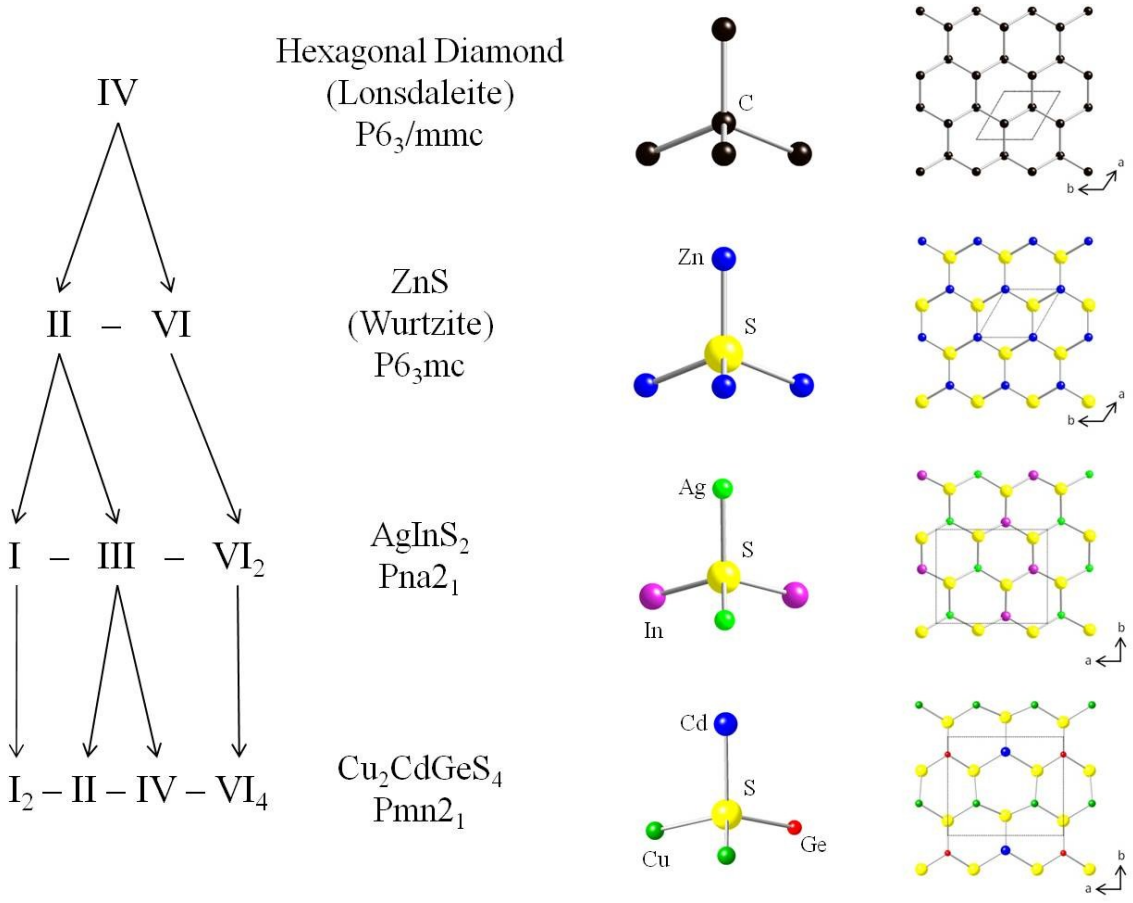

Figure 3.1 Structural progression of the hexagonal family of DLSs, showing the most common space groups at each level.

The above compounds are all diamond-like, i.e. they have a structure that resembles either cubic or hexagonal diamond[145,146], Figure 3.1. These materials follow a set of guidelines which include; i) each atom must have an average valence electron concentration of 4, ii) the average concentration of valence electrons for each anion must be 8,[145,146] iii) each atom must have a tetrahedral coordination, and iv) the octet of each anion must be satisfied by its nearest neighbors.[145,146,147] These conditions can be used not only to classify known compounds, but also to predict new compounds. Furthermore, combining these rules with an understanding of how the structure of these materials

relates to the physical properties could prove useful in predicting properties of yet to be discovered materials.

This work presents the crystal structure, electronic band structure, and density of states (DOS) of the DLS Ag_2ZnSiS_4 as well as the experimentally determined band gap. Ag_2ZnSiS_4 is a quaternary DLS of the formula I_2-II-IV-VI_4, which can be derived from that of the I-III-VI_2 family, with $AgGaS_2$ being its closest ternary relative. The structure of Ag_2ZnSiS_4 can be obtained from $AgGaS_2$ by replacing every two Ga atoms in a doubled structure of $AgGaS_2$ with one Zn and one Si in an ordered fashion (see Figure 3.1).Therefore the band structure and DOS are compared with that of $AgGaS_2$ computed using the same method.[148]

3.2 Experimental

3.2.1 Reagents

Chemicals used in this work were utilized as obtained unless otherwise noted : (1) silver powder, ~325 mesh, 99.99%, Cerac Milwaukee, WI; (2) zinc powder, 99.999%, Strem Newburyport, MA; (3) silicon powder, 99.999%, Strem Newburyport, MA; (4) sulfur powder, sublimed, 99.5%, Fisher Scientific Pittsburgh, PA.

3.2.2 Synthesis

Single crystals of Ag_2ZnSiS_4 were produced by weighing 4 mmol of Ag, 2 mmol of Zn, 2 mmol of Si, and 8 mmol of S in an argon-filled glove box. These reagents were combined using an agate mortar and pestle until the sample appeared homogeneous (~ 20 min). The sample was then transferred to a graphite crucible, which was then placed

within a 12 mm O.D. fused-silica tube. The tube was then flame-sealed under a vacuum of approximately 10^{-3} mbar and placed in a programmable muffle furnace. The sample was heated to 800°C over 12 hrs and held at that temperature for 96 hrs, after which the sample was slow-cooled to 500°C at 5°C/hr (60 hrs) and then allowed to cool radiatively to ambient temperature.

The product was a gray colored ingot with colorless needle-like crystals slightly tinted green protruding from the surface. Energy dispersive spectroscopy (EDS) detected the presence of all four elements in the translucent green crystals.

3.2.3 Physical Property Measurements

3.2.3.1 Scanning Electron Microscopy and Energy Dispersive Spectroscopy

Scanning electron microscopy and energy dispersive spectroscopy (SEM/EDS) was performed on a Hitachi S-3400N scanning electron microscope equipped with a Bruker Quantax model 400 energy dispersive spectrometer using an XFlash® 5010 EDS detector with a 129 eV resolution. Samples were mounted on double-sided carbon tape affixed to an aluminum specimen holder. Images were taken at a working distance of 10 mm with an accelerating voltage of 15 kV. EDS spectra were also collected under these same conditions for 2 minutes live time.

3.2.3.2 Single-Crystal X-ray Diffraction: Data Collection and Reduction

A Bruker SMART Apex 2 CCD single crystal X-ray diffractometer employing graphite monochromatized molybdenum K_α radiation with a wavelength of 0.7107 Å and operating with a tube power of 50 kV and 30 mA was used to collect the data for 40 s/frame at ambient temperature. A total of 4283 measured reflections were collected with 1456 of them unique. The program SAINT[149] was used to integrate the data and SADABS[150] was employed to perform the absorption correction. XPREP was used for space group determination and to create files for SHELXTL.[151] Based on systematic absences, two space groups were initially considered, *Pn* and *P2/n*. The space group *Pn* (No. 7) was selected because all DLSs are noncentrosymmetric due to all of the tetrahedra pointing in the same direction along a crystallographic axis.

3.2.3.3 Single-Crystal X-ray Diffraction: Solution and Refinement

Using the SHELXTL-PC[151] software package, the structure was solved and refined in the noncentrosymmetric space group *Pn*, Figure 3.2. Eight atoms were located on general positions; 2 Ag site, 1 Zn site, 1 Si site and 4 S sites. The structure was refined with an R1(all data) of 0.0210. Other crystallographic and experimental details are reported in Table 3.1. Fractional atomic coordinates and equivalent isotropic displacement parameters are given in Table 3.2 while refined bond distances and angles are shown in Table 3.3. The program CrystalMaker®[152] was used to generate the crystal structure figures.

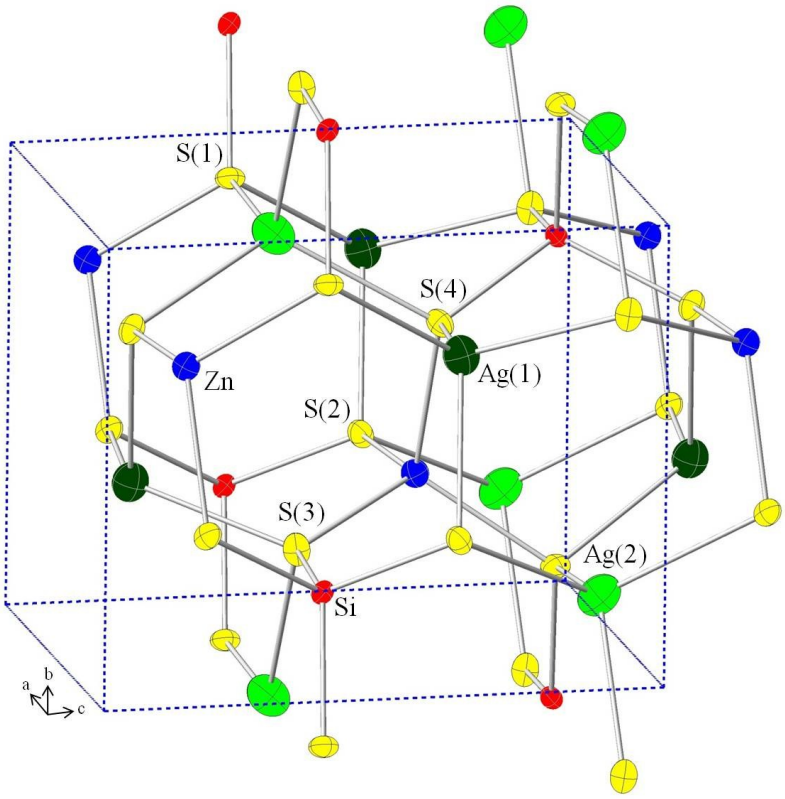

Figure 3.2 Unit cell of Ag_2ZnSiS_4 using thermal ellipsoids with 50% probability.

Table 3.1 Crystallographic data and experimental details for Ag_2ZnSiS_4

Empirical Formula	Ag_2ZnSiS_4
Size	0.025 x 0.032 x 0.237 mm
Color	Green
Habit	Needle
Formula weight	437.44 g mol^{-1}
Temperature	296(2)K
Wavelength	0.71073 Å
Space group	*Pn*
Unit cell dimensions	a = 6.4052(1) Å
	b = 6.5484(1) Å
	c = 7.9340(1) Å
	α = γ = 90°
	β = 90.455(1)°
Volume	332.772(8) $Å^3$
Z	2
Calculated density	4.366 Mg m^{-3}
Flack parameter	0.04(1)
F(000)	404
Reflections collected/unique	4283 / 1456
Data/restraints/parameters	1456 / 2 / 75
Completeness to theta=27.11	100.0%
Goodness of Fit	1.272
Final R indices [I>2sigma(I)]	$R1$ = 0.0197, w$R2$ = 0.0402
R indices (all data)	$R1$ = 0.0210, w$R2$ = 0.0411

Refinement of F^2 was made against all reflections. $R_1 = \frac{\Sigma||F_o|-|F_c||}{\Sigma|F_o|}$, $wR_2 = \sqrt{\frac{\Sigma\left[w\left(F_o^2-F_c^2\right)^2\right]}{\Sigma\left[w\left(F_o^2\right)^2\right]}}$,

$w = \frac{1}{(\sigma^2(F_o^2)+(aF_o)^2+bP)}$, $P = [2F_c^2 + Max(F_o^2, 0)]/3$

Table 3.2 Fractional atomic coordinates and equivalent isotropic displacement parameters, Uiso ($Å^2x10^3$) for Ag_2ZnSiS_4.

Site	x	y	z	$U_{(eq)}$*
Ag(1)	0.23428 (4)	0.31806 (5)	0.32726 (3)	29 (1)
Ag(2)	0.71991 (6)	0.15354 (4)	0.57873 (5)	33 (1)
Si(1)	0.7199 (3)	0.1844 (1)	0.0732 (2)	11 (1)
Zn(1)	0.22232 (7)	0.31373 (7)	0.82066 (5)	16 (1)
S(1)	0.1161 (1)	0.1248 (1)	0.5868 (1)	14 (1)
S(2)	0.5879 (1)	0.3163 (1)	0.8534 (1)	15 (1)
S(3)	0.0504 (1)	0.2008 (1)	0.0614 (1)	16 (1)
S(4)	0.6239 (1)	0.3398 (1)	0.2966 (1)	14 (1)

* $U_{(eq)}$ is defined as 1/3 the trace of the orthogonal tensor U_{ij}.

Table 3.3 Selected bond distances (Å) and angles (°) for Ag_2ZnSiS_4.

Bond	Distance (Å)	Bond	Angle (°)
Ag(1) - S(1)	2.537(1)	S(1) - Ag(1) - S(2)	106.65(3)
Ag(1) - S(2)	2.5802(8)	S(1) - Ag(1) - S(3)	112.69(3)
Ag(1) - S(3)	2.527(1)	S(1) - Ag(1) - S(4)	114.18(3)
Ag(1) - S(4)	2.513(1)	S(2) - Ag(1) - S(3)	100.47(3)
		S(2) - Ag(1) - S(4)	108.48(3)
		S(3) - Ag(1) - S(4)	113.14(4)
Ag(2) - S(1)	2.545(1)	S(1) - Ag(2) - S(2)	110.08(4)
Ag(2) - S(2)	2.575(1)	S(1) - Ag(2) - S(3)	110.86(3)
Ag(2) - S(3)	2.565(1)	S(1) - Ag(2) - S(4)	106.46(4)
Ag(2) - S(4)	2.618(1)	S(2) - Ag(2) - S(3)	106.14(4)
		S(2) - Ag(2) - S(4)	117.02(3)
		S(3) - Ag(2) - S(4)	106.21(4)
Zn(1) - S(1)	2.327(1)	S(1) - Zn(1) -S(2)	112.09(5)
Zn(1) - S(2)	2.354(1)	S(1) - Zn(1) -S(3)	110.33(4)
Zn(1) - S(3)	2.333(1)	S(1) - Zn(1) -S(4)	111.71(4)
Zn(1) - S(4)	2.3623(9)	S(2) - Zn(1) -S(3)	112.81(5)
		S(2) - Zn(1) -S(4)	105.46(4)
		S(3) - Zn(1) -S(4)	104.08(5)
Si(1) - S(1)	2.135(1)	S(1) - Si(1) - S(2)	107.84(9)
Si(1) - S(2)	2.116(2)	S(1) - Si(1) - S(3)	111.18(8)
Si(1) - S(3)	2.122(3)	S(1) - Si(1) - S(4)	108.5(1)
Si(1) - S(4)	2.138(2)	S(2) - Si(1) - S(3)	109.6(1)
		S(2) - Si(1) - S(4)	111.91(8)
		S(3) - Si(1) - S(4)	107.8(1)

3.2.3.4 Laboratory X-ray Powder Diffraction

X-ray powder diffraction studies were performed on a Panalytical X'Pert Pro MPD powder X-ray diffractometer using copper Kα radiation with a wavelength of 1.541871 Å and operating with a tube power of 45 kV and 40 mA. Data were collected from 5° to 145° 2θ with a step size of 0.0083556° and scan rate of 0.010644°/sec. The incident beam optics were comprised of a 0.02 rad soller slit, a divergent slit of 1/4° and an anti-scatter slit of 1/2°; whereas, the diffracted beam optics were comprised of a 0.02 rad soller slit and an anti-scatter slit of 1/4°. The samples were prepared for analysis using a top fill method where the sample powder is added from bottom to top of a sample holder and spread out using random chops of a razor blade to minimize preferred orientation. Phase identification of crystalline components was carried out using the X'Pert HighScore Plus software package[153] and the International Center for Diffracted Data (ICDD) database.

3.2.3.5 Diffuse Reflectance UV/Vis/NIR Spectroscopy

Diffuse reflectance UV/Vis/NIR spectroscopy was performed using a Varian Cary 5000 spectrometer equipped with a Harrick Praying Mantis diffuse reflectance accessory. The sample was ground, placed in the sample cup and compared to a similarly prepared 100% reflectance standard, $BaSO_4$. Data were collected from 2500 to 200 nm at a scan rate of 600 nm/min. The collected percent reflectance was converted to absorbance using the Kubelka-Munk equation[154] and wavelength was converted to energy in eV.

3.2.3.6 Electronic Structure Calculations

Density functional theory (DFT) calculations were performed with the help of Dr. Balamurugan Karuppannan using the solid state electronic structure package, Wien2k (version 11.1).[155] Wien2k uses a hybrid full potential linear augmented plane wave (LAPW) and augmented plane wave + local orbitals (APW + lo) schemes for solving the Kohn-Sham (KS) equations of the total energy of crystalline solids within DFT. In the LAPW method, the unit cell of a crystal is partitioned into non-overlapping atomic spheres and interstitial regions. The basis functions are constructed using the muffin-tin approximation (MTA), in which spherically symmetric potential within the atomic spheres and constant potential outside the spheres are assumed. The electronic states are classified as core, semi-core and valence states. The core states are completely confined within the atomic sphere while the semi-core states are high-lying core states that are not completely confined within the atomic sphere. The valence states are (partly) delocalized.[156] The APW + lo method increases the computation speed while its results are comparable in accuracy with that of LAPW method.[157] The results presented here are based on the calculations using APW + lo methods of Wien2k.

The refined structure of Ag_2ZnSiS_4 (obtained in the single crystal XRD studies in this work) and the structure of $AgGaS_2$ given by Laksari *et al*[148] were used in the DFT calculations. For the case of Ag_2ZnSiS_4, the Ag, Zn, Si and S atoms with electronic configurations, [Kr] $4d^{10}$ $5s^1$, [Ar] $3d^{10}$ $4s^2$, [Ne] $3s^2$ $3p^2$ and [Ne] $3s^2$ $3p^4$ were modeled to have MT spheres of radii (R_{MT}) 2.48, 2.29, 1.97 and 1.97 bohr respectively. On the other hand, following Laksari *et al*,[148] the MT spheres of radii 2.2, 2.0 and 1.8 for Ag, Ga ([Ar] $3d^{10}$ $4s^2$ $4p^1$) and S respectively are taken for the case of $AgGaS_2$. In both cases, the

initial densities of the core, semi-core, and valence states were determined using the relativistic approach of local spin density approximations (LSDA). These calculations were carried out along with the use of the Perdew–Burke–Ernzerhof generalized gradient approximation (PBE-GGA) for treating the exchange and correlation effects.[158] The calculations for the case of $AgGaS_2$ were also repeated using LSDA to approximate the exchange and correlation effects in order to more directly compare to calculations already found in the literature.[148,159] The product of the minimum of R_{MT} and $K_{\max}$ (RK_{max}) was set to be 7.0 for the case Ag_2ZnSiS_4 and 8.0 for $AgGaS_2$. The peak energy cutoff separating the core from the valence states was -6.0Ry and the calculations were carried out using a radial mesh approach of 1000 points.

In all cases, self consistent calculations were carried out using a series of subroutines; LAPW0, LAPW1, LAPW2, LCORE, and MIXER which were repeated, in order, until the total energy of the system converged.[157] The first subroutine, LAPW0, is carried out to calculate the total potential energy of the system as the sum of the Coulomb energy and exchange-correlation potential. The Coulomb energy is calculated using the multi-polar Fourier expansion developed by Weinert in 1981.[160] The exchange-correlation potential is then calculated for each orbital using a least squares approach for the core states, a 3-dimensional fast Fourier transform (FFT) for the semi-core states, and the PBE-GGA for the valence states.[158] The contribution from the plane wave to the Hamiltonian matrix is then determined by adjusting the Fourier series to have zero potential within the atomic sphere while retaining the potentials in the semi-core and valence states according to the formalization of Weinert *et al*.[161] After which the

Hellmann-Feynman force is calculated from the total potential energy using the method of Yu *et al.*[162]

The second subroutine, LAPW1, is then utilized to set up the Hamiltonian matrix for the k-mesh according to the method of Koelling and Arbman in order to calculate the eigenvalues and eigenvectors through diagonalization.[163] These values are then used by the third subroutine, LAPW2, to calculate the Fermi-energy and the expansion of the electronic charge densities for each occupied state and each *k*-vector. Afterward, the subroutine LCORE calculated the eigenvalues, densities, and contribution to atomic forces for the core states. This, spherical portion of the potential is modeled using the relativistic LSDA basis set established in 1969 by Desclaux.[164,165] The final subroutine, MIXER, is then utilized to add and "mix" the charge densities of the core states (LCORE), semi-core states (LAPW0), and the valence states (LAPW2). This process incorporates the multi-secant mixing scheme, developed by Marks and Luke in 2008, as a normalization step which utilizes the expansion coefficients from up to 10 proceeding iterations to calculate the optimal mixing fraction for each coefficient.[166] The convergence criteria for this set of routines was an energy change less than 0.1 mRy/unit cell while the *k*-mesh was generated using a total of 1000 *k*-points over the whole Brillouin zone (BZ) utilizing the high symmetry points taken for plotting the band structure within the irreducible Brillouin zone (IBZ) based on the template files of Wien2k.

3.3 Results and Discussion

3.3.1 Morphology and Composition

Reactions to prepare Ag_2ZnSiS_4 produced a gray ingot consisting of colorless crystals with what appeared to be a very slight green tint on the surface. When the ingot was broken, cavities were observed within the ingot where more crystals were found. EDS analysis of the gray ingot showed regions of Ag_2ZnSiS_4, ZnS and an Ag-Si-S phase. X-ray powder diffraction of the ground ingot (Figure 3.3) shows the presence of the quaternary phase Ag_2ZnSiS_4. The powder pattern also shows the presence of two unwanted phases, ZnS and Ag_2SiS_3, in the bulk sample. EDS spectra of the crystals show the presence of all four elements (Figure 3.4) in the measured ratio of $Ag_{1.97}Zn_1Si_{1.15}S_{4.13}$ in agreement with the predicted stoichiometry. A higher concentration of Zn was detected within the crystals than on the surface which is due to a possible surface coating of an impurity phase.

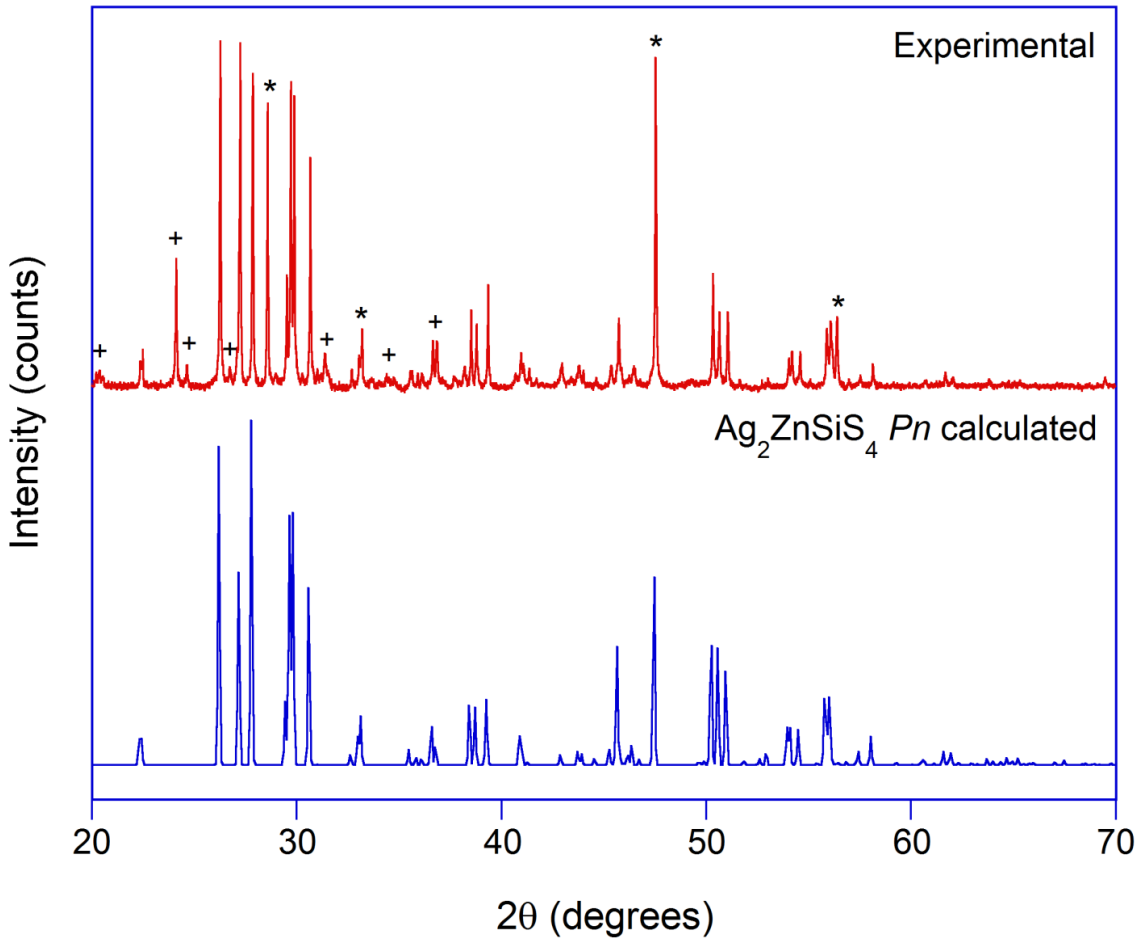

Figure 3.3 X-ray powder diffraction pattern of the ground ingot (top) compared to the calculated pattern of Ag_2ZnSiS_4 (bottom). Peaks indexed to the impurity phases ZnS (*) and Ag_2SiS_3 (+) are also indicated.

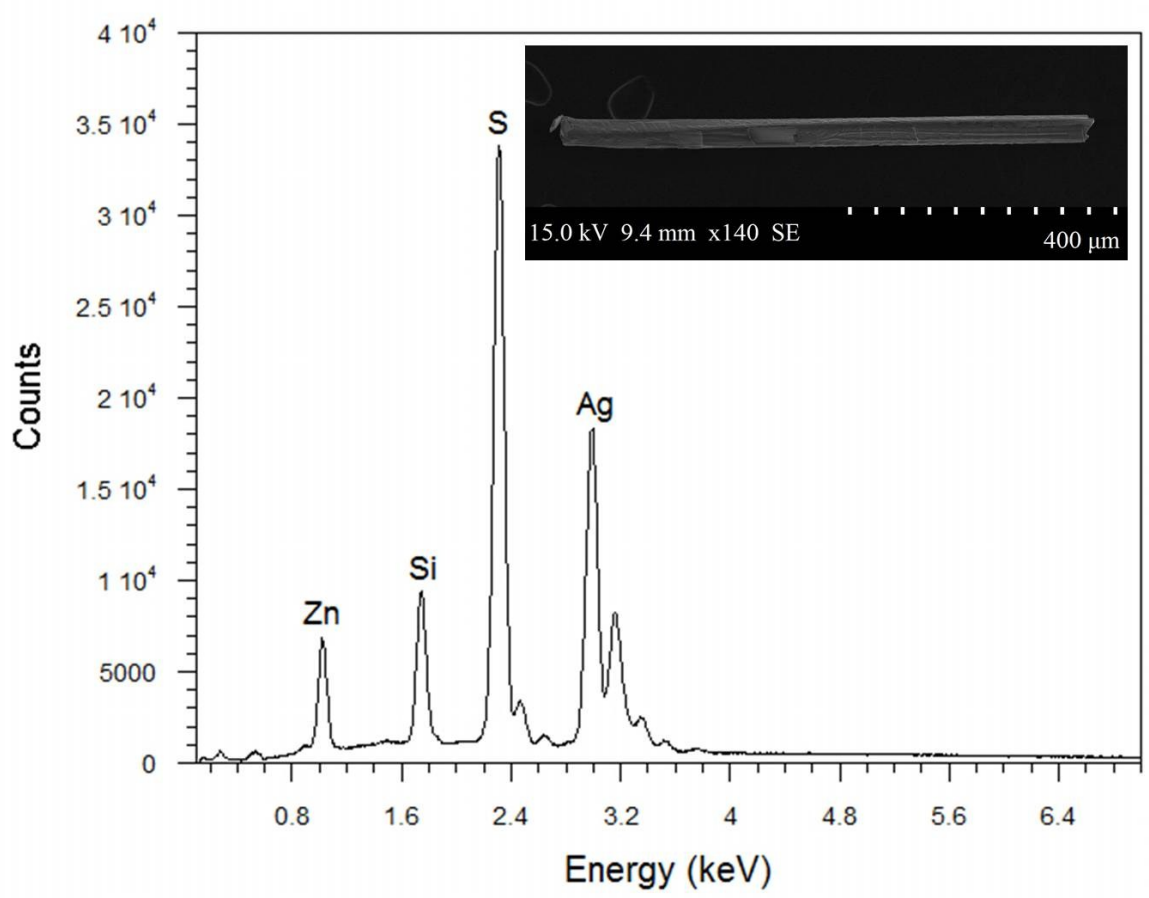

Figure 3.4 Energy dispersive spectrum of Ag_2ZnSiS_4 crystal with an inlayed scanning electron micrograph of the same crystal.

3.3.2 Structure

Single crystal X-ray diffraction data reveal that Ag_2ZnSiS_4 crystallizes in the monoclinic noncentrosymmetric space group *Pn*. All ions are tetrahedrally coordinated and reside in general positions. Each sulfur anion is surrounded by two silver cations, one zinc cation, and one silicon cation in accordance to Pauling's 2nd rule of local electroneutrality.[147] In this ordered structure the metal-sulfur bond lengths can be separated into three distinct categories. Bond distances for Ag-S show an average length of 2.539(1) Å for Ag(1) and 2.575(2) Å for Ag(2). These distances compare well to those

found for the quaternary DLS compounds Ag_2HgSnS_4 with an average Ag-S bond length of 2.43(2) Å[167] and the related compound Ag_2ZnGeS_4 with an average Ag-S bond length of 2.578(5) Å.[168] The Zn-S bond has an average length of 2.344(2) Å, which corresponds well with the average of 2.372(1)Å and 2.35(2) Å found in Ag_2ZnGeS_4[168] and Li_2ZnSnS_4, respectively.[169] The distances of the Si-S bonds average 2.128(4) Å in accordance to the bond lengths found in Cu_2MnSiS_4 and Cu_2ZnSiS_4 which have averages of 2.136(1) Å[170] and 2.136(1) Å [171] respectively.

Although a less common structure type for diamond-like compounds, the *Pn* space group was first observed in these materials in 1969 by Joubert-Bettan *et. al.* for Na_2ZnSiO_4.[172] This wurtz-kesterite structure type was also observed in the more recent study by Lekse *et. al.* in 2008 for the compound Li_2ZnSnS_4.[169] However, the structure of Ag_2ZnSiS_4 was not completely unexpected, due to the predictions from Chen *et. al.* in 2010 who preformed Madelung energy calculations for different structure types on a number of known and predicted diamond-like compounds and determined *Pc* (equivalent to *Pn*) to be the most energetically favorable for this predicted compound.[173]

The structure of Ag_2ZnSiS_4 can be described as a hexagonal, closest-packed array of sulfur anions with Ag^{1+}, Zn^{2+} and Si^{4+} occupying tetrahedral holes. The structure can be viewed as a corner-sharing, three-dimensional network of MS_4 tetrahedra. When viewed down the *b*-axis one can notice (Figure 3.5) the alternating nature of the cations. Rows along the *a*-axis of alternating Ag(1)-S_4 and Zn(1)-S_4 tetrahedra (ABAB) are separated by rows of Ag(2)-S_4 and Si(1)-S_4 tetrahedra (CDCD). The pattern is then alternated (BABA) and (DCDC) after which it repeats. This structure differs from the more common diamond-like wurtz-stannite structure, $Pmn2_1$ in the cation ordering. In

Pmn2₁ there is only one unique site for the M^{1+} ions and they are aligned in rows down the *c*-axis, which is demonstrated by the comparison to the previously reported Cu_2ZnSiS_4 compound (Figure 3.5).[171] Similarly, the difference between the *Pn* and *Pna2₁* space groups is the cation ordering, specifically the location of the Zn^{2+} ion in respect to the Si^{4+} site as illustrated by the comparison to Ag_2CdGeS_4 in Figure 3.5.[174]

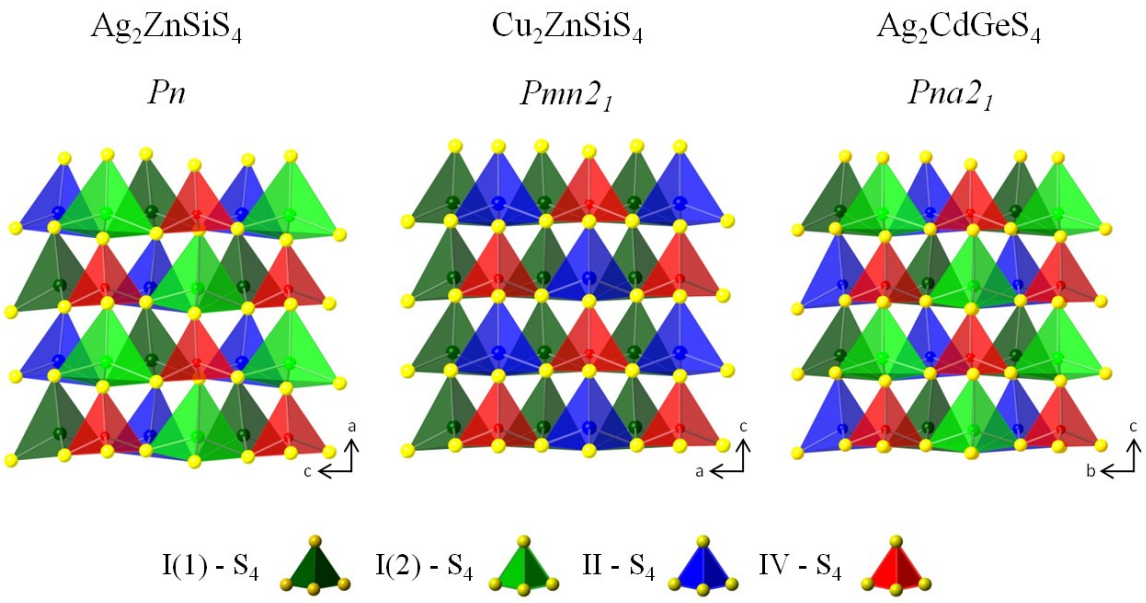

Figure 3.5 Polyhedral view of Ag_2ZnSiS_4 extended to show long range cation ordering in comparison to the equivalent views of the similar compounds Cu_2ZnSiS_4 and Ag_2CdGeS_4.

3.3.3 Electronic Band Structure and Density of States

The calculated electronic band structures of Ag_2ZnSiS_4 and $AgGaS_2$ are shown in Figure 3.6 and 3.7 respectively. In both compounds the valence band maximum (VBMa) and the conduction band minimum (CBMi) are at the Γ-point of the BZ, indicating that the compounds are direct band gap semiconductors. The difference between the CBMi and VBMa yields a band gap (E_g) of 1.88 eV for Ag_2ZnSiS_4. The value of E_g for $AgGaS_2$ is 1.21 eV. The experimentally determined band gap of $AgGaS_2$ is 2.51 eV, a positive 1.3 eV difference from our calculated value,[159,173,175] while UV/Vis/NIR spectroscopic analysis of Ag_2ZnSiS_4 sample yielded an estimated band gap of 3.28 eV (Figure. 3.8), a positive 1.4 eV difference from our calculated value.

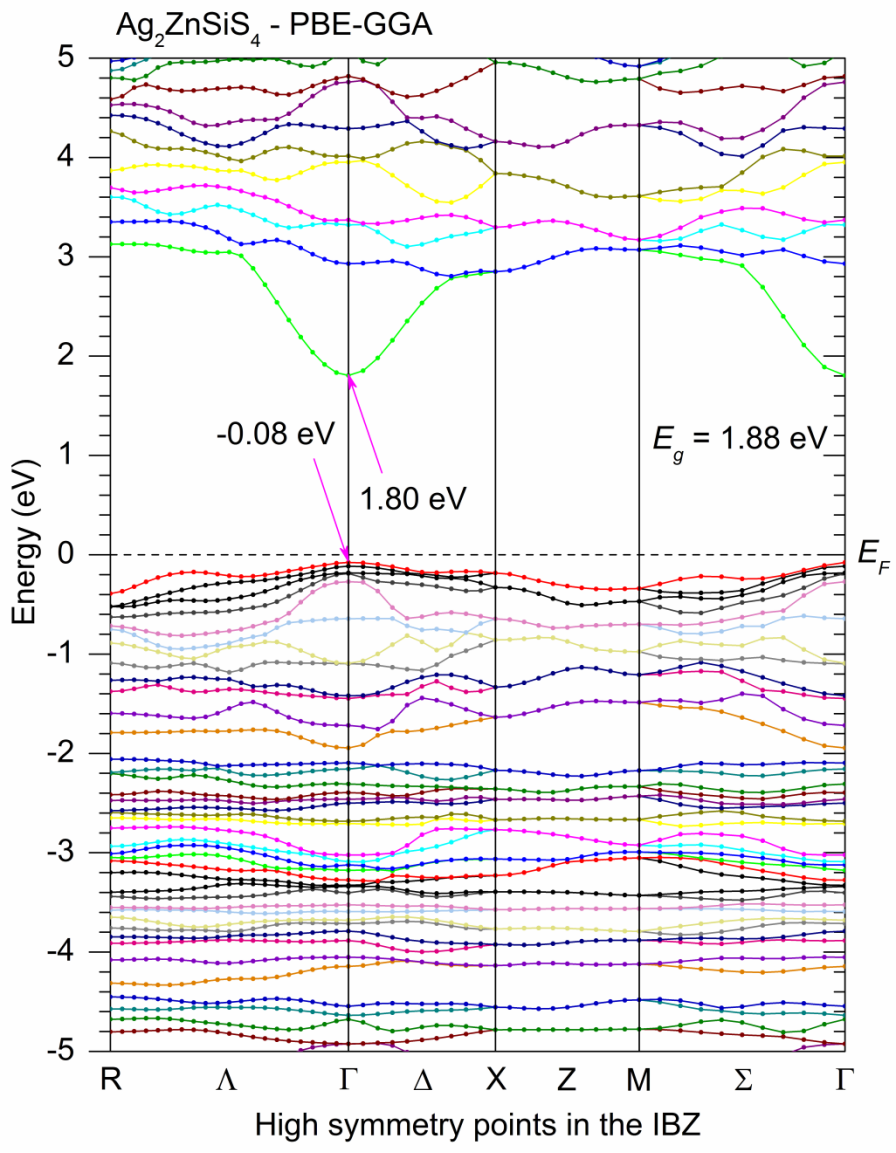

Figure 3.6 Calculated electronic band structure of Ag_2ZnSiS_4. The graph is scaled for 0 eV at the Fermi level (E_F).

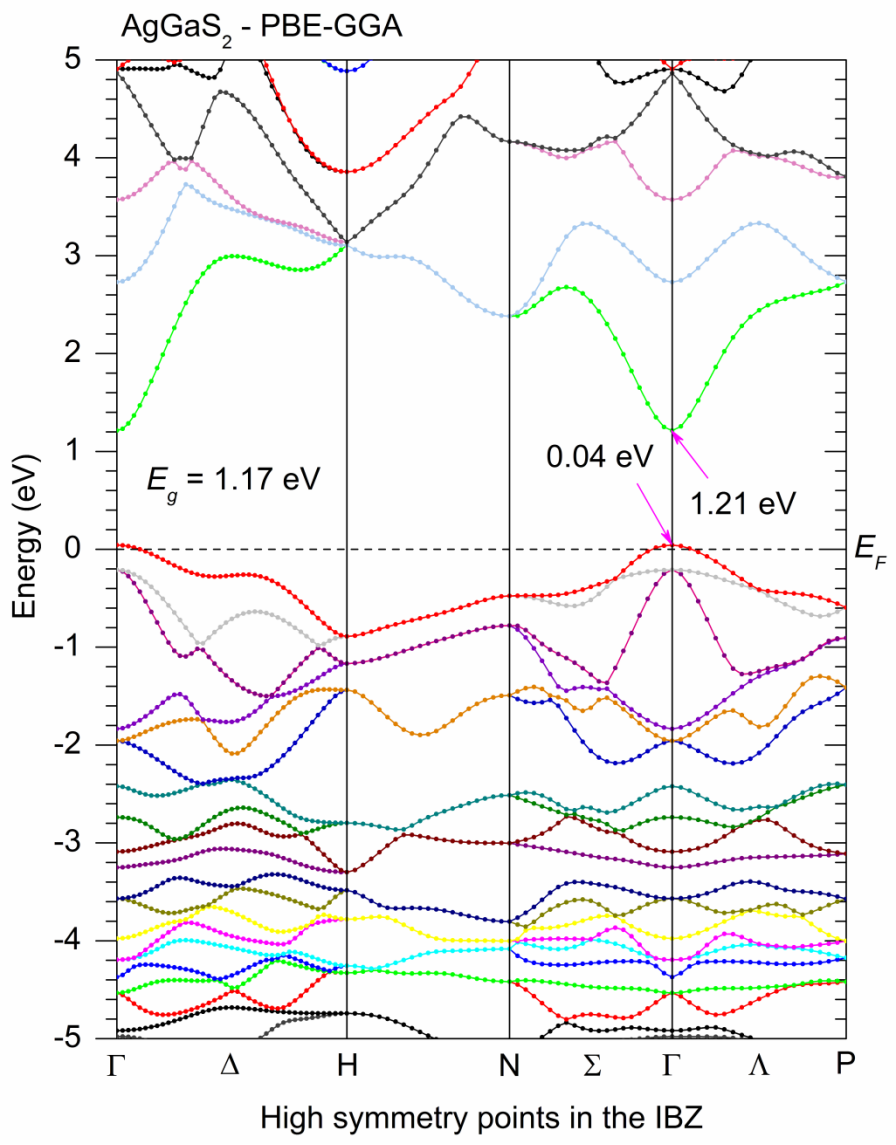

Figure 3.7 Calculated electronic band structure of $AgGaS_2$. The graph is scaled for 0 eV at the Fermi level (E_F).

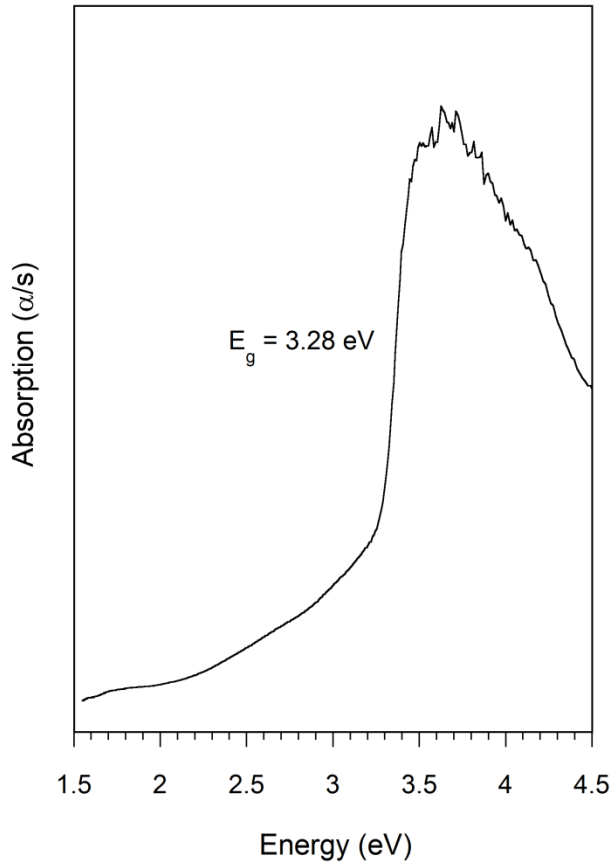

Figure 3.8 Optical diffuse reflectance UV/Vis/NIR spectrum converted to absorption for Ag_2ZnSiS_4.

Since the band structure of $AgGaS_2$ has been determined previously, a comparison was made between the present and published results. Even though the same PBE-GGA has been used, the calculated E_g in the work reported here is a little higher and closer to the experimentally determined value, than that which was reported by M. G. Brik (1.00 eV) using Materials Studio 4.0 package with CASTEP.[159] It is also noted that both Laksari *et al*[148] and Chahed *et al*[176] have reported that $AgGaS_2$ has a direct band gap of 0.95 eV both calculated using the local density approximation (LDA) in Wien2k. In fact, calculations using LSDA in Wien2k in this work also yielded the same 0.95 eV band

gap for $AgGaS_2$ with details given in the supplementary material. Therefore, it is clear that the PBE-GGA provides a relatively better, even though underestimated, estimation of the band gap, in comparison to LDA/LSDA using the Wien2k program. It is also worth noting here that there are new exchange correlation functionals such as the Heyd-Scuseria-Ernzerhof (HSE) hybrid functional.[177] Paier *et. al.* was able to calculate a band gap for the quaternary diamond-like semiconductor Cu_2ZnSnS_4 (CZTS) that was equal to the measured 1.5 eV band gap of the material.[177] This functional is yet to be implemented for Wien2k so although it underestimates the band gap, (PBE-)GGA is used in this study. Therefore the underestimation of the band gap considered in this comparison is expected.

The calculated DOS and partial DOS plots for Ag_2ZnSiS_4 and $AgGaS_2$ shown in Figure 3.9 and 3.10 clearly demonstrate the semiconducting nature of these compounds. In both Ag_2ZnSiS_4 and $AgGaS_2$, the valence band (VB) close to the Fermi level has major contribution from the Ag-4*d* and S-3*p* states although there is significant, but relatively small, contribution from the 3*p* states of Zn and Si or the 3*p* and 4*p* states of Ga. A very weak contribution in this region from the Zn-3d states can also be seen. The hybridization of the Ag-4*d* states with the S-3*p* and the *p* states of other atoms in the crystal is well known as the *p-d* hybridization, which is responsible for the red-shift of the optical band gap in these materials with reference to that of their binary analogs.[178] For example the binary DLSs, ZnS and GaS have an optical band gap of 3.6 and 2.5 eV respectively.[179] The states around the CBMi are mostly contributed to by the Zn-4*s*/Ga-4*s* and Si-3*s* and 3*p* states. There is also a small contribution from the Zn-3*p* states and S-3*s* and 3*p* states, and a weak contribution from the Ag-5*s* and 4*p* states. The majority of the Zn-3*d* states lie deep in the VB in the energy range of −6.0 to −8.0 eV and

the major contribution of Si-3*s* states are also deep in the valence band in the energy range of −6.0 to −8.0 eV as well as around −14.0 eV. Similarly, the major portion of Ga-3*d* states are in the energy range of −12 to −15.3 eV in the core of the VB. The major part of S-3*s* states are also in the core of the valence band in the energy range of −12.0 to −14.2 eV with considerably less contribution around −7.5 eV. Ultimately, the presence of strong *p*-*d* hybridization (more of 4*d* states of Ag and less of Zn/Ga) mainly constitutes the VBMa while the conduction band is mainly constructed from the mixing of *s* and *p* states and very little of the d orbitals of the atoms. The same effects of *p*-*d* hybridization have also been reported in $CuGaS_2$.[159,178]

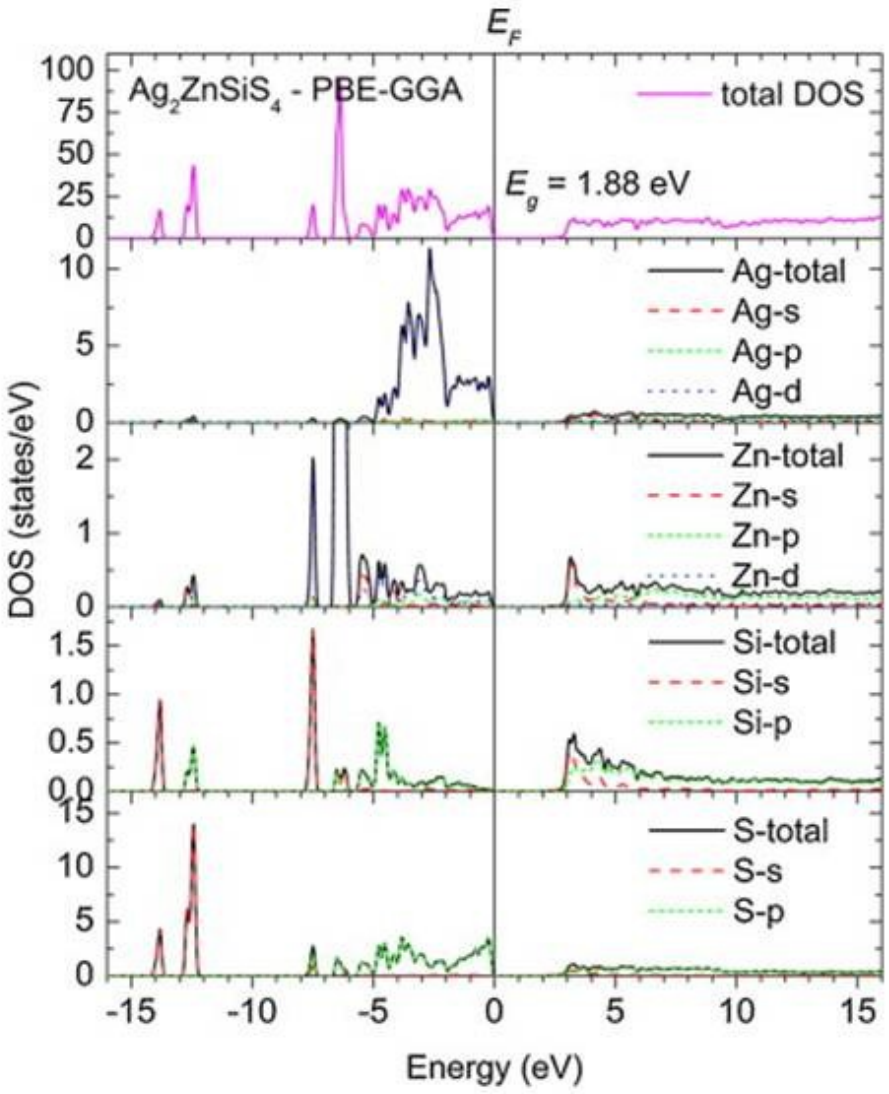

Figure 3.9 The calculated total and partial density of states for Ag_2ZnSiS_4. The graph is scaled for 0eV at the Fermi level (E_F).

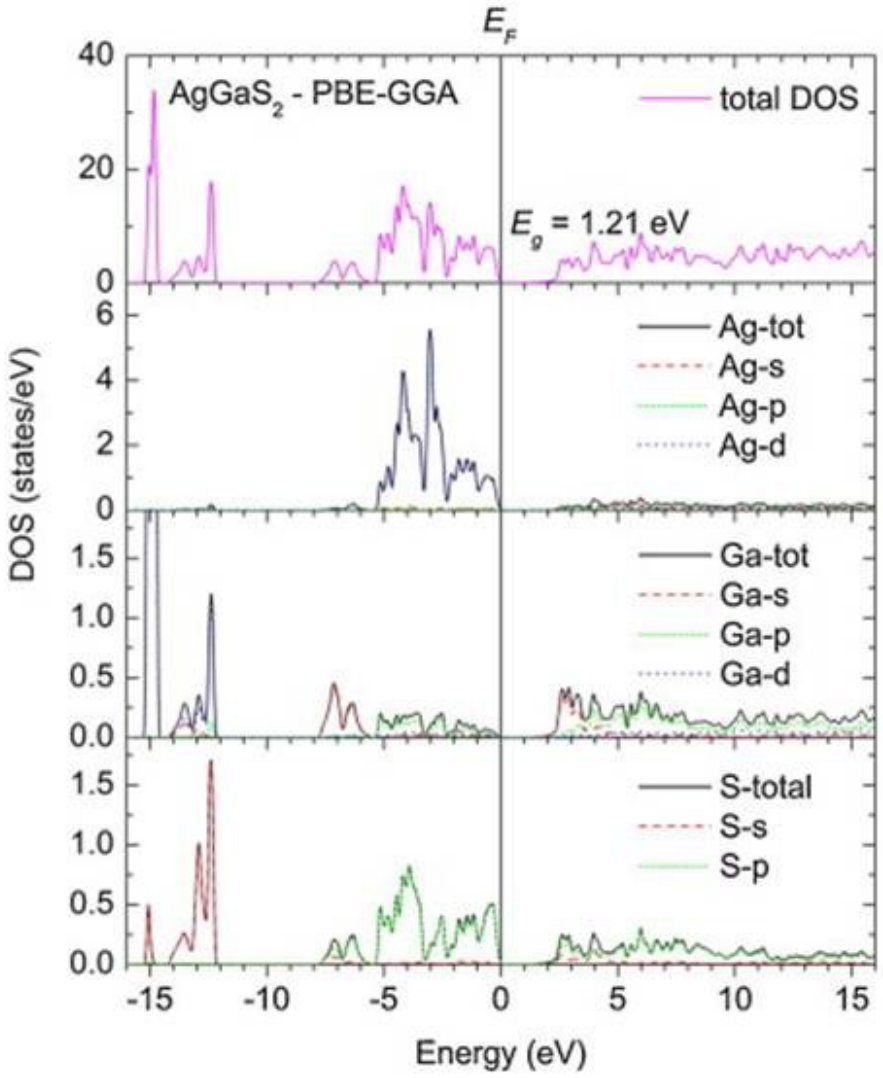

Figure 3.10 The calculated total and partial density of states for $AgGaS_2$. The graph is scaled for 0eV at the Fermi level (E_F).

3.4 Conclusion

Single crystals of the quaternary diamond-like semiconductor Ag_2ZnSiS_4 have been synthesized via high-temperature, solid-state synthesis. The crystal structure was solved in the monoclinic space group *Pn*. Electronic band structure calculations show a direct energy gap of 1.88 eV, which suggests that the title compound is suitable for applications in optoelectronic devices such as LEDs.[180] Partial (or full) replacement of Zn by magnetic ions such as those of Cr, Mn, Fe, Co, or Ni could establish interesting magnetic properties in the material, while retaining the semiconducting and optical properties for applications in spin-based electronics.[181,181,182] Substitution would also help in the fine-tuning of the band gap due to the finite, but small contribution of 3d-orbitals to the valence band maximum and conduction band minimum of the band structure. Since the zinc metal states have less influence on the energy gap and are mostly confined deep in the valence band, this system is suitable for localizing the magnetic moments while retaining the semiconducting behavior.[183]

3.5 References

Reprinted from the Journal of Alloys and Compounds, 516, Carl D. Brunetta, Balamurugan Karuppannan, Kimberly A. Rosmus, Jennifer A. Aitken, *The crystal and electronic band structure of the diamond-like semiconductor Ag_2ZnSiS_4*, 65-72,

139 Shi, X.; Xi, L.; Fan, J.; Zhang, W.; Chen, L. "Cu-Se bond network and thermoelectric compounds with complex diamondlike structure" *Chem. Mater.* **2010**, *22(22)*, 6029-6031.

140 Shi, X. Y.; Huang, F. Q.; Liu, M. L.; Chen, L. D. "Thermoelectric properties of tetrahedrally bonded wide-gap stannite compounds $Cu_2ZnSn_{1-x}In_xSe_4$" *Appl. Phys. Lett.* **2009**, *94(12)*, 122103.

141 Steinhagen, C.; Panthani, M. G.; Akhavan, V.; Goodfellow, B.; Koo, B.; Korgel, B. A. "Synthesis of Cu_2ZnSnS_4 nanocrystals for use in low-cost photovoltaics" *J. Am. Chem. Soc.* **2009**, *131(35)*, 12554-12555.

142 Lekse, J. W.; Moreau, M. A.; McNerny, K. L.; Yeon, J.; Halasyamani, P. S.; Aitken, J. A. "Second-harmonic generation and crystal structure of the diamond-like semiconductors Li_2CdGeS_4 and Li_2CdSnS_4" *Inorg. Chem.* **2009**, *48(16)*, 7516-7518.

143 Ruderman, W.; Maffetone, J.; Zelman, D.; D. Poirier, D. "Laser damage studies of silver gallium sulfide single crystals" *Mater. Res. Soc. Symp. Proc.* **1998**, *484*, 519-524.

144 Catella, G. C.; Burlage, D. "Crystal growth and optical properties of $AgGaS_2$ and $AgGaSe_2$" *MRS Bull.* **1998**, *23(7)*, 28-36.

145 E. Parthé, E. *Crystal Chemistry of Tetrahedral Structures*; Gordon and Breach Science Publishers: New York, NY, **1964**.

146 Goryunova, N.A. *The Chemistry of Diamond-Like Semiconductors*; Anderson, J.C. Ed.; The MIT Press: Cambridge, U.K. **1965**.

147 Pauling, L. "The principles determining the structure of complex ionic crystals" *J. Am. Chem. Soc.* **1929**, *51*, 1010-1026.

148 Laksari, S.; Chahed, A.; Abbouni, N.; Benhelal, O.; Abbar, B. "First-principles calculations of the structural, electronic and optical properties of $CuGaS_2$ and $AgGaS_2$" *Comp. Mater. Sci.* **2006**, *38(1)*, 223-230.

149 Bruker **1998** SMART and SAINT, Bruker AXS Inc., Madison, Wisconsin, USA.

150 Sheldrick, G. M. **2002** SADABS. University of Göttingen, Germany.

151 Bruker **2007** SHELXTL-PC, release 6.14, Bruker AXS Inc., Madison, Wisconsin, USA.

152 Palmer, D. **2010** Crystal Maker, CrystalMaker Software Ltd., Oxfordshire, England.

153 X. P. H. Plus, PANalytical B.V., Almelo, the Netherlands.

154 Kubelka, P.; Munk, F. "An article on optics of paint layers" *Zeit. Für Tekn. Physik* **1931**, *12*, 593-601.

155 Schwarz, K.; Blaha, P.; Madsen, G. K. H. "Electronic structure calculations of solids using the WIEN2k package for material sciences" *Comp. Phys. Commun.* **2002**, *147*, 71-76.

156 Schwarz, K. "DFT calculations of solids with LAPW and WIEN2k" *J. Solid State Chem.* **2003**, *176(2)*, 319-328.

157 Blaha, P.; Schwarz, K.; Madsen, G. K. H.; D. Kvasnicka, D. *WIEN2k Users Guide* J. Luitz, Vienna University of Technology, Vienna, Austria **2011**.

158 Perdew, J. P.; Burke, K.; Ernzerhof, M. “Generalized gradient approximation made simple” *Phys. Rev. Lett.* **1996**, *77(18)*, 3865-3868.

159 Brik, M. G. “First-principles study of the electronic and optical properties of $CuXS_2$ (X = Al, Ga, In) and $AgGaS_2$ ternary compounds” *J. Phys.: Condens. Matter* **2009**, *21(48)*, 485502.

160 Weinert, M. "Solution of Poisson's equation: Beyond Ewald-type methods" *J. Math. Phys.* **1981**, *22(11)*, 2433-2440.

161 Weinert, M.; Wimmer, E.; Freeman, A.J. "Total-energy all-electron density functional method for bulk solids and surfaces" *Phys. Rev. B.* **1982**, *26(8)*, 4571-4578.

162 Yu, R.; Singh, D.; Krakauer, H. "All-electron and pseudopotential force calculations using the linerized-augmented-plane-wave method" *Phys. Rev. B.* **1991**, *43(8)*, 6411-6422.

163 Koelling, D. D.; Arbman, G. O. "Use of energy derivative of the radial solution in an augmented plane wave method: application to copper" *J. Phys. F.* **1975**, *5(11)*, 2041-2054.

164 Desclaux, J. P. "Hartree Fock Slater self consistent field calculations" *Comp. Phys. Commun.* **1969**, *1(3)*, 216-222.

165 Desclaux, J. P. "A multiconfiguration relativistic DIRAC-FOCK program" *Comp. Phys. Commun.* **1975**, *9(1)*, 31-45.

166 Marks, L. D.; Luke, R. "Robust mixing for *ab initio* quantum mechanical calculations" *Phys. Rev. B.* **2008**, *78(7)*, 075114.

167 Parasyuk, O. V.; Chykhrij, S. I.; Bozhko, V. V.; Piskach, L. V.; Bogdanyuk, M. S.; Olekseyuk, I. D.; Bulatetska, L. V.; Pekhnyo, V. I. "Phase diagram of the Ag_2S-HgS-SnS_2 system and single crystal preparation, crystal structure and properties of Ag_2HgSnS_4" *J. Alloys Compd.* **2005**, *399*, 32-37.

168 Parasyuk, O. V.; Fedorchuk, A. O.; Kogut, Yu. M.; Piskach, L. V.; Olekseyuk, I. D. "The Ag_2S-ZnS-GeS_2 system: phase diagram, glass-formation region and crystal structure of Ag_2ZnGeS_4" *J. Alloys Compd.* **2010**, *500*, 26-29.

169 Lekse, J. W.; Leverett, B. M.; Lake, C. H.; Aitken, J. A. "Synthesis, physicochemical characterization and crystallographic twinning of Li_2ZnSnS_4" *J. Solid State Chem.* **2008**, *181(12),* 3217-3222.

170 Bernert, T.; Pfitzner, A. "$Cu_2MnMIVS_4$ (MIV = Si, Ge, Sn) analysis of crystal structures and tetrahedral volumes of normal tetrahedral compounds" *Z. Kristallogr.* **2005**, *220(11)*, 968-972.

171 Rosmus, K. A.; Aitken, J. A. "Cu_2ZnSiS_4" *Acta Cryst.* **2011**, *E67(4)*, i28.

172 Joubert-Bettan, C. A.; Lachenal, R.; Bertaut, E. F.; Parthé, E. "Crystal structures of Na_2ZnSiO_4, Na_2ZnGeO_4, and Na_2MgGeO_4" *J. Solid State Chem.* **1969**, *1(1)*, 1-5.

173 Chen, S.; Walsh, A.; Luo, Y.; Yang, J. H.; Gong, X. G.; Wei, S. H. "Wurtzite-derived polytypes of kesterite and stannite quaternary chalcogenide semiconductors" *Phys. Rev. B* **2010**, *82(19)*, 195203.

174 Brunetta, C. D.; Minsterman, W. C.; Lake, C. H.; Aitken, J. A. "Cation ordering and physicochemical characterization of the quaternary diamond-like semiconductor Ag_2CdGeS_4" *J. Solid State Chem.* **2012**, *187*, 177-185.

175 Honeyman, W. N.; Wilkinson, K. H. "Growth and properties of single crystals of Group I-III-VI_2 ternary semiconductors" *J. Phys. D: Appl. Phys.* **1971**, *4(8)*, 1182-1185.

176 Chahed, A.; Benhelal, O.; Laksari, S.; Abbar, B.; Bouhafs, B.; Amrane, N. "First-principles calculations of the structural, electronic and optical properties of $AgGaS_2$ and $AgGaSe_2$" *Physica B* **2005**, *367*, 142-151.

177 Paier, J.; Asahi, R.; Nagoya, A.; Kresse, G. "Cu_2ZnSnS_4 as a potential photovoltaic material: a hybrid Hartree-Fock density functional theory study" *Phys. Rev. B.* **2009**, *79(11)*, 115126.

178 Shay, J. L.; Tell, B.; Kasper, H. M.; Schiavone, L. M. "p-d Hybridization of the valence bands of I-III-VI_2 compounds" *Phys. Rev. B* **1972**, *5(12)*, 5003-5005.

179 Madelung, O.; Schulz, M. Eds. *Numerical Data and Functional Relationships in Science and Technology. New Series. Group III: Crystal and Solid State Physics. Semiconductors. Supplements and Extensions to Volume III/17. Intrinsic Properties of Group IV Elements and III–V, II–VI and I–VII Compounds, Vol. 22a*, Springer, Berlin, **1982**.

180 Shay, J. L.; Tell, B.; Kasper, H. M. "Visible stimulated emission in ternary chalcopyrite sulfides and selenides" *Appl. Phys. Letters* **1971**, *19(9)*, 366-368.

181 Pearton, S. J.; Abernathy, C. R.; Norton, D. P.; Hebard, A. F.; Park, Y. D.; Boatner, L. A.; Budai, J. D. "Advances in wide bandgap materials for semiconductor spintronics" *Mater. Sci Eng. R.* **2003**, *40(4)*, 137-168.

182 Wolf, S. A.; Awschalom, D. D.; Buhrman, R. A.; Daughton, J. M.; von Molnár, S.; Roukes, M. L.; Chtchelkanova, A. Y.; Treger, D. M. "Spintronics: a spin-based electronics vision for the future" *Science* **2001**, *294*, 1488-1495.

183 Sato, K.; Bergqvist, L.; Kudrnovský, J.; Dederichs, P. H.; Eriksson, O.; Turek, I.; Sanyal, B.; Bouzerar, G.; Katayama-Yoshida, H.; Dinh, V. A.; Fukushima, T.; Kizaki, H.; Zeller, R. "First-principles theory of dilute magnetic semiconductors" *Rev. Mod. Phys.* **2010**, *82(2)*, 1633-1690.

4 The Impact of Three New Quaternary Sulfides on the Current Predictive Tools for Structure and Composition of Diamond-Like Materials

4.1 Introduction

Diamond-like semiconductor (DLS) materials are normal valence compounds whose structures can be derived from either the cubic or hexagonal form of diamond.[184-186] The configuration of these structures can, therefore, be envisioned by taking the carbon lattice of cubic diamond or hexagonal lonsdaleite and replacing the carbon with cations and anions in an orderly fashion (Figure 4.1). Due to their relative ease of synthesis, binary diamond-like materials are well represented in the literature; however, as the number of components increases to ternary, the synthesis becomes more challenging and, considering the greater number of predicted stoichiometries, relatively few have been reported. For example, Zeng *et al.* computationally predicted 75 possible compositions for DLSs of the form I-III-VI_2, where the Roman numerals represent the valence of the atom and the subscript indicates the stoichiometry.[187] Only ~1/3 of these predicted compounds have been synthesized and characterized. In the case of quaternary DLSs, such as the I_2-II-IV-VI_4 family, the number of possible compositions is even greater, yet there still remains many to be reported.

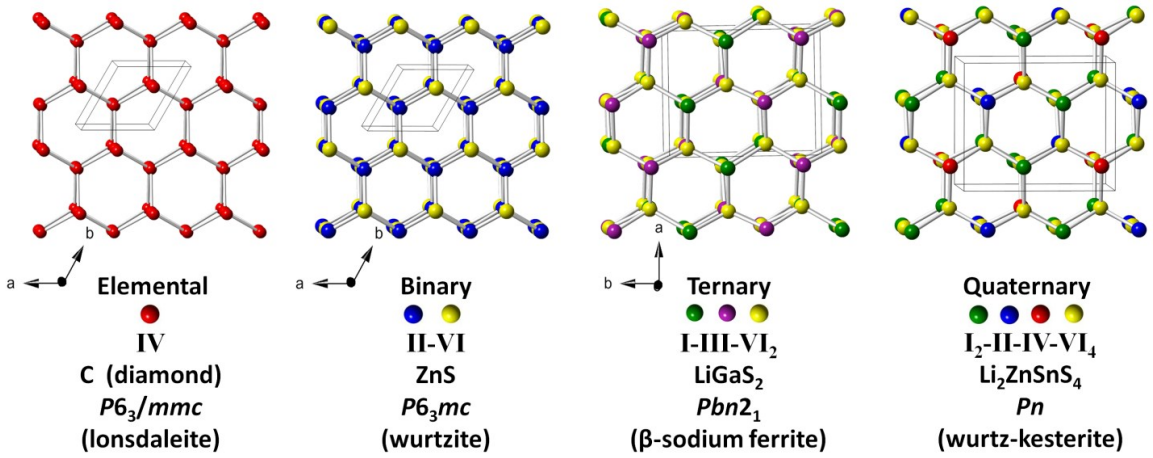

Figure 4.1 The structural progression of DLS's derived from lonsdaleite.

Due to the large variety of possible compositions, quaternary diamond-like materials can possess numerous technologically useful properties. These materials are of interest for applications such as tunable semiconductors,[188-191] photovoltaics,[188,192,193] spintronics,[194,195] non-linear optics,[196,197] and thermoelectrics.[189,198,199] The interest in applying these materials in such applications stems from the inherently tunable properties of band gap,[188,192,200,201] magnetism,[190,194] second harmonic generation,[196,201,202] and electrical properties.[203] However a complete understanding of the roles of structure and composition in determining the resulting physicochemical properties has not yet been realized. Furthermore, due to limitations of the predictive tools, the development of new materials for specific applications is challenging.

For decades, four guidelines have been used to predict compositions that will have diamond-like structures. The first is that the average number of valence electrons per atom is four. Next, the average number of valence electrons per anion must be eight.[184,185] Also, the octet of each anion must be satisfied by nearest neighbor cations and each atom must be tetrahedrally coordinated. For the last guideline, Pauling's radius

ratio rule is commonly used to predict coordination geometry.[184,185,204] It is well known that this rule is effective in its application to relatively hard anions. However, many examples of diamond-like materials with softer anions exist, yet violate this rule.

Here we present three new quaternary DLSs: Ag_2FeSiS_4, Li_2FeGeS_4,[205] and Li_2FeSnS_4.[205] These three compounds crystallize with the wurtz-kesterite structure in the space group *Pn*, raising the number of quaternary DLSs in this space group from 2 to 5. Using several sets of ionic and crystal radii, radius ratios of r^+/r^- for all ions in these materials are significantly out of the range for tetrahedral coordination, thus violating Pauling's radius ratio rule. This prompts the re-evaluation of the predictive tools used for diamond-like materials even though the other guidelines for these materials are followed.[204] In addition to examining the three new compounds reported here, the adherence of diamond-like structures to Pauling's radius ratio rule has been assessed by considering all previously reported structures of quaternary diamond-like chalcogenides solved by single crystal X-ray diffraction methods and selected DLS structures refined from X-ray powder diffraction.[206-234] Since several sets of tetrahedral radii have appeared in the literature, we also evaluated how well the experimental bond lengths from this set of compounds correspond to those predicted using the radii sets from various authors.[235-239] Furthermore, the cation tetrahedral volumes from this set of compounds were calculated and examined to determine whether or not they can be used to predict either a cubic- or hexagonal-derived diamond-like phase as proposed by Pfitzner *et al.*[217,225]

4.2 Experimental

4.2.1 Reagents

Chemicals used in this work were utilized as obtained unless otherwise noted: (1) silver powder, ~325 mesh, 99.99%, Cerac Milwaukee, WI; (2) lithium sulfide powder, ~200 mesh, 99.9%, Cerac Milwaukee, WI; (3) iron powder, 99.999%, Strem Newburyport, MA; (4) silicon powder, 99.999%, Strem Newburyport, MA; (5) germanium pieces were first ground using an impact mortar and pestle until the large pieces were broken up into a coarse powder and then ground for 5 min in a ceramic mortar and pestle before use, 99.999%, Strem Newburyport, MA; (6) tin powder, ~200 mesh, 99.99%, Cerac Milwaukee, WI; (7) sulfur powder, sublimed, 99.5%, Fisher Scientific Pittsburgh, PA.

4.2.2 Synthesis

Single crystals of Ag_2FeSiS_4, Li_2FeGeS_4[205] and Li_2FeSnS_4[205] were produced by weighing stoichiometric amounts of each element or binary starting material in an argon-filled glove box. For each material reagents were combined in an agate mortar, ground for 20 min with a pestle and then transferred to a 9 mm o.d. graphite crucible which was then placed in a 12 mm o.d. fused-silica tube. The tube was then flame-sealed under a vacuum of approximately 10^{-3} mbar and placed in a programmable furnace. For Ag_2FeSiS_4, the reactants were heated to 700°C over 12 hours, held at that temperature for 96 hours and then cooled to 420°C over 50 hours after which the sample was allowed to cool radiatively. For Li_2FeGeS_4 and Li_2FeSnS_4, the reactants were heated at 750 °C for

96 hours, slowly cooled to 500 °C in 50 hours and then allowed to cool to room temperature naturally. In the case of Li_2FeGeS_4 and Li_2FeSnS_4, products were rinsed with N,N'-dimethylformamide and hexane. In all cases dark red, plate-like crystals were selected for single crystal X-ray diffraction.[205]

4.2.3 Physical Property Measurements

4.2.3.1 Single Crystal X-ray Diffraction: Data Collection and Reduction

A Bruker SMART Apex 2 CCD single crystal X-ray diffractometer utilizing graphite monochromatized molybdenum K_α radiation was used to collect data at ambient temperature with a tube power of 50 kV and 30 mA for 35 sec per frame. SAINT[240] was used to integrate the data and SADABS[241] was employed to perform the absorption correction. XPREP was used for space group determination and to create files for SHELXTL.[242] Based on systematic absences, two space groups were initially considered, *Pn* and *P2/n*. The space group *Pn* (No. 7) was selected because all DLSs are noncentrosymmetric.

4.2.3.2 Single-Crystal X-ray Diffraction: Solution and Refinement

The SHELXTL-PC[242] software package was used to solve and refine the crystal structures of Ag_2FeSiS_4, Li_2FeGeS_4[205] and Li_2FeSnS_4.[205] Each structure consists of eight atoms located on general positions: two (I) sites, one Fe site, one (IV) site, and four S sites (where I=Ag, Li and IV=Si, Ge, Sn). The structures were refined with R1(all data) of 0.0249, 0.0346 and 0.0310, respectively. Crystallographic parameters and details for each compound are shown in Table 4.1. Atomic coordinates and equivalent atomic

displacement parameters for Ag_2FeSiS_4 as well as the bond distances and bond angles of Ag_2FeSiS_4 can be found in Tables 4.2 and 4.3. The program CrystalMaker®[243] was used to generate the crystal structure figures.

Table 4.1 Crystallographic data and experimental details for Ag_2FeSiS_4, Li_2FeSnS_4, and Li_2FeGeS_4.

Empirical formula	Ag_2FeSiS_4	Li_2FeSnS_4[205]	Li_2FeGeS_4[205]
Size (mm)	0.13 x 0.30 x 0.84	0.02 x 0.05 x 0.06	0.01 x 0.05 x 0.09
Color	Dark red	Dark red	Dark red
Habit	Plate	Plate	Plate
Formula weight	427.92 g mol^{-1}	316.66 g mol^{-1}	270.56 g mol^{-1}
Temperature	296 K	173 K	173 K
Wavelength of X-ray	0.71073 Å	0.71073 Å	0.71073 Å
Space group	*Pn*	*Pn*	*Pn*
Unit cell dimensions	a = 6.4220(1) Å	a = 6.3727(3) Å	a = 6.2286(2) Å
	b = 6.6185(1) Å	b = 6.7776(3) Å	b = 6.6029(2) Å
	c = 7.8650(1) Å	c = 7.9113(4) Å	c = 7.7938(2) Å
	α = γ = 90°	α = γ = 90°	α = γ = 90°
	β = 90.614(1)°	β = 90.207(3)°	β = 90.047(2)°
Volume	334.275(8) $Å^3$	341.70(3) $Å^3$	320.53(2) $Å^3$
Z	2	2	2
Calculated density	4.242 Mg m^{-3}	3.078 Mg m^{-3}	2.803 Mg m^{-3}
Flack parameter	-0.05(3)	0.08(3)	0.10(1)
F(000)	396	292	256
Reflections collected/unique	4330/1470	4042/1483	4074/1392
Data/restraints/parameters	1470/2/75	1483/2/64	1392/2/64
Completeness to theta = 27.11°	100%	100%	100%
Goodness of fit	1.144	1.059	1.229
Final R indices [*I*>2sigma(*I*)]	R1 = 0.0235	R1 = 0.0254	R1 = 0.0290
	wR_2 = 0.0627	wR_2 = 0.0493	wR_2 = 0.0605
R indices (all data)	R1 = 0.0249	R1 = 0.0310	R1 = 0.0346
	wR_2 = 0.0641	wR_2 = 0.0421	wR_2 = 0.0623

Refinement of F^2 was made against all reflections. $R_1 = \frac{\Sigma||F_o|-|F_c||}{\Sigma|F_o|}$, $wR_2 = \sqrt{\frac{\Sigma\left[w(F_o^2-F_c^2)^2\right]}{\Sigma\left[w(F_o^2)^2\right]}}$,

$w = \frac{1}{(\sigma^2(F_o^2)+(aF_o)^2+bP)}$, $P = [2F_c^2 + Max(F_o^2, 0)]/3$

Table 4.2 Selected bond distances (Å) and angles (°) for Ag_2FeSiS_4.

Bond	Distance	Bond	Angle
Ag(1)—S(1)	2.547(2)	S(1)—Ag(1)—S(2)	107.74(6)
Ag(1)—S(2)	2.581(2)	S(1)—Ag(1)—S(3)	110.80(5)
Ag(1)—S(3)	2.529(2)	S(1)—Ag(1)—S(4)	113.50(6)
Ag(1)—S(4)	2.518(2)	S(2)—Ag(1)—S(3)	100.75(6)
		S(2)—Ag(1)—S(4)	109.06(5)
Ag(2)—S(1)	2.544(2)	S(3)—Ag(1)—S(4)	114.03(7)
Ag(2)—S(2)	2.569(2)	S(1)—Ag(2)—S(2)	111.36(6)
Ag(2)—S(3)	2.560(2)	S(1)—Ag(2)—S(3)	111.36(6)
Ag(2)—S(4)	2.609(2)	S(1)—Ag(2)—S(4)	106.07(6)
		S(2)—Ag(2)—S(3)	107.19(7)
Fe(1)—S(1)	2.336(2)	S(2)—Ag(2)—S(4)	106.30(6)
Fe(1)—S(2)	2.371(2)	S(3)—Ag(2)—S(4)	106.30(6)
Fe(1)—S(3)	2.339(2)	S(1)—Fe(1)—S(2)	111.42(8)
Fe(1)—S(4)	2.369(2)	S(1)—Fe(1)—S(3)	108.84(7)
		S(1)—Fe(1)—S(4)	114.46(8)
Si(1)—S(1)	2.133(2)	S(2)—Fe(1)—S(3)	112.83(9)
Si(1)—S(2)	2.112(4)	S(2)—Fe(1)—S(4)	104.71(7)
Si(1)—S(3)	2.125(4)	S(3)—Fe(1)—S(4)	104.43(9)
Si(1)—S(4)	2.147(4)	S(1)—Si(1)—S(2)	108.4(2)
		S(1)—Si(1)—S(3)	110.4(1)
		S(1)—Si(1)—S(4)	108.5(2)
		S(2)—Si(1)—S(3)	109.8(2)
		S(2)—Si(1)—S(4)	111.9(1)
		S(3)—Si(1)—S(4)	107.9(2)

Table 4.3 Fractional atomic coordinates and equivalent isotropic displacement parameters, U_{iso} ($Å^2x10^3$) for Ag_2FeSiS_4.

Site	x	y	z	$U_{(eq)}$*
Ag(1)	0.23458(7)	0.3196(1)	0.32677(6)	32(1)
Ag(2)	0.72118(9)	0.14939(8)	0.58073(9)	34(1)
Fe(1)	0.2194(1)	0.3160(1)	0.8188(1)	16(2)
Si(1)	0.7184(4)	0.1857(1)	0.0724(4)	12(3)
S(1)	0.1162(3)	0.1205(2)	0.5855(2)	16(3)
S(2)	0.5869(3)	0.3190(2)	0.8521(2)	17(3)
S(3)	0.0486(3)	0.1986(2)	0.0606(2)	17(3)
S(4)	0.6245(3)	0.3387(2)	0.2997(2)	15(3)

*$U_{(eq)}$ is defined as 1/3 the trace of the orthogonal tensor U_{ij}.

4.3 Results and Discussion

4.3.1 Structure

The isostructural Ag_2FeSiS_4, Li_2FeGeS_4, and Li_2FeSnS_4 crystallize in the space group *Pn* and can be described using the hexagonal, closest-packed model of sulfur anions with 1+, 2+, and 4+ cations occupying half the tetrahedral holes. In this structure, all tetrahedra point in the same direction, demonstrating the noncentrosymmetric nature of the structure that can be clearly seen when viewed down the b-axis. As shown in Figure 4.2, each compound consists of isolated IV-S_4 tetrahedra, where each corner is shared by one II-S_4 tetrahedron and two I-S_4 tetrahedra. All three existing structure types of the hexagonally derived DLSs have an identical IV-S_4 array. The wurtz-kesterite structure (*Pn*) found for the new compounds presented here differs in the ordering of the I-S_4 and II-S_4 tetrahedra from the more commonly encountered DLSs with the wurtz-stannite structure ($Pmn2_1$) and the less common diamond-like materials that crystallize in the space group $Pna2_1$. Looking down the *b*-axis of the wurtz-kesterite structure, alternating rows of I-II-I-II and IV-I-IV-I along the *a*-axis can be observed.

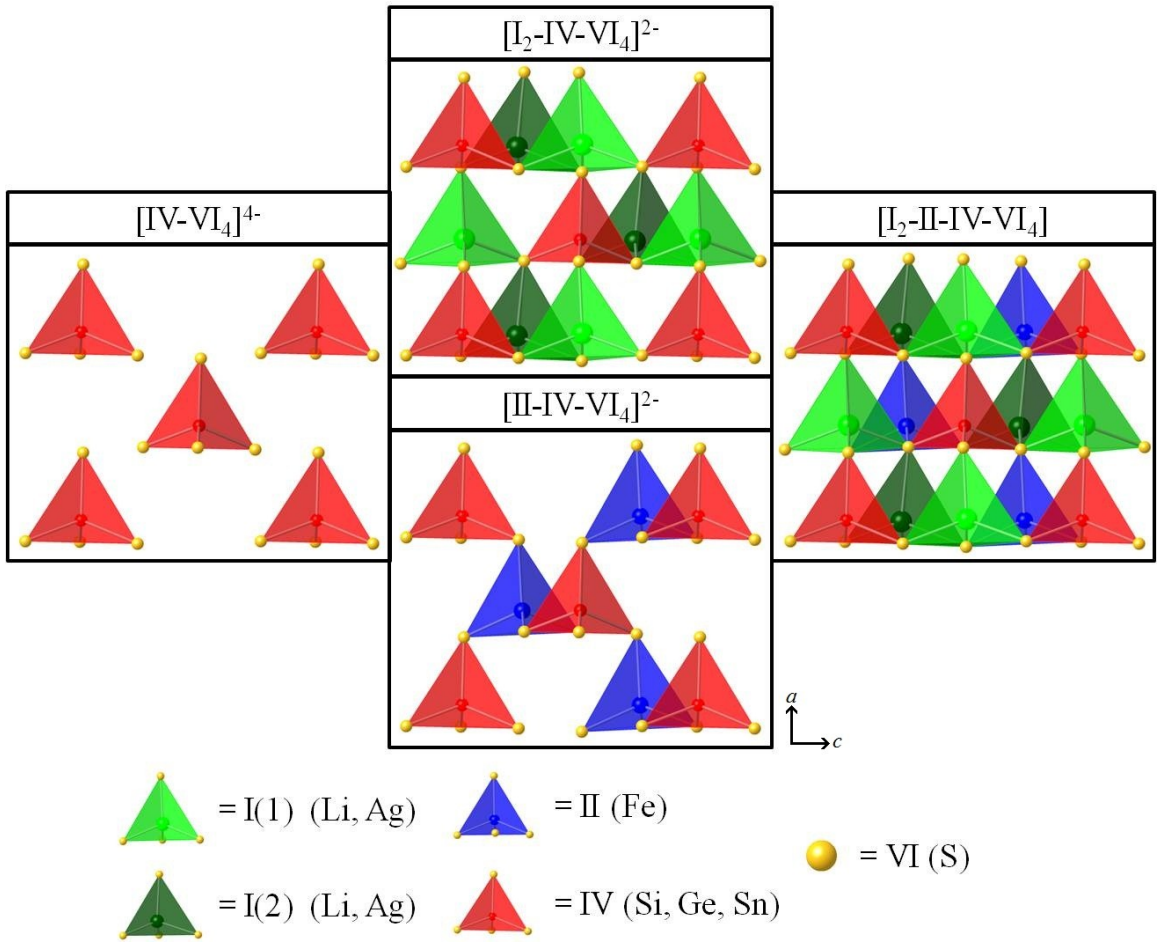

Figure 4.2 The arrangement of metal-sulfur tetrahedra in the *Pn* structure, as seen in Ag_2FeSiS_4, Li_2FeSnS_4, and Li_2FeGeS_4.

Bond distances found in these compounds are comparable to those found in the literature for similar diamond-like materials. The Ag-S bond distances found in Ag_2FeSiS_4 range from 2.428(2) Å to 2.609(2) Å with an average of 2.546(1) Å, analogous to the bond lengths found in Ag_2CdGeS_4 and Ag_2ZnSiS_4, which range from 2.513(1) Å to 2.618(1) Å with an average of 2.558(1) Å.[206,210] The Li-S bond lengths in Li_2FeSnS_4 and Li_2FeGeS_4 were found to have a range of 2.36(2) Å to 2.53(2) Å with each compound possessing an average Li-S bond length of 2.43(2) Å. This is similar to those found in the previously reported DLS materials Li_2CdGeS_4 and Li_2CdSnS_4, which

possess a range of 2.402(9) Å to 2.45(4) Å and an average of 2.43(2) Å.[233] The range of Fe-S bond lengths in Ag_2FeSiS_4, Li_2FeSnS_4, Li_2FeGeS_4 is relatively narrow with a range of ~0.02 to 0.04 Å, averaging 2.354(1), 2.358(1), and 2.328(1) Å, respectively. These distances match up to those found in Ag_2FeSnS_4 and Cu_2FeSnS_4.[208,220] The Si-S bond lengths found in Ag_2FeSiS_4 are between 2.112(4) Å and 2.147(4) Å, averaging 2.129(2) Å, which closely measures up to the bond lengths found in Ag_2ZnSiS_4 with an average of 2.128(1) Å.[210] The Sn-S bonds in Li_2FeSnS_4, varying only by ~0.01 Å and averaging 2.393(1) Å, are akin to the average distance of 2.386(1) Å in Li_2CdSnS_4. The Ge-S bond distances in Li_2FeGeS_4, varying ~0.02 Å and averaging 2.236(1) Å, are similar to the average bond distance of 2.212(1) Å in Li_2CdGeS_4.[233]

4.3.2 Comprehensive Literature Comparison

A critical examination of these new diamond-like materials and those previously reported was made in order to re-evaluate the predictive tools for DLSs, Table 4.4.[206-234] Due to the similarities among DLS structure types, and in some cases the existence of isoelectronic ions, X-ray powder diffraction patterns of these materials can be very similar and in some cases nearly indistinguishable.[206] Therefore, a majority of compounds whose structures have been assigned based on X-ray powder diffraction data have been excluded from this comparison. To the best of our knowledge, the structures of only 29 quaternary DLS chalcogenides, including the three reported here, have been solved from single crystal X-ray diffraction data. Herein the bond distances and tetrahedral volumes found in these structures are used to assess adherence to Pauling's radius ratio rule and Pfitzner's theory.[204,217,225]

Table 4.4 Radius ratios, r^+/r^-, and tetrahedral volumes for 41 selected quaternary diamond-like materials.

Compound	Space Group	X-ray Method	Radius Ratio*			Tetrahedral Volumes (Å^3)**					Ref.
			I/VI	II/VI	IV/VI	I(1)-VI	I(2)-VI	II-VI	IV-VI	Dev.	
Ag_2CdGeS_4	*Pna2$_1$*	SC	0.655	0.541	0.312	8.629	8.108	8.171	5.529	1.406	[206]
Ag_2CdGeS_4	*Pmn2$_1$*	P	0.655	0.541	0.312	8.127		8.202	5.806	1.362	[207]
Ag_2FeSiS_4	***Pn***	**SC**	**0.655**	**0.453**	**0.235**	**8.381**	**8.669**	**6.501**	**5.009**	**1.715**	**this work**
Ag_2FeSnS_4	*I-42m*	SC	0.655	0.453	0.406	7.310		7.578	8.290	0.506	[208]
$Ag_2HgSnSe_4$	*Pmn2$_1$*	P	0.655	0.647	0.406	9.667		8.758	7.723	0.973	[209]
Ag_2ZnSiS_4	*Pn*	SC	0.655	0.435	0.235	8.356	8.637	6.509	4.995	1.705	[210]
Cu_2CdGeS_4	*Pmn2$_1$*	SC	0.435	0.541	0.312	6.439		8.588	5.574	1.552	[211]
$Cu_2CdGeSe_4$	*Pmn2$_1$*	SC	0.435	0.541	0.312	7.624		7.951	7.397	0.279	[212]
$Cu_2CdGeSe_4$	*I-42m*	P	0.435	0.541	0.312	5.064		6.860	7.349	1.203	[212]
$Cu_2CdGeTe_4$	*I-42m*	SC	0.435	0.541	0.312	8.545		10.829	9.229	1.173	[213]
Cu_2CdSiS_4	*Pmn2$_1$*	SC	0.435	0.541	0.235	6.412		6.376	6.422	0.025	[214]
Cu_2CdSiS_4	*Pmn2$_1$*	SC	0.435	0.541	0.235	6.653		8.506	4.877	1.815	[215]
$Cu_2CdSnSe_4$	*I-42m*	P	0.435	0.541	0.406	7.284		9.788	8.063	1.282	[216]
Cu_2CoGeS_4	*I-42m*	SC	0.435	0.424	0.312	5.689		6.764	6.313	0.540	[217]
Cu_2CoSiS_4	*I-42m*	P	0.435	0.424	0.235	6.076		6.841	4.983	0.934	[218]
Cu_2CoSnS_4	*I-42m*	P	0.435	0.424	0.406	6.029		6.723	7.485	0.728	[218]
$Cu_2CoSnSe_4$	*I-42m*	P	0.435	0.424	0.406	7.327		7.120	8.607	0.806	[218]
Cu_2FeGeS_4	*I-42m*	SC	0.435	0.453	0.312	6.257		6.728	5.721	0.504	[219]
Cu_2FeSnS_4	*I-42m*	SC	0.435	0.453	0.406	5.064		6.860	7.349	1.203	[220]
Cu_2FeSnS_4	*I-42m*	SC	0.435	0.453	0.406	6.474		6.506	7.222	0.423	[221]
Cu_2FeSnS_4	*P-4*	SC	0.435	0.453	0.406	6.401		6.553	7.038	0.333	[222]
$Cu_2FeSnSe_4$	*I-42m*	SC	0.435	0.453	0.406	7.123		7.644	8.626	0.763	[223]
Cu_2HgGeS_4	*Pmn2$_1$*	P	0.435	0.647	0.312	6.183		8.820	5.556	1.732	[224]
$Cu_2HgGeSe_4$	*I-42m*	P	0.435	0.647	0.312	6.983		9.552	7.043	1.466	[224]
$Cu_2HgSnSe_4$	*I-42m*	P	0.435	0.647	0.406	7.056		9.710	8.590	1.332	[216]
Cu_2MnGeS_4	*Pmn2$_1$*	SC	0.435	0.418	0.312	6.369		6.385	6.369	0.009	[225]
Cu_2MnGeS_4	*Pmn2$_1$*	SC	0.435	0.418	0.312	6.324		7.581	5.671	0.971	[226]
Cu_2MnSiS_4	*Pmn2$_1$*	SC	0.435	0.418	0.235	6.545		7.543	5.031	1.265	[225]
Cu_2MnSnS_4	*I-42m*	SC	0.435	0.418	0.406	6.667		7.448	7.156	0.395	[225]
Cu_2MnSnS_4	*I-42m*	SC	0.435	0.418	0.406	6.326		7.066	7.085	0.443	[226]
Cu_2MnSnS_4	*I-42m*	SC	0.435	0.418	0.406	6.381		7.336	7.136	0.503	[227]
$Cu_2MnSnSe_4$	*I-42m*	P	0.435	0.418	0.406	6.474		6.506	7.222	0.423	[228]
Cu_2ZnGeS_4	*I-42m*	SC	0.435	0.435	0.312	6.474		5.991	5.499	0.488	[229]
$Cu_2ZnGeSe_4$	*I-42m*	P	0.435	0.435	0.312	7.312		7.415	6.841	0.306	[230]
$Cu_2ZnGeTe_4$	*I-42m*	P	0.435	0.435	0.312	8.766		8.747	8.766	0.011	[231]
Cu_2ZnSiS_4	*Pmn2$_1$*	SC	0.435	0.435	0.235	6.453		6.543	5.006	0.863	[232]
Li_2CdGeS_4	*Pmn2$_1$*	SC	0.429	0.541	0.312	7.260		8.494	5.469	1.521	[233]
Li_2CdSnS_4	*Pmn2$_1$*	SC	0.429	0.541	0.406	7.371		8.398	6.872	0.778	[233]
Li_2FeGeS_4	***Pn***	**SC**	**0.429**	**0.453**	**0.312**	**7.347**	**7.317**	**6.427**	**5.750**	**0.769**	**this work**
Li_2FeSnS_4	***Pn***	**SC**	**0.429**	**0.453**	**0.406**	**7.353**	**7.362**	**6.698**	**7.007**	**0.318**	**this work**
Li_2ZnSnS_4	*Pn*	SC	0.429	0.435	0.406	7.433	7.392	6.673	6.933	0.368	[234]

* Radius Ratio calculated using Shannon's 4-coordinate crystallographic radii for metals and 6-coordinate crystallographic radii for sulfur [37].

**Tetrahedral volumes calculated from solved and/or refined crystal structures.

SC – Structures solved from single crystal X-ray diffraction.

P – Structures refined from powder X-ray diffraction.

4.3.3 Comparison of Tetrahedral Volumes

It has been proposed by Pfitzner and coworkers that the volumes of cation tetrahedra in quaternary DLSs can be used to predict whether the ensuing structure will exhibit cubic or hexagonal closest packing. They proposed that if all the tetrahedra are of similar size (volume) the structure will be related to cubic diamond and if there is greater disparity in the sizes (volumes) then the structures will be derived from lonsdaleite. This theory was deduced from the experimental data of several ternary DLSs. Pfitzner and coworkers then selected three quaternary diamond-like compounds, Cu_2MnSiS_4, Cu_2MnGeS_4, and Cu_2MnSnS_4, as well as their solid solutions, in order to extend this hypothesis to quaternaries.[217,225]

According to this theory, the title compounds Ag_2FeSiS_4, Li_2FeSnS_4, and Li_2FeGeS_4 should all exhibit large differences in the volumes of the tetrahedra since the structures are derived from lonsdaleite. However, Pfitzner *et al.* did not establish a range in volume variations that would predict each packing type. For the purpose of this comparison, variations greater than 1 $Å^3$ were considered significant and used to predict a hexagonal-derived structure. The tetrahedral volumes calculated from the bond distances for Ag_2FeSiS_4 show a variation of 3.660 $Å^3$, the smallest tetrahedra volume is 5.009 $Å^3$ for Si-S_4 and the largest is 8.669 $Å^3$ for the Ag(2)-S_4 tetrahedra. This predicts a hexagonal-derived diamond-like structure, which agrees with the structure solution reported here. Likewise, Li_2FeGeS_4 also possesses a tetrahedral volume range of 1.597 $Å^3$, further confirming this hypothesis. However Li_2FeSnS_4 is comprised of tetrahedra ranging from 6.698 $Å^3$ for the Sn-S_4 tetrahedra to 7.362 $Å^3$ for the Li(2)-S_4

tetrahedra. This range of only 0.664 $Å^3$ corresponds to a cubic-derived diamond-like structure in contrast to the structure reported here.

Analysis of the 41 reported quaternary diamond-like chalcogenides selected here demonstrates that the tetrahedral volumes alone do not provide an indication of the preferred type of closest packing. When considering the reported cubic-derived structures, many of the materials with *I-42m* symmetry display significant variations in tetrahedral volumes. The most notable examples are that of the $Cu_2CdGeTe_4$ with tetrahedral volumes ranging from 8.542 $Å^3$ for Cu-Te_4 to 10.829 $Å^3$ for Cd-Te_4 and $Cu_2CdGeSe_4$ with volumes ranging from 6.632 $Å^3$ for Ge-Te_4 to 9.642 $Å^3$ for Cd-Te_4.[213] These large variations contradict the hypothesis that dissimilar tetrahedral volumes can be used as a predictive tool for hexagonal-derived structures and that uniform tetrahedral volumes forecast a cubic-related structure. In fact, two of the three compounds with the smallest variances in tetrahedral volumes posses hexagonally derived structures. Cu_2MnGeS_4 has the smallest variance in tetrahedral volumes and exhibits hexagonal closest packing.[225,226] Likewise, Cu_2CdSiS_4 with the third smallest variance also exhibits hexagonal closest packing, see Table 4.4.[214,215]

To determine if tetrahedral volumes could be used to predict a structure of hexagonal lineage, standard deviations of the volumes as well as their ratios were considered. Among the tetrahedral volumes in the 41 diamond-like chalcogenides considered here, the IV-VI_4 tetrahedra are the most regular in size and arrangement. In the three observed hexagonal-derived structure types, the anions can be found in a hexagonal closest packed array with the IV cations in the same tetrahedral holes (looking down the *a*-axis in $Pna2_1$, and the b-axis in $Pmn2_1$ and *Pn*). The group I and group II

ions occupy the remaining tetrahedral holes, leading to structural differentiation. No pattern was observed in the variance of the tetrahedral volumes that can be used to predict the preference of cation arrangement. Moreover, the difference in tetrahedral volumes across one structure type was found to vary greatly. For example, among the five DLSs crystallizing with the wurtz-kesterite (*Pn*) structure, the standard deviation of the tetrahedral volumes ranges from 0.318 $Å^3$ for Li_2FeSnS_4 to 1.715 $Å^3$ for Ag_2FeSiS_4. This difference is even more dramatic for the wurtz-stannite (*$Pmn2_1$*) structure type where the standard deviation of the tetrahedral volumes ranges from 0.009 $Å^3$ for Cu_2MnGeS_4 to 1.732 $Å^3$for Cu_2HgGeS_4.[224-226] Thus the degree of variance does not favor the formation of a particular hexagonal-derived structure type.

As demonstrated by this library of structures, somewhat larger deviations from ideal tetrahedral angles for one ion can often be compensated by lesser variance in the angles of another ion in the structure. Usually the angles in the I-VI_4 and the II-VI_4 tetrahedra exhibit the greatest deviation from ideal, relative to the IV-VI_4 tetrahedra. Therefore the averaged tetrahedral bond angles for the total structure are very close to 109.5°. Consequently the examination of tetrahedral volumes certainly demonstrates the flexibility of the diamond-like framework, although it does not provide any predictive ability.

4.3.4 Evaluation of Pauling's First Rule

Traditionally, one of the defining criteria for predicting tetrahedral structures is adherence to Pauling's first rule, the radius ratio rule.[204] This rule states that the ratio of the cation radius to the coordinating anion radius can be used to predict the ensuing

coordination geometry. If this ratio is in the range of 0.225 to 0.414 the geometry is predicted to be tetrahedral, a prerequisite for diamond-like materials.[184,185] However, most researchers are aware that Pauling's first rule can only be used as a guideline. In Pauling's seminal 1929 paper describing his rules, a number of example compounds were reported, mostly limited to simple binary oxides. However, O^{2-} is considered to be a hard base, while S^{2-} and Se^{2-} are softer anions and often do not display the same behavior. The range of ratios yielding diamond-like chalcogenides has not yet been reported. As a consequence of examining the selected 41 reported DLSs, the radius ratio for tetrahedral coordination is expanded from that specified by Pauling's first rule and may result in the prediction of additional diamond-like materials.[204]

For example when the radius ratios of the new quaternary DLSs reported here are considered using Shannon's revised radii and Pauling's range of 0.225 to 0.414, it can be found that none of these compounds are predicted to be diamond-like.[204,237] For Ag_2FeSiS_4 the radius ratios range from 0.23 for Si^{4+}/S^{2-} and 0.67 for Ag^{+}/S^{2-}. This is the largest spread in radius ratios among all quaternary DLS structures determined from single crystal X-ray data. For the lithium containing compounds, the radius ratios are closer to ideal, however, ratios of Li^{+}/S^{2-} (0.42) and Fe^{2+}/S^{2-} (0.45) are slightly above Pauling's predicted range for tetrahedral geometry. In fact any sulfides containing Ag^{+}, Cd^{2+}, Cu^{+}, Fe^{2+}, Li^{+}, Hg^{2+}, Mn^{2+}, and Zn^{2+} are not predicted to adopt tetrahedral geometry according to Pauling's first rule. Therefore, Pauling's established range of tetrahedral radius ratios is not applicable to diamond-like chalcogenides and may eliminate pursuit of particular compounds if the desired coordination is not predicted. In conclusion, the radius ratio rule should only be used as a guideline and the acceptable ratio for tetrahedral

coordination should be expanded to at least 0.67 for diamond-like compounds incorporating softer anions.

4.3.5 Evaluation of Available Radii Sets

To advance predictions of structures and properties of diamond-like chalcogenides, the accuracy of the radii sets put forth is investigated herein. The radii sets of Pauling and Huggins,[235] Philips and VanVechten,[236] Shannon,[237] Koga,[238] and Pyykkö[239] were chosen for evaluation. Figure 4.3 provides a comparison between the bond distances calculated from the various sets of radii to those of the measured bonds lengths found in the quaternary diamond-like materials listed in Table 4.4.

The covalent radii set presented by Pauling and Huggins in 1934 was derived from half the bond distance of homonuclear bonds.[235] This radii set should not be confused with Pauling's tetrahedral covalent radii set from 1960 that will be discussed later with Pyykkö's radii. A comparison of the X-S bonds calculated from Pauling's radii, based on a hard-sphere model of the atom, to the measured bond lengths is shown in Figure 4.4. This comparison demonstrates that, for the metals that were included in Pauling's radii set, the calculated metal-sulfur bond lengths are somewhat overestimated in comparison to the weighted average of the bond lengths observed in quaternary diamond-like materials. Although, Pauling's radii can be used to predict metal-sulfur bond lengths within the range of bond lengths from single crystal X-ray diffraction measurements, many elements were not considered at the time due to a lack of data on homonuclear bonds.

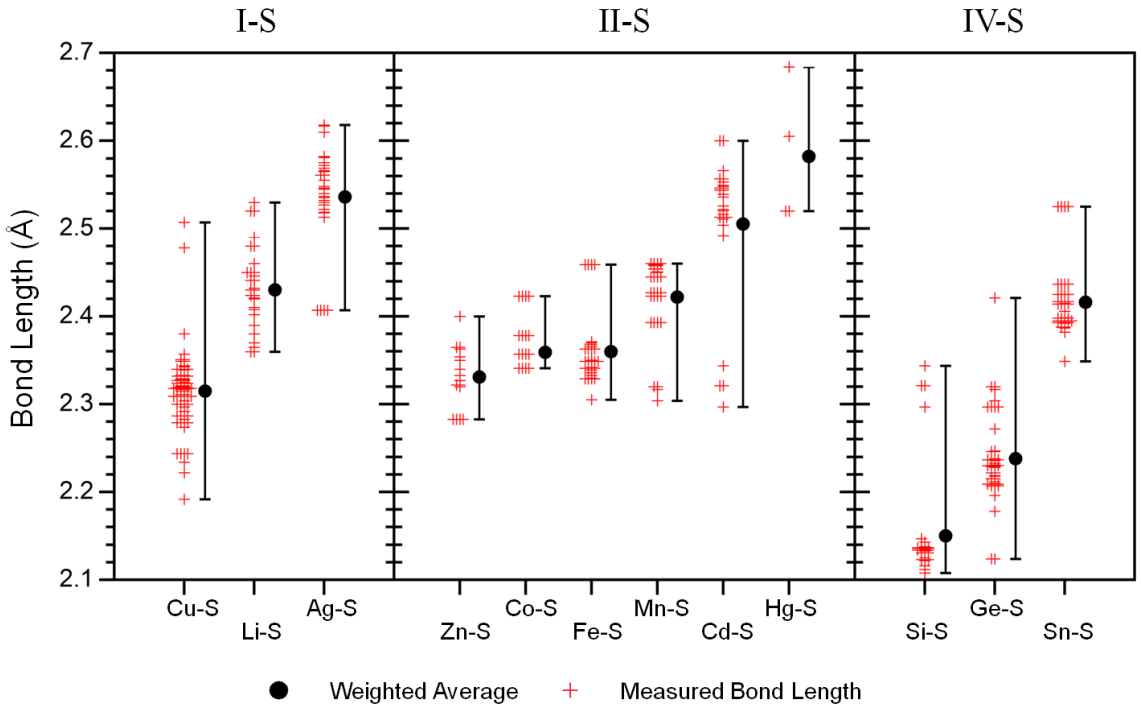

Figure 4.3 Measured metal-sulfur bond distances from single crystal experiments of quaternary DLS's depicting the weighted average and the range.

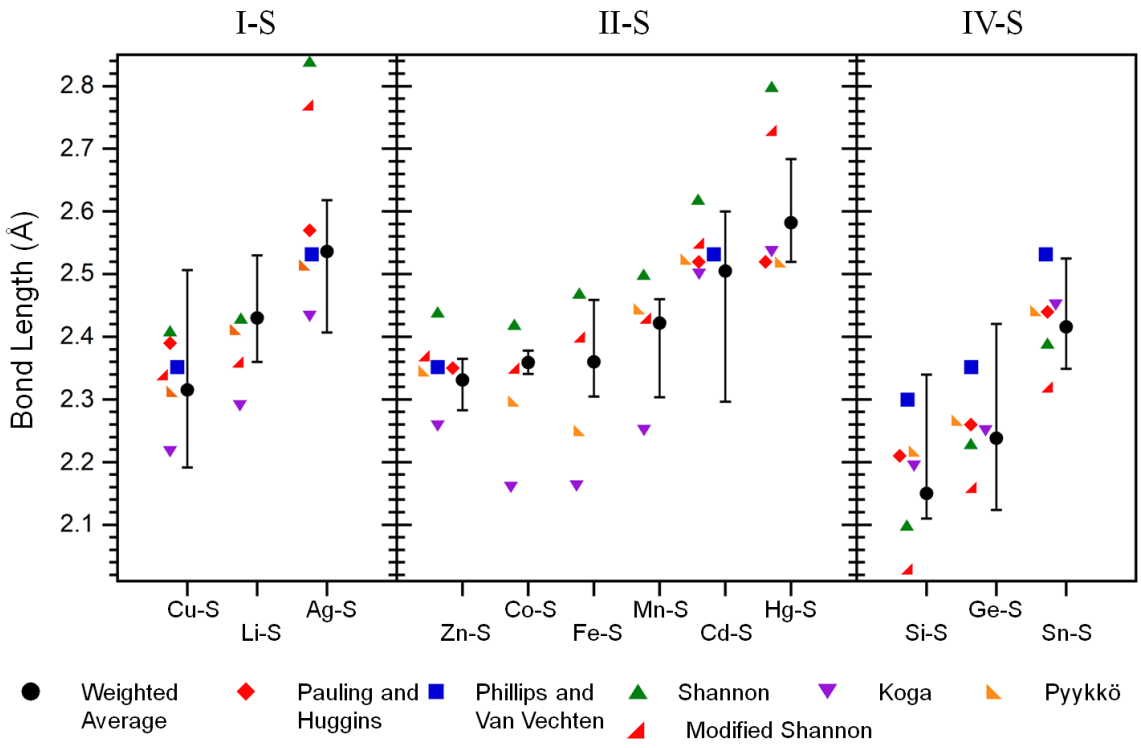

Figure 4.4 A comparison of the range and weighted average of measured metal-sulfur bond lengths to the bond lengths calculated from Pauling, Phillips, Shannon, Koga, and Pyykkö radii as well as a modified Shannon radii using 4-coordinate sulfur radius determined from single crystal data of quaternary DLSs.

In a later 1970 study, Phillips and Van Vechten calculated radii using the classical model of the atom and the Z_{eff} of the outermost *s* or *p* orbitals to formulate a "core size" correction. In their study, measured data from the diamond-like structures of C, Si, Ge, and α-Sn were used to generate correction factors for their respective rows of the periodic table.[236] Their results can be used to predict metal-sulfur bond lengths within experimental ranges; however, all of the metal-sulfur bond lengths are overestimated in comparison to the weighted average of the measured values and this is most pronounced in the bonds predicted for IV-S (Figure 4.4).

The set of crystal and ionic radii reported by Shannon in 1976 is one of the most commonly used because it takes into account both coordination number and oxidation state of the ions. This radii set was calculated from a compilation of mostly binary compounds, and some ternary compounds, where the initial cation radii were determined by subtracting the previously established Ahrens' covalent radii for the anions from the measured bond distances.[244] The radii for each ion with identical coordination and charge were averaged. A correction factor was determined by plotting these average radii with respect to unit cell volumes for isostructural binary compounds with the same anion. The values for the cation radii were then adjusted according to the assumption that this relation is linear. The adjusted cation radii were then used to determine the anion radius in the same fashion and the process was repeated.[245] Although quite complete, Shannon's set does not contain a crystal radius for S^{2-} in four-coordinate geometry.[237] Most subsequent studies that use this set of radii employ the crystal radius for six-coordinate S^{2-} in place of a four-coordinate S^{2-}, which is not an appropriate substitution. The use of the Shannon radii results in overestimating most of the metal-sulfur bond lengths, especially II-S bonds for which the predicted values are greater than any observed data.

In this work, a crystal radius for four-coordinate S^{2-} was calculated from the averaged bond lengths of metal-sulfur bonds within the quaternary diamond-like materials considered here, by subtracting the Shannon four-coordinate radius for the respective metal cation. This approach produced a crystal radius of 1.62(8) Å for four-coordinate S^{2-} compared to Shannon's reported 1.70 Å crystal radius for six-coordinate S^{2-}.[237] This result was further substantiated using a "leave-one-out" cross validation study.[246] In this method a data point is left out and the remaining data points are used to

predict the value of the missing data point. A deviation is then calculated for the predicted point compared to the actual data point. Predicted data points with deviations greater than 10% of its actual value are considered outliers; however, no data points in this study fell into this category. This process was repeated for each data point and the deviations were averaged to assess the error in the radius. Additionally, a separate dataset comprised of 40 ternary DLSs was also evaluated in the same manner.[247-271] The average radius for four-coordinate S^{2-} was determined to be 1.62(9) Å from the ternary dataset after cross validation. The metal-sulfur bond lengths predicted from this four-coordinate S^{2-} radius and Shannon's cation radii are closer to the measured values then those calculated using Shannon's six-coordinate S^{2-} radius, Figure 4.4. This modification to Shannon's radii set decreases the degree of overestimation for metal-sulfur bond lengths for the I and II metal cations; conversely, this adjustment leads to significant underestimation of the IV-S bond distances.

In 2001, Koga re-evaluated covalent radii by considering only carbon bonds to elements and subtracting half the C-C distance in ethane. Due to the difficulty of varying coordination patterns and spin states, this method is difficult to apply to transition metals; therefore, Koga preformed density functional theory (DFT) calculations to predict these radii.[238] Figure 4.4 depicts that the use of this radii set provides metal-sulfur bond distances that are comparable to those of the IV-S bond distances; however, the bond lengths of I-S and II-S are severely underestimated.

The most recent study put forth describing tetrahedral covalent radii has been presented by Pyykkö in 2012.[239] In his study he considered interatomic distances found in the crystal structures of 41 binary compounds and the computationally predicted bond

distances from 48 ternary compositions. Pyykkö used the same principles and assumptions that Pauling used in the determination of his tetrahedral covalent radii set in 1960, while incorporating more data points and employing computationally determined structures containing elements for which no experimental data was available.[272] Pyykkö reports radii for Li, Sc, Mn, Fe, Co, Tl, Pb, Bi, and Po, which Pauling did not. Additionally, an error correction was implemented in the case of elements for which both homonuclear and heteronuclear bond distances were known. For those radii that are common to both sets the agreement is within 0.02 Å, with the following notable exceptions: Pauling predicts a radius of 1.35 Å for Cu while Pyykkö predicts 1.271 Å, Pauling predicts a radius of 1.52 Å for Ag while Pyykkö predicts 1.473 Å. In comparison to Pauling's radii, Pyykkö overestimates the radii of all halogens except F which is underestimated. Due to the similarity between the datasets and the mutual assumption that the tetrahedral compounds primarily consist of single covalent bonds, only Pyykkö's radii are used here, Figure 4.4. The bond lengths predicted using Pyykkö's radii agree well with the measured metal-sulfur bond distances of the 41 quaternary DLSs considered here. This comparison shows good agreement for the I-S and IV-S bond lengths, even though the predicted value for the Si-S bond is higher than the weighted average. On the other hand, this model was found to underestimate the bond lengths for half of the II-S bond distances considered.

The comparison of measured bond distances with those calculated from several sets of radii shows that there is not one set of radii that can be reliably used to predict all of the bond distances in quaternary diamond-like sulfide materials with great accuracy. The metal-sulfur bond lengths predicted from Pauling's radii set shows the smallest

average deviation, 0.03 Å, from the weighted average for quaternary diamond-like materials; however, Mn, Fe, and Co radii are not included in this set, thus these metal-sulfur bond lengths cannot be calculated, Table 4.5. On the other hand, Mn-S, Fe-S, and Co-S bond lengths can be calculated using Pyykkö's radii set and the average deviation of all predicted metal-sulfur bond distances is only 0.01 Å greater than those predicted by Pauling. The degree of ionic and covalent character of the bonding that depends on the electronegativity differences of the ions is responsible for the discrepancies between the measured bond distances and those calculated from radii.[272] Although some researchers have attempted to account for this phenomenon, namely Phillips and Van Vechten[236] and Shannon,[237] they fall short of properly capturing the ionocovalent character of all bonds as evidenced by the significant inaccuracy in the prediction of some metal-sulfur bonds. For example, the Ag-S bond distance predicted from Shannon's radii set is 0.30 Å greater than the weighted average. Likewise, Phillips and Vechten predict a Si-S bond distance that is 0.15 Å greater than the weighted average. In conclusion, considering both accuracy and completeness of the radii set, we recommend the use of Pyykkö's radii for the prediction of metal-sulfur bonds in quaternary DLSs.

Table 4.5 The average S^{2-} (CN=4) deviation for predicted metal-sulfide bond lengths compared to the weighted average of reported data from quaternary diamond-like materials. The lowest deviations for each metal-sulfide bond are indicated in red.

Metal	Pauling (Å)	Philips-Van Vechten (Å)	Shannon (Å)	Modified Shannon (Å)	Koga (Å)	Pyykkö (Å)
Li	-	-	**0.01**	0.07	0.14	0.02
Cu	0.04	**0.01**	0.06	0.02	0.13	0.03
Ag	0.03	**0.01**	0.30	0.23	0.11	0.02
Mn	-	-	0.08	**0.01**	0.17	0.02
Fe	-	-	0.11	**0.04**	0.20	0.11
Co	-	-	0.06	**0.01**	0.20	0.06
Zn	**0.02**	**0.02**	0.11	0.04	0.07	**0.02**
Cd	**0.01**	0.03	0.11	0.04	**0.01**	0.02
Hg	0.06	-	0.22	0.15	**0.05**	0.06
Si	0.06	0.15	0.06	0.13	**0.04**	0.06
Ge	0.02	0.12	**0.01**	0.08	**0.01**	0.03
Sn	**0.02**	0.12	0.03	0.10	0.04	0.03
Avg. Dev.	**0.03**	0.06	0.10	0.08	0.10	**0.04**

4.4 Conclusion

In conclusion, the crystal structures of three new, isostructural diamond-like materials have been reported. Ag_2FeSiS_4, Li_2FeGeS_4, and Li_2FeSnS_4 were all found to crystallize in the noncentrosymmetric space group *Pn* increasing the members of this diamond-like structure type by 150%. Furthermore, all three compounds were found to be in violation of Pauling's radius ratio rule.[204] This work, along with a careful comparison to a majority of the published single crystal structures and refined powder structures of quaternary diamond-like materials, demonstrates that this rule can be broken and desired tetrahedral structure can still be produced. Furthermore, it has been determined that the

difference in tetrahedral volumes cannot be used to predict whether a structure will be derived from the cubic or hexagonal diamond structure as proposed by Pfitzner *et al.*[217]

Additionally, five radii sets were used to calculate metal-sulfur bond distances that were compared to the measured bond lengths from quaternary diamond-like materials. In order to improve the prediction of metal-sulfur bonds using the Shannon radii set, a four-coordinate S^{2-} radius was calculated to be 1.62(8) Å and the use of this radius for the prediction of metal-sulfur bond lengths improve the agreement with the measured results. Although, the bond distances determined from Shannon's radii set describe the general trend of the I-S and II-S bond distances, these bond lengths are still markedly overestimated.[237] Overall it was found that the new Pyykkö radii set best describes the weighted average bond lengths found for metal-sulfur bonds in quaternary materials.[239] However, none of the radii sets considered here can be used to predict metal-sulfur bond lengths with great accuracy when compared to the weighted average bond lengths found for quaternary diamond-like semiconductors.

With the growing interest of these materials for technological applications such as photovoltaics[188,192,193] and thermoelectrics,[189,198,199] as well as the daunting amount of imaginable compositions, there is a need for predictive tools in order to better focus synthetic efforts. The realization of these tools depends on high-quality structural studies and physicochemical characterization of known quaternary diamond-like materials to produce the data sets necessary to advance future discovery of materials. Computational predictions of structures and potential properties can only be as accurate as the input data, which includes atomic radii and an intimate understanding of the bonding that occurs. To

this end there is still work to be done on optimizing the sets of radii for these complex systems.

4.5 References

184 E. Parthé, E. *Crystal Chemistry of Tetrahedral Structures*; Gordon and Breach Science Publishers: New York, NY, **1964**.

185 Goryunova, N.A. *The Chemistry of Diamond-Like Semiconductors*; Anderson, J.C. Ed.; The MIT Press: Cambridge, U.K. **1965**.

186 Bundy, F. P.; Kasper, J. S. "Hexagonal diamond – a new form of carbon" *J. Chem. Phys.* **1967**, *46(9)*, 3437-3446.

187 Zeng, Y.; Chua, S. J.; Wu, P. "On the prediction of ternary semiconductor properties by artificial intelligence methods" *Chem. Mater.*, **2002**, *14(7)*, 2989-2998.

188 Ford, G. M.; Guo, Q.; Agrawal, R.; Hillhouse, H. W.; Hugh, W. "Earth abundant element $Cu_2Zn(Sn_{1-x}Ge_x)S_4$ nanocrystals for tunable band gap solar cells: 6.8% efficient device fabrication" *Chem. Mater.* **2011**, *23(10)*, 2626-2629.

189 Shi, X. Y.; Huang, F. Q.; Liu, M. L.; Chen, L. D. "Thermoelectric properties of tetrahedrally bonded wide-gap stannite compounds $Cu_2ZnSn_{1-x}In_xSe_4$" *Appl. Phys. Lett.* **2009**, *94(12)*, 122103.

190 McCabe, G. H.; Fries, T.; Liu, M. T.; Shapira, Y.; Ram-Mohan, L. R.; Kershaw, R.; Wold, A.; Fau, C.; Averous, M.; McNiff, E. J. "Bound magnetic polarons in p-type $Cu_2Mn_{0.9}Zn_{0.1}SnS_4$" *Phys. Rev. B.* **1997**, *56(11)*, 6673-6680.

191 Honig, H.; Shen, H.; Yao, G.; Doverspike, K.; Kershaw, R.; Dwight, K.; Wold, A. "Preparation and characterization of copper zinc manganese germanium sulfide ($Cu_2Zn_{1-x}Mn_xGeS_4$)" *Mater. Res. Bull.* **1998**, *23(3)*, 307-312.

192 Guo, Q.; Ford, G. M.; Yang, W. C.; Walker, B. C.; Stach, E. A.; Hillhouse, H. W.; Agrawal, R. "Fabrication of 7.2% efficient CZTSSe solar cells using CZTS nanocrystals" *J. Am. Chem. Soc.* **2010**, *132(49)*, 17384-17386.

193 Goetzberger, A.; Hebling, C.; Schock, H. W. "Photovoltaic materials, history, status and outlook" *Mater. Sci. Eng. R.* **2003**, *40(1)*, 1-46.

194 Pearton, S. J.; Abernathy, C. R.; Norton, D. P.; Hebard, A. F.; Park, Y. D.; Boatner, L. A.; Budai, J. D. "Advances in wide bandgap materials for semiconductor spintronics" *Mater. Sci Eng. R.* **2003**, *40(4)*, 137-168.

195 Chambers, S. A.; Yoo, Y. K. "New materials for spintronics" *MRS Bull.* **2003**, *28(10)*, 706-710.

196 Levcenco, S.; Dumcenco, D.; Huang, Y. S.; Arushanov, E.; Tezlevan, V. "Polarization-dependent electrolyte electroreflectance study of Cu_2ZnSiS_4 and $Cu_2ZnSiSe_4$ single crystals" *J. Alloys Compd.* **2011**, *509(25)*, 7105-7108.

197 Li, Y.; Fan, W.; Sun, H.; Cheng, X.; Li, P.; Zhao X. "Electronic, optical and lattice dynamic properties of the novel diamond-like semiconductors Li_2CdGeS_4 and Li_2CdSnS_4" *J. Phys. Condens, Matter* **2011**, *23(22)*, 225401.

198 Liu, M. L.; Chen, I. W.; Huang, F. Q.; Chen, L. D. "Improved thermoelectric properties of Cu-doped quaternary chalcogenides of $Cu_2CdSnSe_4$" *Adv. Mater.* **2009**, *21(37)*, 3808-3812.

199 Sevik, C.; Ćağin, T. “Ab initio study of thermoelectric transport properties of pure and doped quaternary compounds” *Phys. Rev. B* **2010**, *82(4)*, 045202.

200 Ellis, A. B.; Geselbracht, M. J.; Johnson, B. L.; Lisensky, G. C.; Robinson, W. R. *Teaching General Chemistry: A Materials Science Companion*, American Chemical Society, Washington, DC, **1993**.

201 Catella, G. C.; Burlage, D. "Crystal growth and optical properties of $AgGaS_2$ and $AgGaSe_2$" *MRS Bull.* **1998**, *23(7)*, 28-36.

202 Ohmer, M. C.; Pandey, R. “Emergence of chalcopyrites as nonlinear optical materials“ *MRS Bull.* **1998**, *23(7)*, 16-20.

203 Shay, J. L.; Wernick, J. H. *Ternary Chalcopyrite Semiconductors: Growth, Electronic Properties, and Applications*, Pergamon Press, Elmsford, NY, **1975**.

204 Pauling, L. “The principles determining the structure of complex ionic crystals” *J. Am. Chem. Soc.* **1929**, *51*, 1010-1026.

205 Brant, J. A.; Aitken, J. A. *Unpublished Work*

206 Brunetta, C. D.; Minsterman, W. C.; Lake, C. H.; Aitken, J. A. “Cation ordering and physicochemical characterization of the quaternary diamond-like semiconductor Ag_2CdGeS_4” *J. Solid State Chem.* **2012**, *187*, 177-185.

207 Parasyuk, O. V.; Piskach, L. V.; Olekseyuk, I. D.; Pekhnyo, V. I. “The quasi-ternary system Ag_2S-CdS-GeS_2 and the crystal structure of Ag_2CdGeS_4” *J. Alloys Compd.* **2005**, *397*, 95-98.

208 Caye, R.; Laurent, Y.; Picot, P.; Pierrot, R.; Levy, C. “Hocartite, Ag_2SnFeS_4, a new mineral species” *Bull. Soc. Fr. Mineral. Cryst.* **1968**, *91(4)*, 383-387.

209 Parasyuk, O. V.; Gulay, L. D.; Piskach, L. V.; Kumanska, Y. O. "The Ag_2Se-$HgSe$-$SnSe_2$ system and the crystal structure of the $Ag_2HgSnSe_4$ compound" *J. Alloys Compd.*, **2002**, *339*, 140-143.

210 Brunetta, C. D.; Balamurugan, K.; Rosmus, K. A.; Aitken, J. A. "The crystal and electronic band structure of the diamond-like semiconductor Ag_2ZnSiS_4" *J. Alloy. Compd.* **2012**, *516*, 65-72.

211 Parthé, E.; Yvon, K.; Dietech, R. H. "Crystal structure of Cu_2CdGeS_4 and other quaternary normal tetrahedral structure compounds" *Acta Crystallogr., Sect. B* **1969**, *25(6)*, 1164-1174.

212 Gulay, L. D.; Romanyuk, Y. E.; Parasyuk, O. V. "Crystal structures of low- and high-temperature modifications of $Cu_2CdGeSe_4$" *J. Alloy. Compd.*, **2002**, *347*, 193-197.

213 Olekseyuk, I. D.; Piskach, L. V.; Sysa, L. V. "Cu_2GeTe_3-CdTe system and structure of the compound $Cu_2CdGeTe_4$" *Russ. J. Inorg. Chem.*, **1996**, *41(9)*, 1420-1422.

214 Chapuis, G.; Niggli, A. "Crystal structure of the 'normal tetrahedral' compound Cu_2CdSiS_4" *Acta. Cryst.*, **1972**, *28*, 1626-1628.

215 Schäfer, W.; Nitsche, R. "Tetrahedral quaternary chalcogenides of the type Cu_2-II-IV-$S_4(Se_4)$" *Mater. Res. Bull.* **1974**, *9(5)*, 645-654.

216 Olekseyuk, I. D.; Gulay, L. D.; Dydchak, I. V.; Piskach, L. V.; Parasyuk, O. V.; Marchuk, O. V. "Single crystal preparation and crystal structure of the $Cu_2Zn/Cd,Hg/SnSe_4$ compounds" *J. Alloys Compd.*, **2002**, *340*, 141-145.

217 Bernert, T.; Pfitzner, A. "Characterization of mixed crystals in the system $Cu_2Mn_xCo_{1-x}GeS_4$ and investigations of the tetrahedra volumes" *Z. Anorg. Allg. Chem.* **2006**, *632(7)*, 1213-1218.

218 Gulay, L. D.; Nazarchuk, O. P.; Olekseyuk, I. D. "Crystal structures of the compounds $Cu_2CoSi(Ge,Sn)S_4$ and $Cu_2CoGe(Sn)Se_4$" *J. Alloys Compd.*, **2004**, *377*, 306-311.

219 Wintenberger, M. "Study of the crystallographic and magnetic structure of dicopper(I) iron(II) germanium sulfide (Cu_2FeGeS_4) and comment on the magnetic structure of dicopper(I) manganese(II) tin(IV) sulfide (Cu_2MnSnS_4)" *Mater. Res. Bull.*, **1979**, *14(9)*, 1195-1202.

220 Brockway L. O. "The crystal structure of stannite, Cu_2FeSnS_4" *Z. Kristallogr. Krist.* **1934**, *89*, 434-441.

221 Bonazzi, P.; Bindi, L.; Bernardini, G. P.; Menchetti, S. "A model for the mechanism of incorporation of Cu, Fe and Zn in the stannite-kesterite series, $Cu_2FeSnS_4 – Cu_2ZnSnS_4$" *Can. Mineral.*, **2003**, *41*, 639-647.

222 Llanos, J.; Tapia, M.; Mujica, C.; Oro-Sole, J.; Gomez-Romero, P. "A new structural modification of stannite" *Bol. Soc. Chil. Quim.*, **2000**, *45(4)*, 605-609.

223 Roque Infante, E.; Delgado, J. M.; Lopez Rivera, S. A. "Synthesis and crystal structure of $Cu_2FeSnSe_4$, a I_2 II IV VI_4 semiconductor" *Mater. Lett.*, **1997**, *33*, 67-70.

224 Olekseyuk, I. D.; Marchuk, O. V.; Gulay, L. D.; Zhbankov, O. Y. "Isothermal section of the Cu_2Se-HgSe-$GeSe_2$ system at 670 K and crystal structures of the

compounds Cu_2HgGeS_4 and HT-modification of Cu_2HgGeS_4" *J. Alloys Compd.*, **2005**, *398*, 80-84.

225 Bernert, T.; Pfitzner, A. "$Cu_2MnM^{IV}S_4$ (M^{IV} = Si, Ge, Sn) analysis of crystal structures and tetrahedra volumes of normal tetrahedral compounds" *Z. Kristallogr.*, **2005**, *220*, 968-972.

226 Allemand, J.; Wintenberger, M. "Neutron-diffraction study of the magnetic structures of Cu_2MnSnS_4 and Cu_2MnGeS_4" *Bull. Soc. Fr. Mineral. Cristallogr.*, **1970**, *93(2)*, 141-145.

227 Fries, T.; Shapira, Y.; Palacio, F.; Carmen Moron, M.; McINtyre, G. L.; Kershaw, R.; Wold, A.; McNiff, E. J. "Magnetic ordering of the antiferromagnet Cu_2MnSnS_4 from magnetization and neutron-scattering measurements" *Phys. Rev. B.*, **1997**, *56(9)*, 5424-5431.

228 Sachanyuk, V. P.; Olekseyuk, I. D.; Parasyuk, O. V. "X-ray powder diffraction study of the $Cu_2Cd_{1-x}Mn_xSnSe_4$ alloys" *Phys. Stat. Sol.*, **2006**, *203(3)*, 459-465.

229 Moodie, A. F.; Whitfield, H. J. "Determination of the structure of copper zinc germanium sulfide (Cu_2ZnGeS_4) polymorphs by lattice imaging and convergent-beam electron diffraction" *Acta. Cryst.*, **1986**, *42(3)*, 236-247.

230 Parasyuk, O. V.; Gulay, L. D.; Romanyuk, Y. E.; Piskach, L. V. "Phase diagram of the Cu_2GeSe_3-ZnSe system and crystal structure of the $Cu_2ZnGeSe_4$ compound" *J. Alloys Compd.*, **2001**, *329*, 202-207.

231 Parasyuk, O. V.; Olekseyuk, I. D.; Piskach, L. V. "X-ray powder diffraction refinement of $Cu_2ZnGeTe_4$ structure and phase diagram of the Cu_2GeTe_3-ZnTe system" *J. Alloys Compd.*, **2005**, *397*, 169-172.

232 Rosmus, K. A.; Aitken, J. A. "Cu_2ZnSiS_4" *Acta. Cryst.*, **2011**, *E67*, i28.

233 Lekse, J. W.; Moreau, M. A.; McNerny, K. L.; Yeon, J.; Halasyamani, P. S.; Aitken, J. A. "Second-harmonic generation and crystal structure of the diamond-like semiconductors Li_2CdGeS_4 and Li_2CdSnS_4" *Inorg. Chem.* **2009**, *48(16)*, 7516-7518.

234 Lekse, J. W.; Leverett, B. M.; Lake, C. H.; Aitken, J. A. "Synthesis, physicochemical characterization and crystallographic twinning of Li_2ZnSnS_4" *J. Solid State Chem.* **2008**, *181(12),* 3217-3222.

235 Pauling, L.; Huggins, M. L. "Covalent radii of atoms and interatomic distances in crystals containing electron-pair bonds" *Z. Kristallogr. Kristallgeom. Kristallphys. Kristallchem.* **1934**, *87*, 205-238.

236 Van Vechten, J. A.; Phillips, J. C. "New set of tetrahedral covalent radii" *Phys. Rev. B.*, **1970**, *2(6)*, 2160-2167.

237 Shannon, R. D. "Revised effective ionic radii and systematic studies of interatomic distances in halides and chalcogenides" *Acta Cryst.*, **1976**, *32(5)*, 751-761.

238 Suresh, C. H.; Koga, N. "A consistent approach toward atomic radii" *J. Phys. Chem.*, **2001**, *105(24)*, 5940-5944.

239 Pyykkö, P. "Refitted tetrahedral covalent radii for solids" *Phys. Rev. B.*, **2012**, *85(2)*, 024115.

240 Bruker **1998** *SMART and SAINT*, Bruker AXS Inc., Madison, Wisconsin, USA.

241 Sheldrick, G. M. **2002** *SADABS*. University of Göttingen, Germany.

242 Bruker **2007** *SHELXTL-PC, release 6.14*, Bruker AXS Inc., Madison, Wisconsin, USA.

243 Palmer, D. **2010** Crystal Maker, CrystalMaker Software Ltd., Oxfordshire, England.

244 Ahrens, L. H. "Use of ionization potentials. I. Ionic radii of the elements" *Geochim. Cosmochim. Acta.*, **1952**, *2*, 155-169.

245 Shannon, R. D.; Prewitt, C. T. "Effective ionic radii in oxide and fluorides" *Acta Cryst. B.*, **1969**, *25*, 925-946.

246 Shao, J. "Linear model selection by cross-validation" *J. Am. Statist. Assoc.* **1993**, *88*, 486-494.

247 Hahn, H.; Frank, G.; Klinger, W.; Meyer, A. D.; Stoerger, G. "Investigations of ternary chalcogenides. V. Ternary chalcogenides with chalcopyrite structures" *Z. Anorg. Allg. Chem.* **1953**, *271*, 153-170.

248 Guittard, M.; Chilouet, A.; Flahaut, J. "Phase diagram of the aluminum sulfide (Al_2S_3)-silver sulfide (Ag_2S) system" *C. R. Seances Acad. Sci.* **1981**, *293(9)*, 661-663.

249 Bindi, L.; Spry, P. G.; Pratesi, G. "Lenaite from the Gies gold-silver telluride deposit, Judith Mountains, Montana, USA. Occurrence, composition, and crystal structure" *Can. Mineral.* **2006**, *44(1)*, 207-212.

250 Brandt, G.; Raeuber, A.; Schneider, J. "ESR and X-ray analysis of the ternary semiconductors copper aluminum disulfide, copper indium disulfide, and silver gallium disulfide" *Solid State Comm.* **1973**, *12(6)*, 481-483.

251 Abrahams, S. C.; Bernstein, J. L. "Crystal structure of piezoelectric nonlinear-optic silver thiogallate" *J. Chem. Phys.* **1973**, *59(4)*, 1625-1629.

252 Vaipolin, A. A.; Rud, Yu. V.; Rozhdestvenskaya, I. V. "Interatomic interaction aspect of phase transition in silver indium sulfide ($AgInS_2$) crystals" *Cryst. Res. Technol.* **1988**, *23(3)*, 337-341.

253 Pauling, L.; Neuman, E. W. "The crystal structure of binnite $(Cu, Fe)_{12}As_4S_{13}$ and the chemical composition and structure of minerals of the tetrahedrite group" *Zs. Krist.* **1934**, *88*, 54-62.

254 Adiwidjaja, G.; Loehn, J. "Structure refinement for enargite, Cu_3AsS_4" *Acta Cryst. B.* **1970**, *26(11)*, 1878-1879.

255 Henao, J. A.; Delgado, G.; Delgado, J. M.; Castrillo, F. J.; Odreman, O. "Single-crystal structure refinement of enargite [Cu_3AsS_4]" *Mater. Res. Bull.* **1994**, *29(11)*, 1121-1127.

256 Karanovic, L.; Cvetkovic, L.; Poleti, D.; Balic-Zunic, T.; Makovicky, E. "Crystal and absolute structure of energite from Bor (Serbia)" *Neues Jahrb. Mineral.* **2002**, *6*, 241-253.

257 Pfitzner, A.; Bernert, T. "The system Cu_3AsS_4-Cu_3SbS_4 and investigations on normal tetrahedral structures" *Zs. Krist.***2004**, *219(1)*, 20-26.

258 Ferrari, A.; Cavalca, L. "The structure of cuprous thiophosphate" *Gazzetta Chimica Italiana* **1948**, *78*, 283-285.

259 Pfitzner, A.; Reiser, S. "Refinement of the crystal structures of Cu_3PS_4 and Cu_3SbS_4 and a comment on normal tetrahedral structures" *Zs. Krist.* **2002**, *217(2)*, 51-54.

260 Garin, J.; Parthé, E. "Crystal structure of Cu_3PSe_4 and other ternary normal tetrahedral structure compounds with composition $1_3 56_4$" *Acta Cryst. B.* **1972**, *28*, 3672-3674.

261 Aksenov, I. A.; Grutso, S. A.; Makovetskaya, L. A.; Popel'nyuk, G. P.; Rubtsov, V. A. "Growth and properties of crystals of the semiconductor solid solutions copper aluminum indium sulfide ($CuAl_xIn_{1-x}S_2$)" *Izv. Akad. Nauk., Neorg. Mater.* **1988**, *24(4)*, 560-562.

262 Gross, R.; Gross, N. "The arrangement of atoms in chalcopyrite and the structure of the surfaces of contact of regularly intergrowing crystals" *Neues. Jahrb., Beil. Bd.* **1923**, *48*, 128-135.

263 Pauling, L.; Brockway, L. O. "The crystal structure of chalcopyrite, $CuFeS_2$" *Z. Kristallogr. Kristallgeom. Kristallphys. Kristallchem.* **1932**, *82*, 188-194.

264 Hall, S. R.; Stewart, J. M. "Crystal structure refinement of chalcopyrite, $CuFeS_2$" *Acta Cryst. B.* **1973**, *29*, 579-585.

265 Digiuseppe, A.; Steger, J.; Wold, A.; Kostiner, E. "Preparation and characterization of the system copper gallium iron sulfide ($CuGa_{1-x}Fe_xS_2$)" *Izv. Akad. Nauk., Neorg. Mater.* **1974**, *13(8)*, 1828-1831.

266 Kratz, T.; Fuess, H. "Simultane Strukturbestimmung von Kupferkies und Bornit an einem Kristall" *Zs. Krist.* **1989**, *186*, 167-169.

267 Bodnar, I. V.; Bologa, A. P. "Copper gallium sulfide selenides ($CuGaS_{2x}Se_{2(1-x)}$) solid solutions" *Izv. Akad. Nauk., Neorg. Mater.* **1982**, *18(8)*, 1257-1261.

268 Bodnar, I. V.; Bodnar, I. T.; Vaipolin, A. A. "Growth and morphology of the copper gallium disulfide, copper aluminum diselenide, copper diselenide, and

copper indium disulfide ternary compounds" *Crystal Res. Technol.* **1984**, *19(12)*, 1553-1557.

269 Do, Y. R.; Kershaw, R.; Dwight, K.; Wold, A. "The crystal growth and characterization of the solid solutions zinc sulfide-copper gallium sulfide ($CuGaS_2$)" *J. Solid State Chem.* **1992**, *96(2)*, 360-365.

270 Leal-Gonzalez, J.; Melibary, S. S.; Smith, A. J. "Structure of lithium gallium sulfide $LiGaS_2$" *Acta Cryst. C.* **1990**, *46(11)*, 2017-2019.

271 Isaenko, L.; Yelisseyev, A.; Lobanov, S.; Titov, A.; Petrov, V.; Zondy, J. J.; Krinitsin, P.; Merkulov, A.; Vedenyapin, V.; Smirnova, J. "Growth and properties of $LiGaX_2$ (X = S, Se, Te) single crystal for nonlinear optical applications in the mid-IR" *Crystal Res. Technol.* **2003**, *38*, 379-387.

272 Pauling L. *The Nature of the Chemical Bond, 3rd ed.*; Cornell University Press: Ithaca, NY, **1960**.

5 Conclusions

5.1 Novel Diamond-Like Materials

The overall focus of this work was on the synthesis and physicochemical characterization of quaternary diamond-like materials with the formula I_2-II-IV-VI_4. To date, fewer than forty of these compounds are known and structurally characterized using single-crystal X-ray diffraction or a combination of X-ray powder diffraction and Rietveld refinement. This work adds two new quaternary diamond-like materials to this list, Ag_2ZnSiS_4[273] and Ag_2FeSiS_4, and increases the number of silver-containing quaternary diamond-like compounds from four to six.

5.2 Physical Structure

In order to correlate physicochemical properties with the crystal structures of these materials, high-quality structural studies are necessary. Early work on these compounds identified structures by simple comparisons of X-ray powder diffraction patterns using laboratory diffractometers.[274,275] However, the work in this dissertation demonstrates that three possible space groups (3 types of cation ordering) for hexagonal quaternary, diamond-like materials have nearly identical X-ray powder diffraction patterns. Using the example Ag_2CdGeS_4, a known quaternary DLS, this work reports a previously unreported space group $Pna2_1$, differing only in cation ordering from the reported $Pmn2_1$ and the predicted Pn.[274,276,277] These subtle differences in structure would be manifested in X-ray powder diffraction patterns by small deviations in the intensity of diffraction peaks and the presence of very small additional diffraction peaks that normally go

unnoticed using laboratory measurement and visual analysis.[278] Another difficulty in this structure determination is that Ag^{1+} and Cd^{2+} are isoelectronic and, therefore, nearly indistinguishable through X-ray analysis. Until this work, no method had been presented to overcome this challenge short of neutron diffraction studies. We proposed the careful examination of the bond lengths around each atomic site in order to identify the elements, as well as the careful consideration of multiple models with subsequent evaluation using the Hamilton R test.[279] These methods were used to identify the structure of Ag_2CdGeS_4 in the space group $Pna2_1$ using laboratory single-crystal X-ray diffraction data which was confirmed using high-resolution synchrotron X-ray powder diffraction data collected at Argonne National Laboratory.

In addition to demonstrating the application of these methods for structural analysis of these materials, this study clearly exemplifies the need for careful structural analysis of diamond-like structures. Since the origin of many properties, such as band gap, second harmonic generation, and the thermoelectric figure of merit, in these materials are not yet fully understood, accurate detailed structural analyses are necessary to elucidate structure-property correlations. Furthermore, the results of this work suggest that re-evaluation of many of the previously reported structures, which were deduced based on visual comparison of X-ray powder diffraction patterns or Rietveld refinement of laboratory X-ray powder diffraction data, may be necessary in order to ascertain structural details that contribute to understanding the relationships between the observed properties and crystal structures.

It is also pertinent to state that the structure solution and refinement of Ag_2CdGeS_4 in the space group $Pna2_1$ is only the second reported quaternary non-oxide

DLS in this space group.[278] Similarly, the structure solution and refinement of Ag_2ZnSiS_4[273]and Ag_2FeSiS_4 in the space group *Pn* adds members to a structure type where only one quaternary diamond-like material had been previously reported.

5.3 Electronic Structure

In addition to the determination of the crystal structures of these materials by X-ray diffraction methods, the electronic structure of quaternary DLSs was probed using the software package Wien2k for the first time.[280] Even though other groups have preformed electronic structure calculations on quaternary materials using other software packages, these data are scarce and calculations of band gap are rarely compared to optically determined band gaps. The software package Wien2k is unique in its application of density functional theory calculations using a linear augmented plane wave approach and the Perdew-Burke-Ernzerhof generalized gradient approximation for exchange and correlation effects.[281,282] This work demonstrates that these calculations are possible and are comparable to the work in the related system $AgGaS_2$ that also uses Wien2k, but employs local spin density approximations for the exchange and correlation effects.[283]

Another significant achievement of this study is the identification of the atomic orbitals at and around the Fermi level (E_F) in Ag_2ZnSiS_4.[273] The orbitals comprising the top of the valence band and bottom of the conduction band of these DLSs are reported. Mostly the Ag-d and S-p contribute to the valence band maximum and mainly the Zn-s, Si-s, and Si-p contribute to the conduction band minimum in these structures. This allowed us to predict that the II-site should be able to accept a first row transition metal such as Fe or Mn as a dopant, without drastically affecting the band gap of the material.

This suggests the potential for incorporating magnetic characteristics without altering the optical properties and provides a possible avenue of research for others to pursue.

5.4 Predictive Tools

Through a comparison of published quaternary compounds it has been demonstrated that the radius ratio rule[284] should not be used as a predictive tool for tetrahedral coordination, and, therefore, diamond-like structure, in non-oxide compounds. Although this result is not unexpected due to the softer nature of the anions in these materials and, therefore, the higher degree of covalent bonding, it has yet to be explicitly stated in the literature. The present work clearly states that this should no longer be considered as a prerequisite for diamond-like materials. Furthermore, it was also found that the tetrahedral volumes of these materials cannot be used to predict the packing arrangement (hexagonal-derived or cubic-derived) of the subsequent structures as predicted by Pfitzner *et al.*[285] Instead, predictions of tetrahedral coordination can be made upon finding examples of tetrahedral coordination for other compounds containing the same ions in the literature. For example, if the other guidelines of diamond-like materials are used to predict the diamond-like structure of the compound Ag_2MnSiS_4, the potential for tetrahedral coordination to occur is evaluated by searching the literature for examples of Ag-S, Mn-S, and Si-S tetrahedra. However, it should be noted that the absence of examples in the literature does not rule out the existence of a diamond-like phase being accessible.

The present work also compared the metal-sulfide bond distances predicted by using various radii sets to those distances resulting from single crystal X-ray diffraction

studies. Although this work has already demonstrated the inaccuracy of using radii for coordination prediction, these sets of radii are still extremely useful for computational studies as starting parameters for optimization calculations. For those reasons, we compared the various available sets of radii used in solid-state chemistry to their effectiveness at predicting bond distances in quaternary diamond-like sulfides.[286-290] Overall this work concludes that Pyykkö's covalent radii set,[290] an extension of Pauling's covalent tetrahedral radii set from 1960,[291] is the most complete and accurate set for predicting bonding distances in these materials.

5.5 Future Work

This work stresses the importance of careful structural studies toward the establishment of structure-property relationships in quaternary diamond-like materials. The implementation of bonding environment considerations, the Hamilton R test, synchrotron X-ray powder diffraction methods have been applied to quaternary diamond-like materials, as well as DTF calculations based on the linear augmented plane wave approach to understand crystal structure and electronic structure details. Furthermore, the electronic structure calculations for Ag_2ZnSiS_4 can be used to predict further quaternary diamond-like compounds, for example Ag_2CoSiS_4. In addition to the prediction of these compounds, the reconsideration of how the radius ratio rule applies to the guidelines of diamond-like semiconductors leads to the prediction of many compositions of new compounds that may have been previously disregarded. In conclusion, this work demonstrates the need for similar, thorough studies for all quaternary DLS materials in order for the origin of their properties to be understood.

5.6 Reference

273 Brunetta, C. D.; Balamurugan, K.; Rosmus, K. A.; Aitken, J. A. "The crystal and electronic band structure of the diamond-like semiconductor Ag_2ZnSiS_4" *J. Alloy. Compd.* **2012**, *516*, 65-72.

274 Parthé, E.; Yvon, K.; Dietech, R. H. "Crystal structure of Cu_2CdGeS_4 and other quaternary normal tetrahedral structure compounds" *Acta Crystallogr., Sect. B* **1969**, *25(6)*, 1164-1174.

275 Schäfer, W.; Nitsche, R. "Tetrahedral quaternary chalcogenides of the type Cu_2-II-IV-$S_4(Se_4)$" *Mater. Res. Bull.* **1974**, *9(5)*, 645-654.

276 Parasyuk, O. V.; Piskach, L. V.; Olekseyuk, I. D.; Pekhnyo, V. I. "The quasi-ternary system Ag_2S-CdS-GeS_2 and the crystal structure of Ag_2CdGeS_4" *J. Alloys Compd.* **2005**, *397*, 95-98.

277 Chen, S.; Walsh, A.; Luo, Y.; Yang, J. H.; Gong, X. G.; Wei, S. H. "Wurtzite-derived polytypes of kesterite and stannite quaternary chalcogenide semiconductors" *Phys. Rev. B* **2010**, *82(19)*, 195203.

278 Brunetta, C. D.; Minsterman, W. C.; Lake, C. H.; Aitken, J. A. "Cation ordering and physicochemical characterization of the quaternary diamond-like semiconductor Ag_2CdGeS_4" *J. Solid State Chem.* **2012**, *187*, 177-185.

279 Hamilton, W. C. "Significance tests on the crystallographic R factor" *Acta Cryst.* **1965**, *18(3)*, 502-510

280 Schwarz, K.; Blaha, P.; Madsen, G. K. H. "Electronic structure calculations of solids using the WIEN2k package for material sciences" *Comp. Phys. Commun.* **2002**, *147*, 71-76.

281 Blaha, P.; Schwarz, K.; Madsen, G. K. H.; D. Kvasnicka, D. *WIEN2k Users Guide* J. Luitz, Vienna University of Technology, Vienna, Austria **2011**.

282 Perdew, J. P.; Burke, K.; Ernzerhof, M. "Generalized gradient approximation made simple" *Phys. Rev. Lett.* **1996**, *77(18)*, 3865-3868.

283 Laksari, S.; Chahed, A.; Abbouni, N.; Benhelal, O.; Abbar, B. "First-principles calculations of the structural, electronic and optical properties of $CuGaS_2$ and $AgGaS_2$" *Comp. Mater. Sci.* **2006**, *38(1)*, 223-230.

284 Pauling, L. "The principles determining the structure of complex ionic crystals" *J. Am. Chem. Soc.* **1929**, *51*, 1010-1026.

285 Bernert, T.; Pfitzner, A. "Characterization of mixed crystals in the system $Cu_2Mn_xCo_{1-x}GeS_4$ and investigations of the tetrahedra volumes" *Z. Anorg. Allg. Chem.* **2006**, *632(7)*, 1213-1218.

286 Pauling, L.; Huggins, M. L. "Covalent radii of atoms and interatomic distances in crystals containing electron-pair bonds" *Z. Kristallogr. Kristallgeom. Kristallphys. Kristallchem.* **1934**, *87*, 205-238.

287 Van Vechten, J. A.; Phillips, J. C. "New set of tetrahedral covalent radii" *Phys. Rev. B.*, **1970**, *2(6)*, 2160-2167.

288 Shannon, R. D. "Revised effective ionic radii and systematic studies of interatomic distances in halides and chalcogenides" *Acta Cryst.*, **1976**, *32(5)*, 751-761.

289 Suresh, C. H.; Koga, N. “A consistent approach toward atomic radii” *J. Phys. Chem.*, **2001**, *105(24)*, 5940-5944.

290 Pyykkö, P. “Refitted tetrahedral covalent radii for solids” *Phys. Rev. B.*, **2012**, *85(2)*, 024115.

291 Pauling L. *The Nature of the Chemical Bond, 3rd ed.*; Cornell University Press: Ithaca, NY, **1960**.

Appendix I Cu_2CdSnS_4

AI.1 Introduction

In addition to silver-containing diamond-like semiconductors (DLS), the diamond-like mineral cernyite,[292] Cu_2CdSnS_4, was also synthetically produced as a potential parent for future doping studies. This mineral was targeted because 1) it had not yet been synthetically produced, 2) in nature it is found heavily doped with Fe, Mn, and Zn on the 2+ site, and 3) the potential end-members of the solid-solution studies; Cu_2ZnSnS_4,[293] Cu_2FeSnS_4,[294] and Cu_2MnSnS_4[295] are known. As a first step for this project a synthesis of phase pure Cu_2CdSnS_4 has been developed and the product has been characterized using powder X-ray diffraction, diffuse reflectance UV/Vis/NIR spectroscopy, and differential thermal analysis.

AI.2 Experimental

AI.2.1 Reagents

Chemicals used in this work were utilized as obtained: (1) copper powder, ~200 mesh, 99.999%, Strem Newburyport, MA; (2) cadmium powder, 99.999%, Strem Newburyport, MA; (3) tin powder, -100 mesh, 99.999%, Strem; (4) sulfur powder, sublimed, 99.5%, Fisher Scientific Pittsburgh, PA.

AI.2.2 Synthesis

Stoichiometric amounts of copper, cadmium, tin, and sulfur were weighed out according to an 4 mmol equivalence of the general formula I_2-II-IV-VI_4. These materials were ground together using a agate mortar and pestle in an argon-filled glovebox. The ground mixture was transferred to 9 mm O.D. fused-silica ampoule and vacuum sealed at approximately 10^{-3} mbar. The sealed tube was then heated to 800°C over 12 hours and held at 800°C for 125 hours. After which the sample was slow cooled at a rate of 6°C/hour for 50 hours. Once the temperature reached 500°C the sample was allowed to cool ambiently. The sample consisted of a gray microcrystalline powder, which was ground for subsequent property measurements.

AI.2.3 Physical Property Measurements

AI.2.3.1 Powder X-ray Diffraction

Powder diffraction patterns were collected using a Panalytical X'Pert Pro MPD powder X-ray diffractometer. Data were collected from 5° to 145° 2θ with a step size of 0.0083556° and scan rate of 0.010644°/sec. The incident beam optics were comprised of a 0.02 rad soller slit, a divergent slit of 1/4° and an anti-scatter slit of 1/2°; whereas, the diffracted beam optics were comprised of a 0.02 rad soller slit and an anti-scatter slit of 1/4°. The samples were prepared for analysis by back-filling a sample holder with finely ground sample. Cu K_α radiation was used with an accelerating voltage of 45 kV and a current of 40 mA, producing X-rays with a wavelength of 1.541871 Å.

AI.2.3.2 Diffuse Reflectance UV/Vis/NIR Spectroscopy

A Cary 5000 UV/Vis/NIR spectrometer was used to collect diffuse reflectance spectra. Samples were measured using a Harrick Praying Mantis diffuse reflectance accessory and $BaSO_4$ was used as a 100 % reflectance standard. Wavelengths from 2500 nm to 200 nm were scanned. Wavelength data were converted to electron volts and the percent reflectance data were converted to absorbance units using the Kubelka-Munk equation.[296]

AI.2.3.3 Differential Thermal Analysis

A Shimadzu DTA-50 thermal analyzer was employed for thermal analysis studies. A three-point calibration curve with indium, zinc and gold was used to calibrate the instrument. Both a reference of Al_2O_3 with comparable mass to the measured sample and the sample were vacuum sealed in fused-silica ampoules. The temperature was programmed to increase at a rate of 10 °C/min from 25 °C to 1000 °C. The temperature then decreased to 100 °C at 10°C/min. Two cycles were preformed in order to distinguish reversible.

AI.3 Results and Discussion

AI.3.1 Powder X-ray Diffraction

Rietveld refinements of laboratory X-ray powder diffraction data were carried out using the GSAS software package with the EXPGUI interface.[115,297] Peak profiles were fitted using a pseudo-Voigt function with asymmetric terms and low angle support.[298,299]

The background was modeled using a shifted Chebyschev polynomial with 6 terms.[300] Phase parameter refinements were carried out for the unit cell, atomic coordinates, and isotropic displacement parameters of the cations. Peaks shapes were expressed through the refinement of the Cagliotti Gaussian terms and a scaling factor.[301]

The previously reported space group *I-42m* and atomic coordinates were used starting points for this refinement.[292] The final refinement converged with a χ^2 of 1.454 and a equivalent wRp of 0.0571. The refinement, Figure AI.1 , does not indicate the presence of any extra phases, suggesting a phase-pure product.

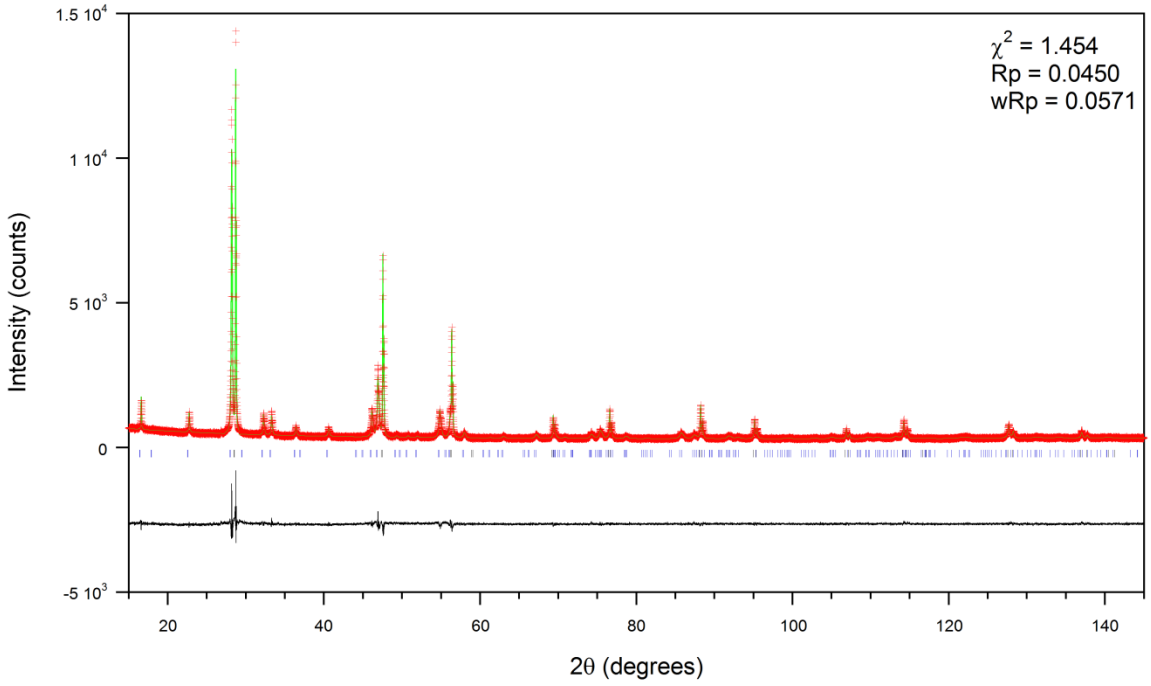

Figure AI.1 Rietveld refinement of Cu_2CdSnS_4 refined in *I-42m*. The observed data (+++) and calculated data (solid line) are overlaid at the top. While tick marks (III) indicating calculated peak locations.

AI.3.2 Diffuse Reflectance UV/Vis/NIR Spectroscopy

The semiconductor nature of this material was accessed using diffuse reflectance UV/Vis/NIR spectroscopy. The material was found to have a band gap of 1.27 eV, as shown in Figure AI.2. The noise in the plot at the top of the band edge is attributed to a physical grating change that takes place in the instrument at that wavelength.

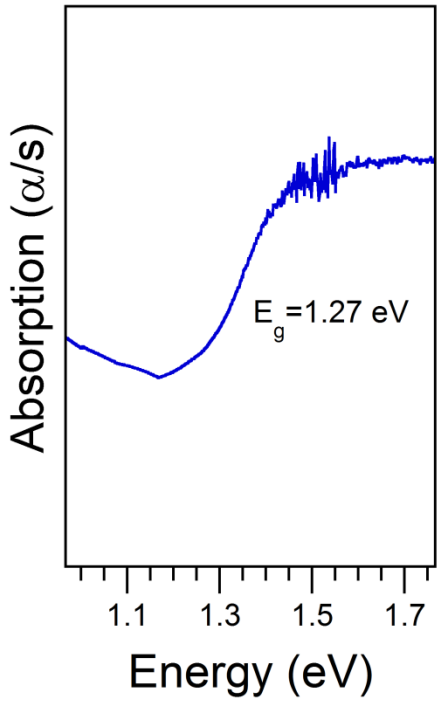

Figure AI.2 Diffuse reflectance spectrum of Cu_2CdSnS_4.

AI.3.3 Differential Thermal Analysis

Differential thermal analysis of Cu2CdSnS4 exhibited two reversible events one on heating and one on cooling. Each cycle displayed an endothermic event upon heating that can be attributed to the melt of the product at approximately 930°C. Likewise, each cycle shows a corresponding exothermic event when cooled which is most likely the

recrystallization of the material at approximately 900°C. The lack of further thermal events supports the conclusion that the material is phase pure.

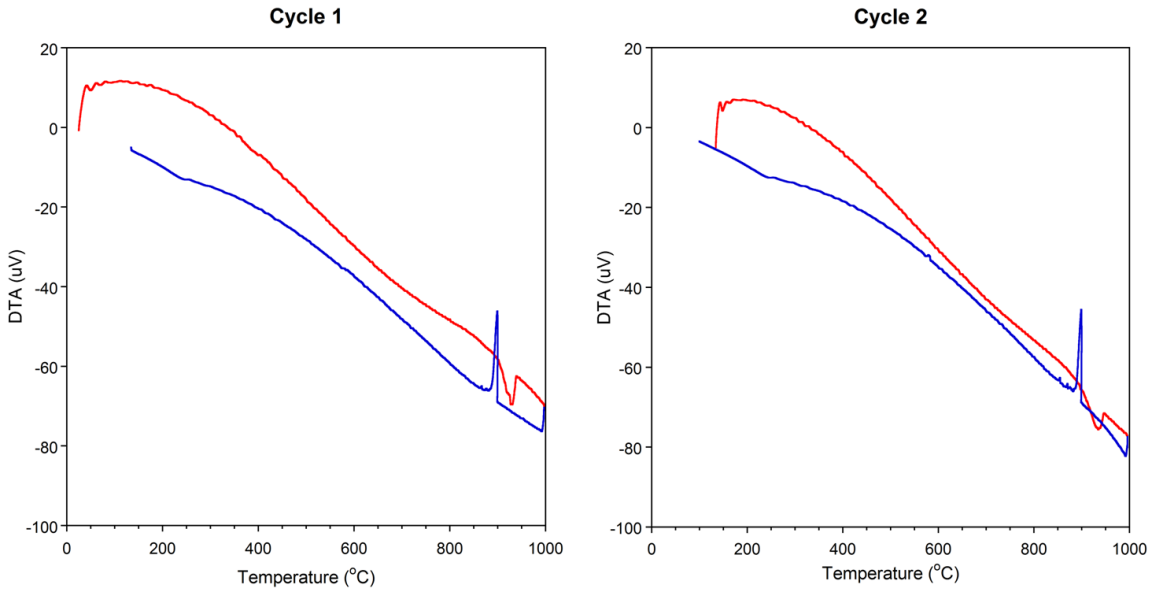

Figure AI. 3 Differential thermal analysis of Cu_2CdSnS_4.

AI.4 Conclusions and Future Work

A synthesis has been developed for the diamond-like semiconductor Cu_2CdSnS_4. The material was confirmed to be a semiconductor with a measured band gap of 1.27 eV. This material and synthesis will be used as an end member for future solid solution studies of the formula $Cu_2Cd_{1-x}M_xSnS_4$, where M=Co, Fe, Mn.

AI.5 References

292 Szymański, J. T. "The crystal structure of cernyite, Cu_2CdSnS_4, a cadmium analog of stannite" *Can. Mineral.* **1978**, *16(2)*, 147-151.

293 Nakayama, N.; Ito, K. "Sprayed films of stannite Cu_2ZnSnS_4" *Appl. Surf. Sci.* **1996**, *92*, 171-175.

294 Brockway L. O. "The crystal structure of stannite, Cu_2FeSnS_4" *Z. Kristallogr. Krist.* **1934**, *89*, 434-441.

295 Allemand, J.; Wintenberger, M. "Neutron-diffraction study of the magnetic structures of Cu_2MnSnS_4 and Cu_2MnGeS_4" *Bull. Soc. Fr. Mineral. Cristallogr.*, **1970**, *93(2)*, 141-145.

296 Kubelka, P.; Munk, F. "An article on optics of paint layers" *Zeit. Für Tekn. Physik* **1931**, *12*, 593-601.

297 Toby, B. H. "EXPGUI, a graphical user interface for GSAS" *J. Appl. Crystallogr.* **2001**, *34(2)*, 210-213.

298 Finger, L. W.; Cox, D. E.; Jephcoat, A. P. "A correction for powder diffraction peak asymmetry due to axial divergence" *J. Appl. Cryst.* **1994**, *27(6)*, 892-900.

299 Van Laar, B.; Yelon, W. B. "The peak in neutron powder diffraction" *J. Appl. Cryst.* **1984**, *17(2)*, 47-54.

300 Abramowitz, M.; Stegun, I.A. eds. *Handbook of Mathematical Functions*, Dover Publications, Dover, NY, **1965**, Ch 22.

301 Caglioti, G.; Paoletti, A.; Ricci, F. P. "Choice of collimators for a crystal spectrometer for neutron diffraction" *Nucl. Instrum. Methods* **1958**, *3*, 223.